Attachment 2 to TMI2-RA-COR-2022-0001

Supplemental Information to License Amendment Request

Three Mile Island Nuclear Station, Unit 2

NRC Possession Only License No. DPR-73

Revision to TMI2-EN-RPT-0001 "Determination of the Safe Fuel Mass Limit for Decommissioning TMI-2"

ENERGYSOLUTIONS	Calculation Package	Doc. No.: TMI2-EN-RPT-0001 Rev.: Rev 1
Title: Determination of the Safe Fuel Mass Limit for Decommissioning TMI-2		
Design Plan No.: TMI2-DPL-N-00-0001		DP Rev.: 1

Signatures	*(printed name, signature, date)*
Preparer	Megan Pritchard
Approval	Guy Rhoden

Record of Verification

Item Verified	Acceptable	N/A - Explain
a) Design Verification by Independent Checking Method	☐	☐
b) Computer Software approved per CG-EN-PR-204	☐	☐
c) Calculation Package complete and per CG-EN-PR-203	☐	☐
Signature	*(printed name, signature, date)*	
Verifier	Derrick Faunce	

Record of Revisions

Rev.	Affected Pages	Affected Media	Description	(Print or Type)	
				Preparer	Verifier
0	-	-	Initial Issue	Megan Pritchard	Derrick Faunce
1	§2, §3, §6	-	- Updates to the description of the validation and USL determination. - Updates to the proposed operational description and upset conditions.	Megan Pritchard	Derrick Faunce

Table of Contents

List of Figures

List of Tables

1. INTRODUCTION

1.1. Purpose and Objectives

The purpose of this calculation and report is to identify a new safe fuel mass limit (SFML) for Three Mile Island (TMI)-2 decommissioning based on realistic but bounding assumptions about the material within the reactor vessel and outside the reactor vessel. It is intended that a single SFML can be utilized for all work in TMI-2 decommissioning and bound all credible operational upsets. This is accomplished through examination and application of material sampling results (i.e., impurities concentration), application of conservative assumptions where conditions are unknown or have associated uncertainty (i.e., fuel geometry, reflector), and taking credit for known phenomena (i.e., radioactive decay, burn-up). The sensitivity of each parameter to overall system reactivity is analyzed such that a balance between known and less certain parameters can be achieved. Documentation and supporting information for the inputs utilized to derive the SFML is outlined in TMI2-EN-RPT-0003, *TMI-2 Safe Fuel Mass Limit Computational Input Consensus* (Ref. [1]).

1.2. Background

1.2.1. Safe Fuel Mass Limit

The SFML is a limit developed through criticality safety analyses as to the amount of fuel-containing debris that may be safely handled at one time. It is intended that this limit bound all remaining fuel-containing debris in the TMI-2 reactor that is subject to decommissioning operations.

Previous defueling operations were performed using SFMLs developed based solely on credible upper bounds for input parameters as opposed to sample data or realistic conditions. However, defueling operations included potential removal of relatively intact fuel rods and fuel debris that varied extensively in its composition. This revision to the SFML is performed with more realistic and less conservative inputs than those used in previous analyses. The primary reasoning behind this approach is that the fuel debris is largely confined to an area with available characterization data, and intact fuel rods are no longer present. These inputs, while less conservative than those used in the original SFML determination, are still considered to be reasonably and sufficiently conservative for their use herein.

1.2.2. Status of TMI-2

The TMI-2 reactor has been undergoing various stages of defueling and clean-up since the accident in 1979. The primary defueling occurred in the late 1980s. The operations removed all fuel to the extent reasonably achievable and ultimately reduced the possibility of an inadvertent criticality under static or accident conditions. Approximately 99% of the original core inventory was removed during these operations with an estimate for residual UO_2 of 1097 kg (~1.2% of initial TMI-2 inventory). The remaining fuel is in the form of finely divided, small particle-size sediment material; re-solidified material either tightly adherent to components or in areas inaccessible to defueling; and adherent films on surfaces contained within piping, tanks, and

other components. The 1097 kg includes fuel debris inside and outside the reactor vessel (RV) with the bulk of the mass residing in the lower head of the RV.

The remaining fuel mass estimates in each major area are provided in Table 1-1. During defueling, the majority of the material in the debris bed of the core was removed. Approximately 12% of the remaining material is estimated to be in the coolant system with some scattered throughout the plant (e.g., steam generators, hot legs, coolant pumps). Evaluation of the ex-vessel residual fuel has demonstrated that no discrete (neutronically de-coupled) location has in excess of 127 kg UO_2, and the total estimate outside of the RV is 170 kg UO_2.

Table 1-1. Remaining Fuel Mass Estimates (Ref. [2], Table 1)

Area	Estimated Mass (kg UO_2)	Uncertainty (kg UO_2)
Plenum	2.1	± 1.9
Letdown Coolers	3.7	± 2.0
Pressurizer	0.3	± 0.2
Reactor Vessel Head	1.3	± 0.9
Reactor Building Basement	1.3	± 0.7
'A' and 'B' Once Through Steam Generator (OTSG)	62.3	± 9.7
Auxiliary and Fuel Handling Buildings	11.5	± 5.8
Reactor Building Miscellaneous Components	64.0	± 26.9
Reactor Coolant System (RCS)	25.8	± 11.1
Reactor Vessel	925	± 370
Total	1097	± 371

Detailed summaries as to how each of these estimates were developed can be found in TMI2-EN-RPT-0003, *TMI2 Safe Fuel Mass Limit Computational Input* Consensus (Ref. [1], §2). Some of the residual quantities included in the estimates are reported as the minimum detectable level, indicating that the measurement technique did not detect a statistically significant number of events (counts) related to fissile nuclides. Physical measurements are subject to imprecisions which is an additional contributor to uncertainty. There are also uncertainties associated with counting statistics. The estimate for residual UO_2 is intended to be an upper bound, but carries an uncertainty in the RV of ± 370 kg UO_2 (Ref. [4]). Including the uncertainty in the estimated mass for the RV results in a total for this area of ~1295 kg UO_2.

1.3. Scope

The existing SFML is the fissile material mass limit for handling within the reactor vessel. The revised SFML derived herein applies to all decommissioning operations including removal from the RV, movement to the reactor cavity or other area intended for segmentation and movement to loading of the transportable storage container (TSC). Once fissile material (in actuality, these are components with damaged core material) is loaded into the TSC, it it outside the scope of the applicable SFML.

2. METHODOLOGY

2.1. General

The SFML is revised through evaluation of planned decommissioning operations and associated operational upsets, remaining fuel estimates, and the associated computation of a bounding mass limit that may be applied to those operations. Inputs to the supporting calculation are supported through review of robust historic sampling data and the conservative application of those results.

2.2. Computational

The approach to developing a new SFML encompasses two computational efforts: first, calculation of the source term (i.e., expected fuel composition) in 2022; and second, the criticality calculations for limiting reactor core fuel arrangements. Analytical software is qualified according to EnergySolutions Quality Assurance Program.

2.2.1. Computer Codes

Derivation of the expected source term is performed using the SCALE 6.2.4 ORIGEN depletion code to decay the previously calculated burned fuel. ORIGEN uses the continuous energy ENDF/B-VII decay data in the decay calculation (SCALE: A Comprehensive Modeling and Simulation Suite for Nuclear Safety Analysis and Design, Ref. [6]).

The criticality results in this report are calculated using Monte Carlo methods in the Monte Carlo n-Particle (MCNP) Version 6.2 code (Ref. [7]) with continuous energy ENDF/B-VIII.0 cross section data (Ref. [8]). MCNP is a general-purpose Monte Carlo particle transport code that can be used for neutron transport. MCNP treats an arbitrary three-dimensional configuration of materials in geometric cells bounded by first- and second-degree surfaces and fourth-degree elliptical tori. The code can be used to perform nuclear criticality safety analyses (k_{eff} eigenvalue calculations). The calculation of the neutron multiplication factor is performed by solving the neutron transport equation as an eigenvalue problem through the employment of Monte Carlo techniques.

2.2.2. USL Determination

Computer codes used to determine the effective neutron multiplication factor, k_{eff}, are to be properly verified and validated in accordance with ANSI/ANS-8.24 (Ref. [9]). The methodology

used in the validation is taken from NUREG/CR-4604 (Ref. [10]) and NUREG/CR-6698 (Ref. [11]).

Calculations are performed to validate MCNP v6.2 nuclear analysis code for neutron multiplication factor calculations performed in support of raising the SFML for TMI-2 decommissioning. The validation report TMI-EN-RPT-0002, *MCNP Version 6.2 Bias Determination for Low Enrichment Uranium Using the ENDF/B-VIII.0 Cross Section Library* (Ref. [12]) determines the calculational margin (MoC) and margin of subcriticality (MoS), in order to establish the Upper Subcritical Limit (USL) for the area of applicability (AOA). The validation is applicable to heterogeneous spherical and annular configurations of low enriched UO_2 and water.

The bias determination report identifies applicable experiments to determine the bias and bias uncertainty for the geometric configuration, enrichment, fissile material distribution, impurity content, and potential soluble poison concentration included in the modeling. The bias and bias uncertainty is then used in combination with an estimate of the margin of subcriticality (MoS) to determine a USL such that for the specific application, calculated reactivity values, k_{calc}, and their associated Monte Carlo uncertainty σ satisfy the relation

$$k_{calc} + 2\sigma < USL$$

This ensures that a system is safely subcritical, in this case at a 95% confidence level. The USL is established by subtracting quantified estimates of the code bias, bias uncertainty, and additional margin from unity.

$$USL = 1 - MoC - MoA - MoS$$

Where,

MoC is the calculational margin and includes the bias and bias uncertainty in addition to any uncertainties related to the trending;

MoA is the Margin of Applicability, where is an allowance for any uncertainties related to extension of the AOA;

MoS is the Margin of Subcriticality, which is an administrative allowance beyond the MoC to ensure subcriticality.

The ANSI/ANS-8.24-2017 standard (Ref. [9]) defines the following terms, which are incorporated in the USL determination defined above.

Bias	The systematic difference between calculated results and experimental data. Note by convention the bias is determined as the calculated value minus the experimental value. Hence, a negative bias indicates that the code underpredicts the experimental result.
Bias Uncertainty	The uncertainty that accounts for the combined effects of uncertainties in the experimental benchmarks, the calculational models of the benchmarks, and the calculational method.

Calculational Margin	An allowance for Bias and Bias Uncertainty plus considerations of uncertainties related to interpolation, extrapolation, and trending (*MoC*)
Margin of Subcriticality	An allowance beyond the calculational margin to ensure subcriticality (*MoS*)
Validation Applicability	A domain, which could be beyond the bounds of the benchmark applicability, within which the margins derived from validation of the calculational method have been applied.

Method

The bias determination is performed in direct support of the SFML work and consists of two parts. The first involves the determination of the MCNP v6.2 computer code bias and bias uncertainty. The second part examines the AOA of the validation benchmark cases. The benchmarks represent a selection of uranium based critical experiments that are determined to be representative of the configurations modeled as part of this report. The benchmark data is examined for potential trends to determine the proper bias determination method. The selection of benchmark cases and calculated bias are reported in TMI-EN-RPT-0002, *MCNP Version 6.2 Bias Determination for Low Enrichment Uranium Using the ENDF/B-VIII.0 Cross Section Library* (Ref. [12]).

The AOA consists of the range or values of various parameters important to the reactivity of the benchmark models. These define the range or values for a system parameter or parameters over which the validation and bias presented above are considered valid without modification. The parameter ranges of the validation models are compared to the models of the system being evaluated. If the system parameter falls within the AOA, no additional margin is necessary beyond the MoS for determining the USL. If one or more of the system parameters are found to fal outside of the AOA, additional margin may be added on the USL to extend the applicability of the validation.

Analysis and Result

The bias determination report validates the use of MCNP Version 6.2 and ENDF/B-VIII.0 library for use in performing the calculations that estimate k_{eff} values for determination of the SFML. There is no notable trend within the data that needs to be compensated for in the determination of the bias, which is calculated as 0.9798. The AOA of the validation is provided in Table 2-1 and is generally sufficient to cover the range of parameters in the SFML calculation.

Table 2-1. Properties of the MCNP6 Benchmark Models

Property	Validated AOA				
Fissile Materials	U (2 – 10 wt. % ^{235}U) in the form of compounds (Uo2, UF4) and solution (UO2F2)				
Basic Geometry of the Fissile Material	Array of fuel rods, array of rectangular parallelepipeds, UO_2 in cubes in a cubic array, finely divided particles in cubes, cylinders, spheres, slabs				
Moderator Materials	Water, Paraffin, Polyethylene				
Reflector Materials	None, Water, Acrylic, Steel, Plexiglas, Paraffin, Polyethylene, Concrete				
Other Significant absorbers, poisons, or structural materials present	Al alloys, steel, borated steel, Boral, boroflex, Ag-In-Cd, Cu, Cu with Cd, Cd, Zircaloy-4, rubber Soluble Boron: 0 – 96 ppm				
Specific Cross Sections and S(α,β) used (MCNP6 identifiers)	1001.00c 5010.00c 5011.00c 6012.00c 6013.00c 7014.00c 8016.00c 8017.00c 9019.00c 11023.00c 12024.00c 12025.00c 12026.00c 13027.00c 14028.00c 14029.00c 14030.00c 15031.00c 16032.00c 16033.00c 16034.00c 16036.00c 17035.00c 17037.00c	19039.00c 19040.00c 19041.00c 20040.00c 20042.00c 20044.00c 20046.00c 20048.00c 22046.00c 22047.00c 22048.00c 22049.00c 22050.00c 24050.00c 24052.00c 24053.00c 24054.00c 25055.00c 26054.00c 26056.00c 26057.00c 26058.00c 27059.00c	28058.00c 28060.00c 28061.00c 28062.00c 28064.00c 29063.00c 29065.00c 30064.00c 30066.00c 30067.00c 30068.00c 30070.00c 40090.00c 40091.00c 40092.00c 40094.00c 40096.00c 42092.00c 42094.00c 42095.00c 42096.00c 42097.00c 42098.00c 42100.00c 47107.00c 47109.00c	48106.00c 48108.00c 48110.00c 48111.00c 48112.00c 48113.00c 48114.00c 48116.00c 49113.00c 49115.00c 50112.00c 50114.00c 50115.00c 50116.00c 50117.00c 50118.00c 50119.00c 50120.00c 50122.00c 50124.00c 92234.00c 92235.00c 92236.00c 92238.00c	h-poly.40t h-h2o.40t
Average Energy of Neutrons Causing Fission (AENCF)	Range (MeV): 2.43E-02 – 2.88E-01 Average (MeV): 1.40E-01				

A single USL is developed for the SFML application for TMI-2 decommissioning. The USL is derived based on the calculated bias using the limiting identified geometric configuration (sphere), fissile material type (low enriched $^{235}UO_2$), soluble poison concentrations (0 – 96 ppm), and distribution (heterogeneous) for the pertinent models.

The additional MoS applied to ensure the calculational results are adequately subcritical typically ranges from 0.02 (at a minimum) to 0.05, and depends on factors such as the systems to be

modeled, the reliability of the calculational method, and knowledge of physical and chemical aspects of the systems to be modeled. There are a large number of experimental benchmarks used in the validation (125 cases covering nine benchmarks), which provides a large set of cases for the statistical evaluation of the bias and bias uncertainty. The additional MoS applied is 0.0298 for an overall USL of 0.95. This MoS is justified through the application of conservative input parameters and bounding configurations to the computational models.

A USL of 0.95 is utilized in the criticality safety analysis and provides adequate margin in supporting the SFML.

3. PROCESS DESCRIPTION

3.1. Operational Description

There are four main areas of core debris in TMI-2. The Reactor Pressure Vessel (also called RV), the Reactor Coolant System (not including the RV), the Reactor Building (not including the RV and Reactor Coolant System), and the Auxiliary/Fuel Handing Building. Table 1-1 provides estimates for these areas, broken down into some smaller areas/systems. Each of the four general areas is handled separately during decommissioning.

The canal above the RV is used to process (i.e., size reduce) and decontaminate large components. The canal is located at the 347 ft elevation, is approximately 25 ft wide, 77 ft long, 20 ft deep in the shallow end and 34 ft deep in the deep end. The RV cavity is located in the approximate center of the canal. A maximum of two volume reduction stations (VRS) are installed at opposite ends of the canal with the working Waste Zone in the central region. The Waste Zone is sized such that it can hold four waste basket liners (WBL). A graphical depiction of the VRS locations within the canal is provided in Figure 3-1 and a potential layout of the Waste Zone is shown in Figure 3-2.

Drawing shows:

VRS 1 & 2

Working Bridge 1&2

Working and Handling space

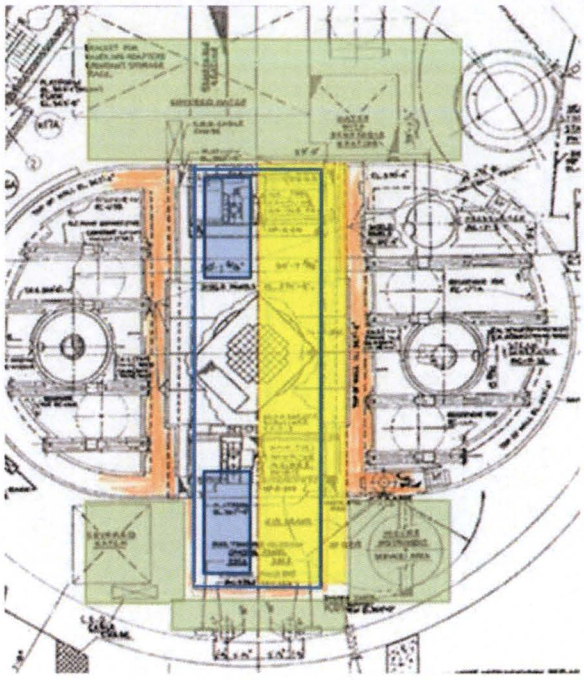

Figure 3-1. Volume Reduction Stations within RV Area

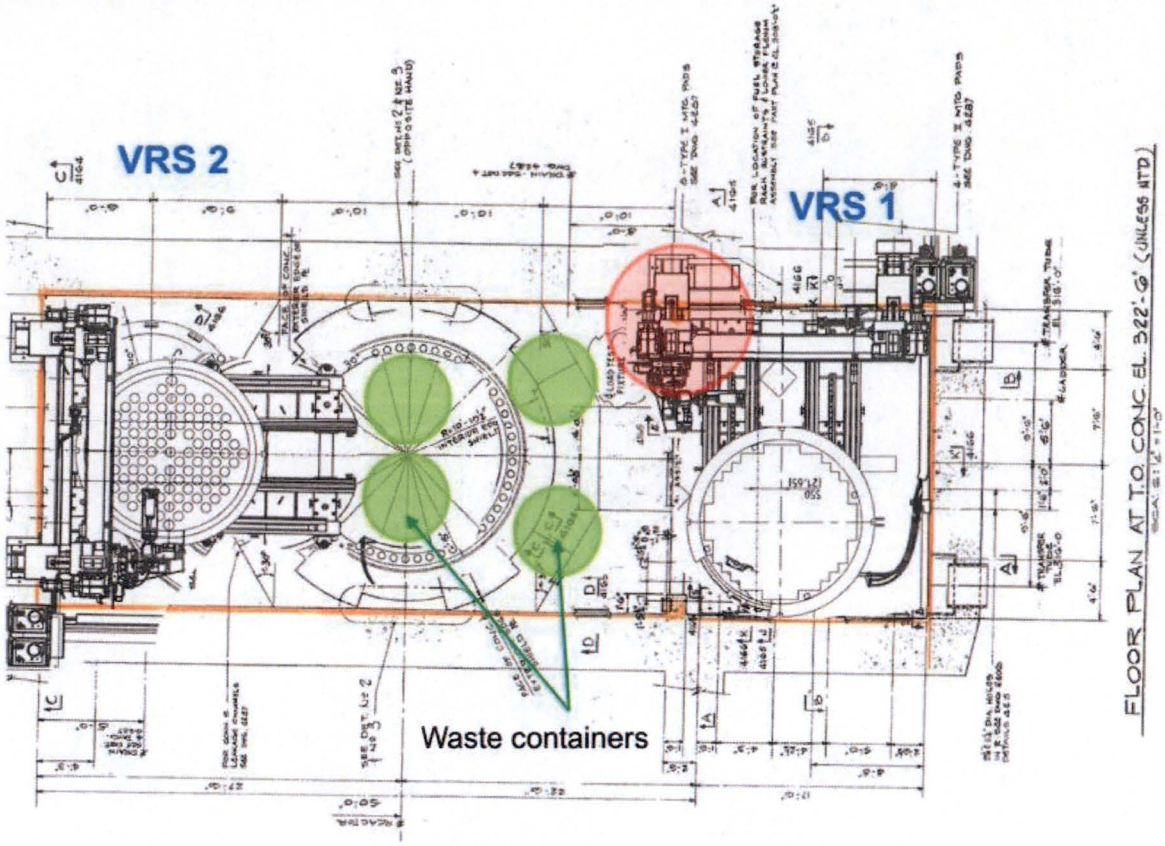

Figure 3-2. Volume Reduction Stations and Work Zone

Core components removed from their in-situ location are moved to a VRS for size reduction, then transferred to the Work Zone for loading into a WBL. Finally, the liners are transferred to be loaded into a TSC. This flow is shown in Figure 3-3.

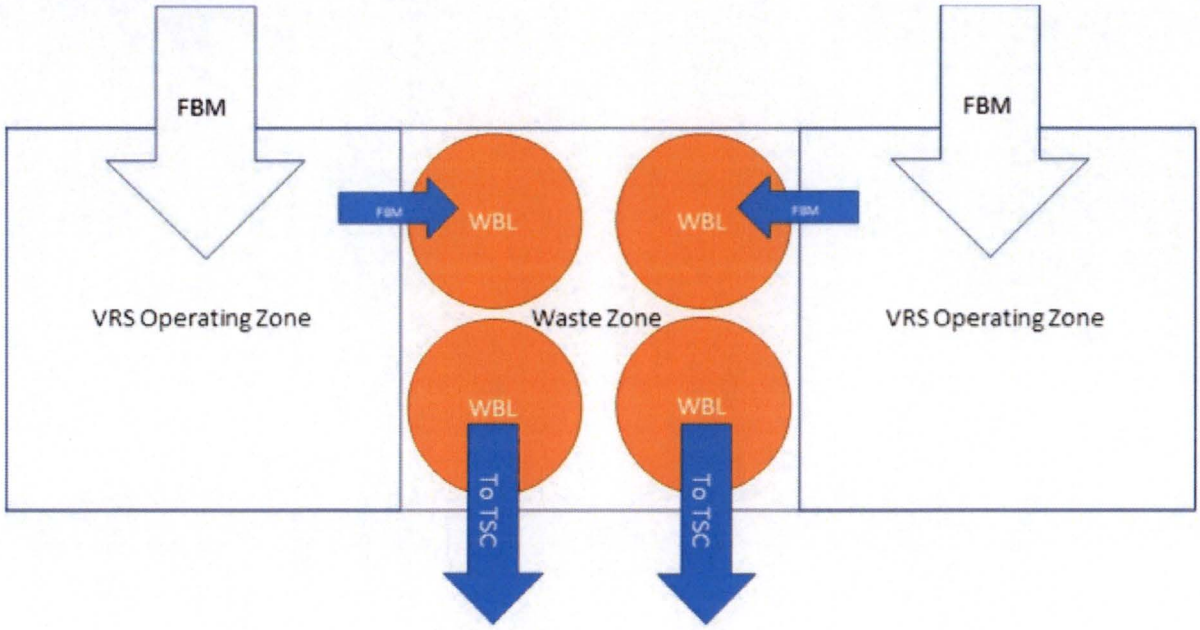

Figure 3-3. Fissile Bearing Material Flow within the Working Area

Prior to the removal of any RV components, the RV and reactor cavity are flooded with water. The types of components to be removed from the RV include core barrel remnants, the thermal shield, and the lower core support plate remnants. After removal of the main components, instrument nozzles and penetrations are cut and moved to the working area (reactor cavity) for loading into the transportation containers. All remaining debris material in the RV following removal of the main components and cut pieces is vacuumed or cleaned up by other mechanical means (e.g., scoops, jaw-type tools).

These components are associated with adhered and non-adhered (i.e., loose) debris material. The three types of debris material (also called damaged core material) associated with the TMI-2 core debris are:

- Type-1 Core Debris – Loose debris consisting of finely-divided, small particle size material;
- Type-2 Core Debris – Surface films consisting of thin films of debris material of varying depth on systems, structures, and components, and;
- Type-3 Core Debris – Re-solidified material and fuel assembly artifacts (average density of 7.1 g/cm^3)

Components with tightly adhered debris material are cut up to fit into open design liner (WBL)/canisters (TSCs) that are compatible with the existing Dry Cask Storage System. Loose debris material chips, and fine granular material are scooped or vacuumed and captured in filter cans that are loaded into TSCs that are also compatible with the existing Dry Cask Storage System. The weight limit for the TSC is 55,000 lbs and they are expected to be loaded to approximately 95% efficiency for a waste weight of 52,250 lbs. Once the debris material is

loaded into the TSCs, the remaining packaging process is identical to a conventional spent nuclear fuel assembly dry storage campaign.

As the components and associated debris are removed, they are moved to the VRS for segmentation and then the Work Zone for loading into a WBL/TSC. Fourteen (14) TSCs are anticipated to be used during the entire operation and multiple are available to receive segmented debris at any one time, which are loaded based on packaging efficiency and/or debris type. Following segmentation, any recovered Type-1 and Type-3 materials from that area during cleanup are loaded into a separate TSC intended for fines and chips collection.

Following cleaning of the RV, the Type-1 and Type-3 debris material in the Once Through Steam Generators is cleaned out and moved to the dry area of the reactor cavity for loading into the TSCs. Lastly, there is also the Auxiliary/Fuel Handing Building with an estimated 11.5 kg of debris material. This material is also moved to the reactor cavity and loaded into the WBL/TSCs.

Only one TSC is removed at a time by placing it into the Dry Storage Canister located inside the Transfer Shield. Once all TSCs are loaded and removed from the reactor cavity, the RV is drained of the remaining water. Loaded TSCs inserted into the Dry Storage Canister are moved from the loading location to a handling facility. Here, the Dry Storage Canister lid is welded on, the Canister is vacuumed dried and backfilled with inert cover gas.

3.2. Normal Conditions

Under anticipated normal conditions, all the of remaining core debris (i.e., fissile material) consists of the three types listed above in the general locations listed in Table 1-1. The total amount of expected fissile material for the entire decommissioning is estimated to be about 1097 kg of irradiated and subsequently decayed UO_2 (i.e., spent fuel) with, on average, 16 wt.% impurities in the fuel debris. Boron is expected to be in the impurities at an average concentration of 0.11 wt.% of the fuel debris. Borosilicate glass is expected to be present in the lower head of the RV.

The four main areas (RV, RCS, Reactor Building, Auxiliary/Fuel Handling Building) are distinctly different and physically separated within the reactor building. Each area (e.g., RV) has specific reactor components (e.g., lower grid assembly [LGA]) or areas made up of components (e.g., the plenum) with an estimated mass. These estimates can be used to visualize a high level packaging plan with some degree of certainty. Some components do not have estimates for the mass or volume so the Canister estimates in the high level packaging plan have relatively high uncertainty.

The segmentation and loading of TSCs occurs in the reactor cavity (canal) where material is transported to after it is removed from its current location. For the majority of component segmentation, it will occur under water in a flooded reactor cavity. Some segmentation (like the OTSG components) may not occur under water and may be on a concrete platform. Additionally, some components may be set on concrete at some time during the operations. For this reason, the reactivity addition from a tight fitting concrete reflector is examined.

Material and component removal from each area is treated as a separate operation, meaning that debris from two areas is not removed at the same time; however, a partially filled TSC from one area may remain for loading from the next facility area if there is remaining void space. Estimates for the number of TSCs for each area based on estimated weight and packing efficiency are provided in Table 3-1.

Table 3-1. Canister Estimates from High Level Cutting and Packaging Plan

Component/Area	Estimated TSCs	Note
LGA, Core Support Assembly (CSA)	3.95 (4)	Assuming payload packing efficiency of 95%. LGA and CSA are majority of Plenum.
Remaining plenum	2.07 (3)	Remainder of 3rd canister may be filled with excess LGA and CSA.
Flow Distributor and ICI Guide Tubes	1	In the "A" D-ring
OTSG	3	
Chip collection	2	Approximately 6,000 lbs
Auxiliary and Fuel Handling Building	1	
Total	**14**	

The design inputs, and specifically reference information, provided in Section 4 and detailed in TMI2-EN-RPT-0003, *Safe Fuel Mass Limit Computational Input Consensus* (Ref. [1]) serves as the basis to develop inputs to the computational models to develop the SFML. The values for input parameters include varied uncertainties: those that are well understood/accepted, those that have some uncertainty, and those that have larger uncertainties. The parameters include ^{235}U enrichment, impurity content, fuel debris composition, UO_2 density, etc. For several input parameters, the selected value is credibly bounding.

Development of the SFML includes optimization of parameters for maximum moderation, reflection and interaction conditions in a bounding geometry (sphere). Using a sphere as the material geometry for SFML minimizes the surface area to volume ratio and does not require taking credit for the distribution of the fuel debris.

4. INPUTS

Over the years since samples were retrieved at TMI-2 and analyzed at various laboratories, substantial effort has been put into using those results to inform operational decontamination and decommissioning (D&D) decisions, validate accident computer codes, estimate fission product release, and understand the nature of the TMI-2 accident. The majority of that work was used for duefueling operations, which occurred in the late 1980s. For the purposes of deriving a SFML for intended D&D operations, the sample results biased toward the bulk of the remaining material are used to develop compuatational input parameters.

The input parameters for consensus include core debris composition (i.e., impurities concentration), fuel enrichment, fuel density, fuel burn-up and resulting composition, fuel pellet geometry, and modeling geometry, including moderation and reflection conditions. Discussion of each of these parameters is provided in TMI2-EN-RPT-0003 (Ref. [1]). Those that rely on historic references (primarily impurities content from sampling and debris composition) are summarized here.

4.1. Design Inputs

Inputs to the design of the SFML come from a combination of historical documents, reactor operation history, previous decommissioning operations, and planned future decommissioning operations. Planned future decommissioning operations, which support the criticality not credible argument for application of the SFML, are laid out in Section 3. The pertinent design input information that feeds into the calculation is further discussed in this section. Inputs that are adjusted as part of the parametric study associated with this calculation (i.e., geometry, enrichment) are in Section 5.

A graded approach is used to apply the design input information to the development of the SFML, which depends on the strength of the basis of that information. For example, known natural phenomena, such as radioactive decay, are applied more assertively than a parameter with less assurance (e.g., exact impurity content) which is applied more judiciously.

4.2. Sampling and Impurities

Samples were retrieved from multiple locations including the lower head region, the core debris bed, and the B-loop steam generator tube sheet, which are summarized here. Note that for each sample retrieved, it was processed into particles which were then analyzed individually. One sample can have multiple particles of varying sizes and elemental makeup.

4.2.1. Reference Data for Lower Vessel Head

In 1985, prior to defueling, 16 particles of debris from the lower reactor vessel (i.e., lower head) were obtained through the annulus. Although the analyses were performed prior to defueling, most of the remaining material is in the same region as the analyzed samples. The samples were intended to be both representative of the region "typical material" and a material that "looked different." The data indicate that the composition of the debris is similar to what would be expected if the principal components of the original core were mixed, melted, and a fraction subsequently relocated to the lower plenum of the reactor. The general appearance of the lower plenum debris and the microstructure of the samples indicate that they were once molten. The particles of pure UO_2 have changes in porosity that indicate it may have been near the melting point (GEND-INF-084, *Examination of the Debris from the Lower Head of the TMI-2 Reactor* Ref. [13]).

Boron was found in measurable concentrations ranging from 0.066 wt.% to 0.36 wt.% on average per debris sample. Gadolinium poison was not readily identifiable in the lower head debris but was more prevalent in the core debris bed. The structural material element with the

highest concentrations in the lower head was iron, ranging from 1.8 to 3.7 wt.% average per debris sample.

For additional summary information on the sample analyses, refer to TMI2-EN-RPT-0003 (Ref. [1]), and for the original analytical information refer to GEND-INF-0084, *Examination of Debris from the Lower Head of the TMI-2 Reactor* (Ref. [13]).

4.2.2. Reference Data for Core Debris Bed

A substantial amount of core debris bed was removed during defueling in the late 1980s. Prior to the defueling, a sampling of core debris from the center and radius was performed in 1983-1984, removing material from three depths: surface of the rubble bed, 3 inches deep into the bed, and 22 inches deep into the bed. A summary of the results is provided below. For reference, the as-built TMI-2 active core region contained about 94.5 wt.% UO_2 + Zr-4 and approximately 2.3 wt.% stainless steel + Inconel. The U/Zr ratio for the active core region was about 3.6.

- The average, normalized, U content was 82.6 wt.%, Zr content was 13.9 wt.%, Fe content was 2.7 wt.%, and Ni content was 0.9 wt.%. The U/Zr ratio was higher than as-built (~5.9) and the Ni, Cr, and Fe was about 1.3 wt.% higher than as-built.
- The degree of mixing and relocation suggests that molten core materials mixed vigorously to produce the degree of homogeneity observed.
- Original as-built uraniuim enrichment for specific fuel assemblies had no correlation to sample results, indicating significant physical relocation of the fuel.

4.2.3. Reference Data for Steam Generator Tube Sheet

Examination of loose core debris from the B-loop steam generator upper tube sheet was part of a fission product inventory evaluation and also provided insight into the deposition of core material outside the reactor vessel. The sample appeared similar to the sample below the surface of the core debris bed, and some of the particles in the lower plenum.

The sample particles were reaction products consisting primarily of U and Zr oxides. Fe, Ni, and Cr were trace elements within the matrix. Two of the 12 particles indicated control rod origen (i.e., Ag, In, and Cd).

4.3. Fuel Debris Composition

References [13], [14], and [15] analytically estimate the peak and sustained temperatures in the core in order to better estimate fission product release and fuel composition. It is estimated that about 20% of the core material in the debris bed experienced temperatures up to fuel melting. The lower plenum material could have attained temperatures of at least 2810 K.

The only historical report that provides the explicit burned composition of the fuel (UO_2 component of the debris) is the 1989 *Criticality Safety Evaluation for Increasing the SFML* (Ref. [16]), which is provided as an attachment to the Defueling Completion Report (Ref. [3]). This composition accounts for burnup effects in all three fuel batches but no melted and comingled cladding or structural material (i.e., impurities) as described above. Comparisons of the

calculated fission product composition with the analytical data indicated, at that time, that the calculational results were appropriate (Ref. [13]).

In each batch, the effects of uranium depletion, fissionable plutonium generation, and rare earth fission product production are considered. The base fuel composition input previously used is provided in Table 4-1. However, because this composition was derived 30-plus years ago, as part of this calculation, it is computationally decayed to the year 2022. The new composition is discussed in Section 6.3.1 as an input to this calculation.

Table 4-1. Burned Fuel Composition (Ref. [16])

Isotope	Number Density (atoms/barn-cm)
^{235}U	5.21E-4
^{238}U	2.25E-2
^{16}O	4.60E-2
^{239}Pu	4.01E-5
^{240}Pu	2.00E-6
^{241}Pu	2.49E-7
^{149}Sm	1.01E-7
^{151}Sm	1.79E-7
^{151}Eu	8.20E-9
^{153}Eu	1.32E-7
^{154}Eu	4.51E-9
^{155}Eu	6.12E-9

4.4. Reference Data Summary

For the purposes of calculating a final SFML, general conclusions can be drawn from the abundance of analytical sample information, particularly that available for the lower head of the reactor vessel.

- The previously derived fuel composition was adequate as a reference composition for burn-up of the original TMI-2 fuel. This composition serves as a starting point to decay each isotope to the year 2022 in order to develop a current fuel composition.
- Impurities, whether from cladding, structural material, or control rods, exist throughout the TMI-2 core. Control rod material was not as commonly found in remaining core debris as structural material.
- The U/Zr compositions in the core are indicative of mixing of all core constituents.
- Boron is evenly distributed throughout sample particles at the same concentration as in the reactor coolant, although it is not known if the elemental boron originated in the coolant or poison rods.
- Gadolinium is distributed among the debris bed material at similar concentrations to the original burnable poison rod loading, indicating vast mixing. Gadolinium was not readily

identified in the lower head or steam generator tube sheet as it was heavily concentrated in the core crusts.

- Most of the control rod material accumulated in the core debris bed or elsewhere, not in the lower head region.
- Temperatures during the accident reached levels to initiate and propagate core melting, peaking at greater than 2800 K. There are few examples of pure UO_2, indicating isolated temperatures greater than 3100 K.
- Mixing of different assemblies' enrichment has occurred, and little or none of the 2.96 wt.% $^{235}U/U$ is contained in the lower head region. The average enrichment of the 34 samples collected in the lower head is 2.23 wt.% $^{235}U/U$.
- Core debris density ranges from about 6 g/cm^3 to less than 9 g/cm^3.

5. CALCULATIONS

5.1. Model Geometry Description

A single criticality model was developed using bounding and anticipated configurations of the remaining spent fuel. A spherical configuration of all remaining spent fuel was filled with a lattice of fuel and moderator. When impurities are included, they are modeled as part of each fuel region. A hexagonal lattice was selected because of the ability to closely pack the fuel elements. Each spherical fuel element is surrounded by water on all sides. The size of the fuel element and spacing between each fuel element (i.e., the H/U ratio) is modified for each base arrangement in order to optimize reactivity in each study. The optimum configuration of fuel and moderator (i.e., H/U ratio) is dependent on multiple parameters and can change with the addition of absorbers to either the fuel or moderator. This adjustment has no physical basis. It is merely a means to maximize the fuel/water intereaction and is bounding of any credible configuration of the material. The base arrangements optimized for further analysis are:

- Sphere with lattice of fuel debris with impurities; pure water moderator and reflector;
- Sphere with lattice of fuel debris; poisoned water moderator and pure water reflector;
- Sphere with lattice of fuel debris with impurities; poisoned water moderator and pure water reflector.

For comparison, a sphere with lattice of fuel debris (no impurities) and pure water as a reflector (no poison) and moderator is also included.

The spherical model assumes all modeled fuel and moderator is in a spherical configuration, surrounded by a close-fitting essentially infinite water reflector. The moderator to fuel ratio is optimized in each base case to achieve the highest reactivity prior to further perturbations on model parameters (e.g., fuel mass). This optimization is done by altering the pitch of the lattice for each unit cell. A graphical depiction of the cross-sectional unit cell lattice is provided in Figure 5-1. The blue area represents the fuel pellet and the red represents the moderator. The hexagonal region surrounding each cell is not a physical attribute but only a computational cell place-holder.

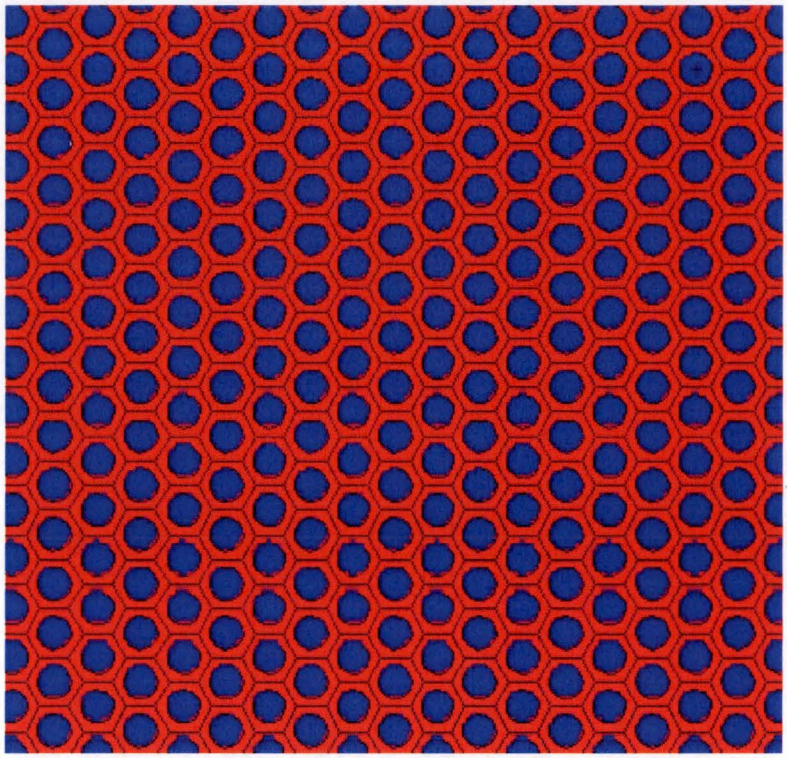

Figure 5-1. Cross Section of Fuel Region Lattice

A graphical depiction of the cross section of the spherical model is provided in Figure 5-2. The interior shaded region is the fuel region lattice and the surrounding red is the effectively infinite reflector.

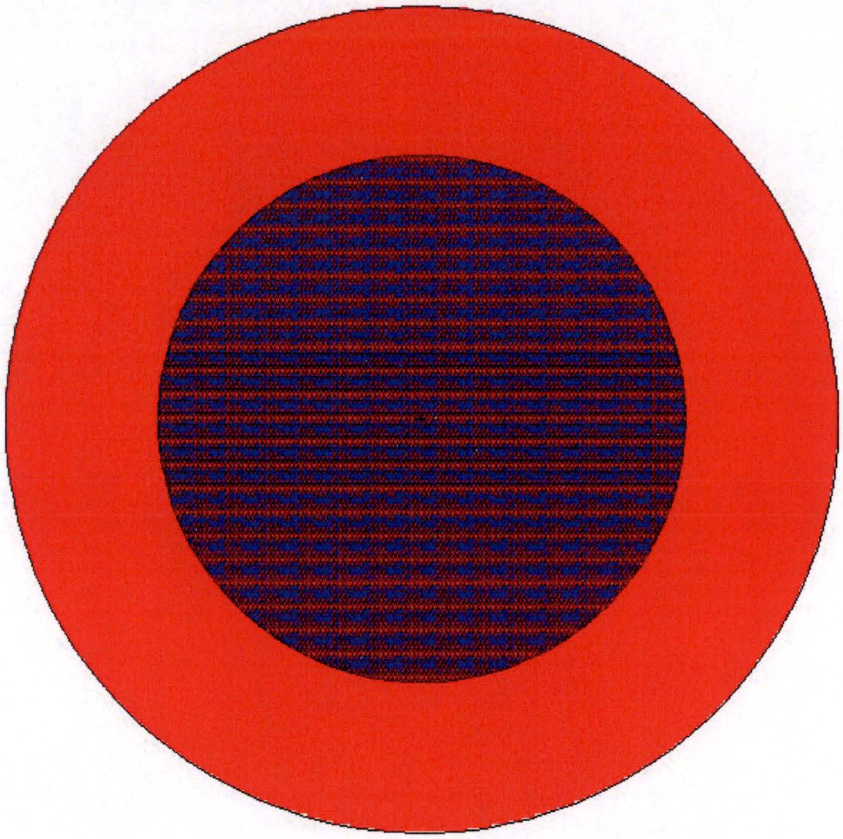

Figure 5-2. Cross Section of Spherical Full Core Model

For each optimized configuration, the total uranium mass, percentage of impurities, and concentration of boron in the water were varied. Sensitivity to a lowered UO_2 density and concrete reflector were also examined on the most limiting configurations. The effect of a lowered UO_2 density was within the margin of error and had little effect of k_{eff}. In all examined cases, the higher UO_2 density was bounding. A concrete reflector is slightly more reactive than the equivalent thickness water reflector. This sensitivity is discussed as an upset condtion in Section 5.4.6.

The range of parameters studied for the spherical configuration are provided in Table 5-1. Parameters such as fuel pellet radius, unit cell separation, and UO_2 density were used as part of scoping calculations to identify an optimum configuration. Once that optimum configuration was identified, uranium mass, impurity weight fraction, boron concentration, and reflector material were adjusted for the reported results. Note that 30 cm of reflection is effectively infinite.

Table 5-1. Parameters and Ranges Examined

Parameter	Range
Uranium Mass	925 kg – 1750 kg
Reflector Thickness	30 cm
Reflector Material	Water, Concrete
Impurity Weight Fraction	5% – 16.21%
Boron Impurity Percentage	10% – 100%
Iron Percentage	90%
UO_2 Density	10.55 – 10.97 g/cm^3
Fuel Pellet Radius	0.2 cm – 0.6 cm
Unit Cell Separation	0.2 cm – 0.4 cm

5.2. Model Assumptions

Because the distribution of the fuel within the RV is unknown, the SFML is derived through bounding assumptions intended to cover any credible upset conditions. The geometric configuration of the fuel is bounding in the heterogeneous spherical model. Because this is low enriched fuel, it is more reactive in a heterogeneous configuration than as a homogeneous model. This was also demonstrated in scoping calculations (NSTS-ES-01 Ref. [17]). A heterogeneous annular model was studied previously and shown to be less reactive than the heterogeneous spherical model (NSTS-ES-01 Ref. [17]). The fuel pellet is spherical, the moderation is optimized, and the fuel region is spherical. This represents a worst-case configuration for the fissile material. Additionally:

- The fuel pellet volume is assumed to be close to that of a standard sized fuel pellet; although a sphere and in a hexagonal lattice;
- Impurities are added as a uniform, homogeneous mix within the fuel sphere;
- The fuel is represented as TMI-2 average fuel (i.e., a homogeneous mixture of the three fuel batches), as discussed in Section 6.3.1;
- An effectively infinite reflector is assumed;
- No credit is taken for existing structural or solid poison materials (e.g., borosilicate glass);
- Only limited credit is taken for the presence of fission product poisons.

5.3. Material Descriptions

5.3.1. Fissile Material

The fissile material is represented as a homogeneous medium assumed as TMI-2 average fuel. The homogeneous medium is a mixture of the three known fuel batches and this is considered conservative because defueling data indicates that most of the batch 3 fuel (at least ~65%), with the highest initial enrichment of 2.96 wt.% has been removed from the RV. Consequently, any

remaining fuel is expected to consist primarily of batch 1 and 2 fuel with 1.98 wt.% and 2.64 wt.% enrichment, respectively.

The composition of the UO_2 component[1] is derived by starting with the composition supplied in the Defueling Completion Report SFML calculation attachment (Ref. [3], Table 5-8). This composition accounts for burnup effects in all three fuel batches through application of a conservative approach to burnup credit. In each batch, the effects of uranium depletion, fissionable plutonium generation, and rare earth fission product production are considered. The gaseous fission products were assumed to be released at the time of the accident and the soluble ones were assumed to have leached out of the fuel matrix. Of the remaining non-soluble fission products, some become volatile under extremely high fuel temperatures and the formation of a zircaloy-fuel eutectic and, thus, were assumed not to remain within the fuel matrix. Of the non-soluble fission products, only the rare earths were considered to be stable under TMI-2 accident conditions. The validity of the presence of rare earth elements, which serve as significant neutron poisons, is discussed extensively in Appendix B of Reference [18] (*Reactor Coolant System Criticality Report).*

The unburned fuel enrichments for the three batches were 1.98 wt.% (56 assemblies), 2.96 wt.% (60 assemblies) and 2.64 wt.% (61 assemblies) $^{235}U/U$. As a homogeneous mixture, the unburned overall enrichment was 2.54 wt.% (Ref. [3]). The TMI-2 fuel experienced the equivalent of approximately 94 effective full-power days of burnup at the time of the accident (Ref. [18]). The actual exposure history for each fuel batch, using existing plant data, was applied to calculate burnup effects. The exposures and core operating history were applied to the ORIGEN-S model to calculate isotopic inventory at the time of the accident. The incorporation of the burnup effects for each fuel batch was used to produce a net ^{235}U enrichment of 2.24% for a homogeneous mixture of the three batches (Ref. [19]). This is in good agreement with samples retrieved from the bottom head with an average enrichment of 2.23 wt.% $^{235}U/U$ (Ref. [20]).

The starting fuel composition is decayed using ORIGEN to the year 2022. Those nuclides that do not have available nuclear data in the ENDF-B/VIII library are not included. Almost all of the neglected nuclides have decayed weight fractions less than 10^{-15}. Attachment B lists the starting fuel composition (Table 9-1) and the decayed composition (Table 9-2) used in the simulations. The neglected components are highlighted.

Nuclides that decreased in the decayed composition are ^{151}Sm, ^{241}Pu, ^{151}Eu, ^{154}Eu, and ^{155}Eu. The largest decrease is in ^{154}Eu and ^{155}Eu. An energy dependent cross section plot for these nuclides can be found in Figure 9-1 in Attachment B. The decrease (decay) in these two europium isotopes has resulted in an increased reactivity. Nuclides that increased in the decayed composition, originally from zero, to be above 1×10^{-7} are ^{241}Am, ^{234}U, and ^{155}Gd; however, they are still pretty low in abundance ($\sim1\times10^{-6}$). A cross section comparison for these nuclides can be found in Figure 9-2 in Attachment B. Based on the abundance of these nuclides and their cross section data, it is expected and confirmed through scoping that the decayed fuel composition is

1. The burnup and decay of UO_2 includes various isotopes other than uranium and oxygen. The table of impurities considers this component as 'fuel composition'.

slightly more reactive than the original burn-up composition. This would present a more conservative fuel composition for the SFML calculation.

Full theoretical density (10.97 g/cm^3), as well as a reduced density (10.55 g/cm^3) based on burn-up history (Ref. [21]), and an as-built density of 92.5% of the theoretical density (10.14 g/cm^3) (Ref. [14]) are all used in the scoping calculations; however, the effect on reactivity is minimal. The relative density as a function of burn-up is expressed as:

$$\frac{\rho}{\rho_{th}} = 0.963 - 1 \cdot 10^{-4} \cdot (burnup)^{3/2}$$

5.3.2. Impurities

All samples of TMI-2 debris accumulations collected have shown that debris contains impurities, whether those be from structural material, control rods, burnable poison rods, coolant poison, or cladding. In many cases, impurities from each category were present in the sample. These are considered long-term impurities of the debris, not surface contaminants. A summary of previous analyses is in Section 4 with additional details in Reference [1]. Substantial fuel, control rod, and structural material mixing to create some degree of homogeneity was shown to have occurred during the TMI-2 accident. Additional justification of this from supporting documentation is also provided in Reference [1].

Core debris in the lower head region of the RV is most representative of what remains in the RV at the present time. For this reason, the impurity concentration is derived from the sampling results for the lower head of the RV. A composition representing the RV lower head was initially derived as 'Mix 3' in the *Defueling Completion Report* (Ref. [3], Table 5-11). In this mix, the fuel composition (UO_2+fission products) makes up 83.79 wt.% of the core debris while the remainder (16.21 wt.%) is impurities. The debris composition with impurities is listed in Table 5-2. Homogenization of the impurity content of the RV lower head in the modeled fuel mixture represents a significant conservatism over what would be derived assuming a homogeneous mixture of the initial core composition, where the UO_2 component is 65.8 wt.% of the TMI-2 core mass (Ref. [22]).

Table 5-2. Impurity Content of Core Debris ('Mix 3')

Component	Weight Percent (%)
Fuel Composition	83.79
Zr	12.70
Fe	2.44
B	0.11
Cd	0.00
Cr	0.75
Mo	0.15
Mn	0.06

The impurity composition within the core debris is varied in the analysis from 0% to 16.21 wt.%. In addition, iron content is fixed at 90% of the relative impurity mixture and boron content is varied independently since the greatest reactivity worth comes from these constituents. This allows the SFML result to not rely on full credit from boron or iron impurities. Calculation of the modeled weight fraction of boron is performed using the following relationship, where B_{mult} is the element's (e.g., boron's) multiplier. The same is done for iron where B_{mult} is replaced with 0.9.

$$B_{modeled} = \frac{Imp\ wf}{core\ debris} \cdot \frac{B_{Mix3}}{Imp\ wf} \cdot B_{mult}$$

The overall fuel debris boron concentration for each multiplier is shown in Table 5-3 for all impurity fractions used. The values shown are weight percent of boron in total fuel debris.

Table 5-3. Overall Boron Concentration in Fuel Debris

B_{mult}	Impurity Fraction (wt.%)			
	5	10	15	16.21
0	0	0	0	0
0.2	0.0068	0.014	0.020	0.022
0.3	0.010	0.020	0.031	0.033
0.5	0.017	0.034	0.051	0.055
0.8	0.027	0.054	0.082	0.088
1	0.034	0.068	0.10	0.11

5.4. Results

Note that calculation results in this section are generally in the form of total uranium, not total UO_2.

5.4.1. Optimum Conditions

An optimum moderation search is performed by adjusting the fuel pellet diameter and lattice pitch (i.e., H/U ratio). Once the most reactive arrangement is identified, that pellet size, pitch and fuel density can be used to examine variations on the total fuel mass, total impurity content, boron concentration, and reflector material.

The fuel pellet radius is varied from 0.2 cm to 0.6 cm, and the pellet separation from 0.1 cm to 0.4 cm in an effort to identify the optimum conditions for maximum reactivity. The fuel volume fraction for randomly packed whole fuel pellets is around 0.63, and a volume fraction of 0.74 corresponds to the maximum that can be achieved for spheres in contact in a hexagonal lattice. A pellet radius of 0.6 cm with a separation of 0.1 cm results in a fuel volume fraction of

approximately 0.634, slightly higher than that for randomly packed spherical pellets. A pellet radius of 0.6 cm with a separation of 0.4 cm results in a fuel volume fraction of 0.34. As the pellet size and separation distance (i.e., unit cell pitch) are varied, the optimum moderation can be found. Since the fuel is low enriched, moderation is necessary to achieve criticality. A higher fuel volume fraction (i.e., less moderator present) in each modeled unit cell results in a reduced reactivity. For this reason, the pellet radius and pitch are not varied beyond these specified values. It is recognized that fuel pellet sizes larger than 1.2 cm may exist due to fuel melting. However, sample data have shown, and temperature-dependent phenomena indicate that particles of pure UO_2 are highly unlikely.

The optimum UO_2 density for all cases is 10.97 g/cm^3.

A graphic depiction of the change in k_{eff} for varying fuel/moderator ratios at 1200 kg U is provided in Figure 5-3. The maximum k_{eff} for the system with minimal impurities occurs around ~1.5. There are multiple fuel radius and pitch values that can produce the same ratio (e.g., 0.4 cm radius; 0.2 cm pitch and 0.6 cm radius; 0.3 cm pitch both have a ratio of 2) with slightly different k_{eff}.

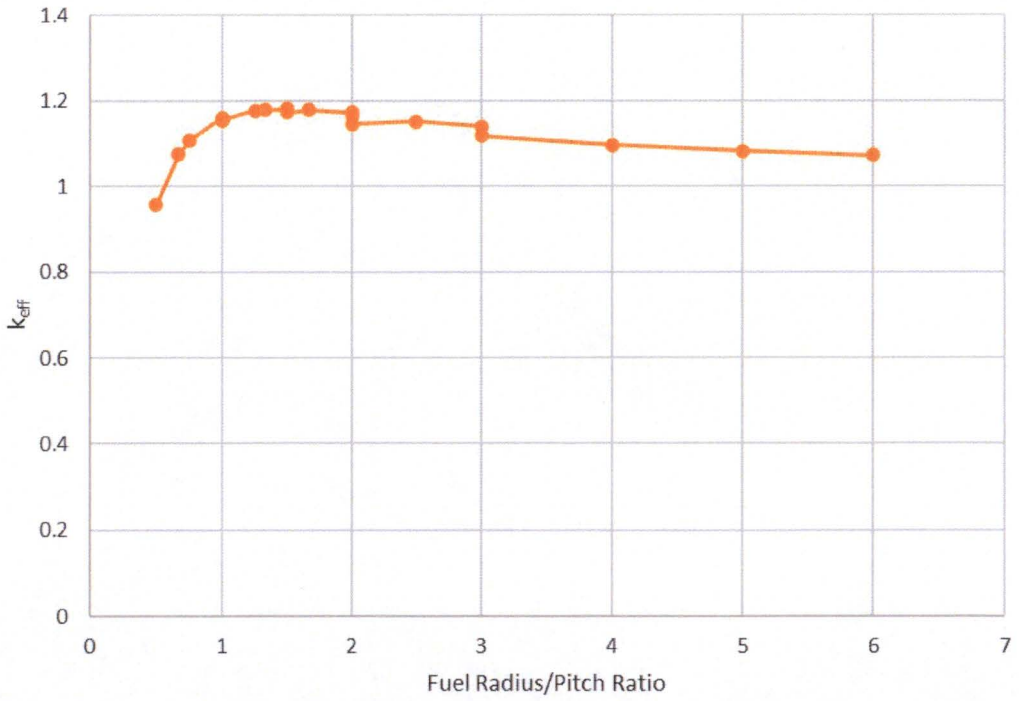

Figure 5-3. Variation in Reproduction Factor as a Function of Fuel-to-Water Volume Ratio and Boron Content

5.4.2. Impurity Content

The weight fraction of the 'Mix 3' impurity applied homogeneously to the fuel composition has a significant effect on the neutron multiplication factor. Although the impurity mix has multiple

constituents, in reality made up from the melting and mixing of structural components and control rods, the boron has the highest neutron absorption cross section for the energy region of interest and therefore the greatest reactivity worth.

To show the effect of overall impurity concentration in the fuel debris on k_{eff}, the uranium mass is fixed at 1200 kg. The boron concentration is adjusted by a multipler on the value provided in 'Mix 3' (i.e., 30% is a 70% reduction). Figure 5-4 displays the negative reactivity worth with each small addition of boron. For 15 and 16.21 wt.% impurity content, 20% of the boron impurity is worth approximately -15.07% Δk/k. In other words, -0.75% Δk/k on average for each 1% addition of boron in the fuel mix. The positive and negative reactivity worth is reported in comparison to the k_{eff} with no boron impurity rather than from unity since deviation from a purely critical state is not part of this study. As the boron impurity increases, it's negative reactivity worth decreases with each addition. This is apparent by looking at the slope of the curve near the 100% multiplier. Over the entire range of boron multipliers, the average worth is -0.48% Δk/k for each 1% addition. For 5 wt.% impurity content, 20% of the boron impurity is worth approximately -5.52% Δk/k. In this case, there is an added 0.27% Δk/k of negative reactivity on average for each 1% addition of boron in the fuel mix. For 10 wt.% impurity content, 20% of the boron impurity is worth -11.4% Δk/k, or -0.57% Δk/k for each 1% addition. As expected, as the impurity weight percent increases, boron has a more significant impact on k_{eff}.

The reactivity worth of boron in the impurities is similar for the range of uranium loadings examined (925 kg – 1750 kg U) but has a slightly higher worth at lower fissile loadings. Note that in all these results, only 90% of the iron is credited.

For a 1200 kg U fuel loading, if 15 wt.% or more of the total impurity content is credited, at least 28% of the boron also has to be credited in order to stay below the USL. If 10 wt.% of the impurities is credited, at least 47% of the boron content must be credited to stay below the USL. With a boron multiplier of 1 (100%), the boron is 0.11 wt.% of the fuel debris (see Table 5-2 and Table 5-3). With a boron multiplier of 0.47, the boron concentration is 0.0517 wt.% of the fuel debris. Using an impurity content of 10 wt.% and boron multiplier of 0.47, the overall boron impurity in the fuel debris required to stay below the USL is a minimum of 0.0319 wt.%.

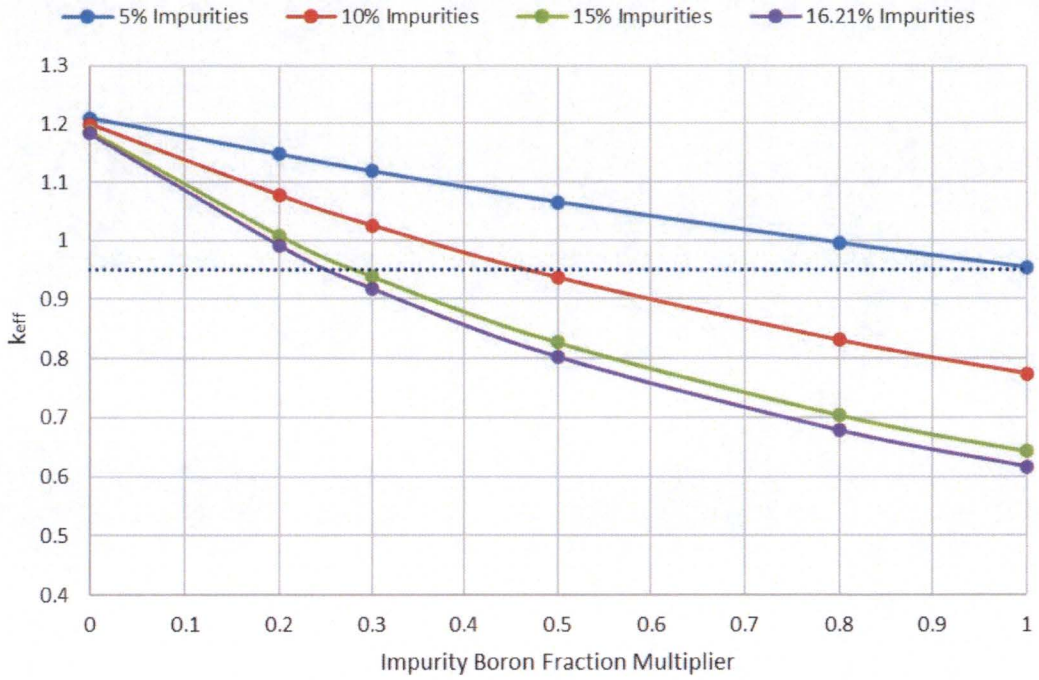

Figure 5-4. Variation in Reproduction Factor for Each Impurity Concentration as a Function of Impurity Boron Content

5.4.3. Reflector Material Sensitivity

The tight fitting (i.e., effectively infinite) water reflector is used in the reported results in this section. The water is replaced with concrete to test the sensitivity of this parameter since concrete is present in the TMI-2 facility and it is possible that decommissioning operations will expose components to it. It is not considered credible that a tight fitting concrete reflector could be realized during decommissioning operations.

Comparison of the neutron multiplication factor for a uranium loading ranging from 925 kg to 1500 kg for 10 wt.% impurities and 50% boron impurity multiplier at optimum moderation for both a water and concrete reflector is provided in Table 5-4. The tight fitting concrete reflector provides approximately +0.0065 $\Delta k/k$ at 1200 kg uranium loading.

Table 5-4. Sensitivity of Reproduction Factor to Concrete Reflector

Reflector	U mass (kg)	$k_{eff} + 2\sigma$
Water	925	0.9235
	1125	0.9334
	1200	0.9365
	1500	0.9465
Concrete	925	0.9313
	1125	0.9401
	1200	0.9427
	1500	0.9519

5.4.4. Summary of Results

These results indicate that the entire remaining amount of uranium in the TMI-2 facility with some margin can be safely handled for decommissioning operations by taking credit for some impurity content. This analysis optimized moderation, fuel density, pellet size, and fuel configuration while taking partial credit, yet still applying conservative assumptions for fuel burn-up, fission products and decay, enrichment, impurity weight fraction and boron and iron content in the fuel debris. It is feasible to apply a SFML of 1200 kg U (1361 kg UO_2) with a $k_{eff} + 2\sigma < 0.95$ through taking credit for 10 wt.% of the impurities, 50% of the sampled boron content of those impurities, and 90% of the iron content of 'Mix 3' ($k_{eff} + 2\sigma = 0.9365$). This equates to 0.034 wt.% of boron in the fuel debris and 1.51 wt.% of iron. Only 31% of the reported boron content and 62% of the reported iron content of the fuel debris (for the lower head RV sample results) is credited in a 1200 kg U SFML. With an estimated remaining core debris inventory of 1097 kg UO_2, of which 90+% is in the RV, this SFML bounds all operations and credible upsets, including concrete reflection, and allows some margin for inventory and impurity uncertainty.

6. UPSET CONDITIONS

There are upset conditions associated with both the expected inventory of total uranium and its associated characteristics, and the decommissioning operations. Some upsets on the input parameters would require gross errors in historical information in addition to the absence of understood phenomena (i.e., nuclear fuel burn-up). Supporting information is provided both in this document and in reference documents on the assertion that anticipated phenomena has occurred and lead to the current conditions. One example of this is evidence of vast mixing of core components during the accident, which leads to impurity content in the fuel debris.

Upset conditions associated with decommissioning operations may include mishandling of components with fissile material to increase moderation, reflection conditions, or interaction conditions. This could potentially occur through removal and accumulation of fissile-bearing components from multiple areas into a single location. Given the size and complexity of the reactor components, and the effort required to remove and move each component, it is at least unlikely that a "pile" of reactor components can develop. Even if such a pile were to develop, the

fissile material is at least partially adhered to structural members such that it's accumulation into a favorable geometry, either under water or not under water is not credible. Water (or gravity) serves to disperse and move any loose uranium thereby aiding in prevention of an ideal formation.

Components removed from their in-situ location are transferred to one of the VRS locations, which is located on the opposite end of the canal from the other VRS. It is not credible that components in one VRS can interact with components in the other VRS given the vast separation distance. Following segmentation, the pieces are moved to the Waste Zone for loading into the WBL and transfer to the TSC. It is possible that pieces that do not fit in the WBL may be placed aside. It is not credible that the segments placed aside could assemble into an ideal configuration with no structural components present. However, even if this were to occur, it would require gross errors in impurity content to erode the safety margin provided by these inherent characteristics of the fuel debris.

Development of the SFML includes optimization of parameters for maximum moderation, reflection and interaction conditions in a bounding geometry. Although the RV canal is flooded with water and a water reflector is considered as the material for all reported calculations, a tight fitting concrete reflector is also examined (see Section 5.4.3) and shown to only slightly increase the reactivity. The slight increase in reactivity offered by a tight fitting concrete reflector bounds any added reactivity from concrete walls or slab during decommissioning operations. There is sufficient margin between the base case reproduction factor and the USL to allow tight-fitting, effectively infinite concrete reflection, which is not considered a credible condition.

The derived SFML bounds the entire expected fissile mass inventory throughout all physically separated areas within the reactor building. The largest uncertainty is associated with the RV at ± 370 kg UO_2. The uncertainties on the fuel debris total mass associated with other areas are considered small, as these areas are better characterized (Ref. [4]). Including the maximum uncertainty, the total fuel debris for the RV could be ~1468 kg UO_2. It is not logistically possible for the entire mass of the RV, which is deposited in a large area, to be removed at one time. Nor is it possible for the entire mass associated with the RV to be placed into a single TSC. The nature of segmentation operations separate and reduce the amount of fissile material in a single area and subsequently any TSC. There is estimated to be approximately 170 kg UO_2 outside of the RV. It would require an unreasonable uncertainty associated with the other remaining areas to approach the estimated mass for the RV, and this is not considered credible. It is estimated that approximately 14 TSCs are necessary to pack the reactor components and internals when they are packed efficiently. There is no credible upset that could lead to a fuel debris mass of greater than 1468 kg UO_2 in a single location, nevermind an idealized configuration.

There are uncertainties associated with the impurity content of 'Mix 3' as detailed in TMI2-EN-RPT-0003 (Ref. [1]) as they apply to the fuel debris for the entire facility. The impurities are reduced by approximately 38% from the specification in the Mix 3. The boron content is further reduced by 50% (~31% of the original B concentration remains) and the iron content by 10% (~56% of the original Fe concentration remains). These conservative reductions provide sufficient margin to encompass uncertainties and heterogeneous flucutuations in the remaining fuel debris material. In comparison to the other mixes, the boron concentration is approximately

half that of Mix 4 (Ref. [3], Table 5-11) which is also derived from the sampling in the lower head of the RV. Additionally, the average boron concentration distribution for the OTSG samples was 0.109 wt.% (Ref. [1], Table 3-4), of which the value used in this calculation (0.034 wt.%) is approximately one third of that.

The above discussion demonstrates that it is not credible to expect all of the remaining fuel material to be collocated and for the resulting mass to exceed the determined 1200 kg U (1361 UO_2) SFML. It is further not considered credible that the segmentation operations would result in the fuel material being placed in an optimal physical arrangement that maximizes reactivity. A conservative approach to adequately represent the inherent characteristics of the remaining fuel debris is taken with respect to the development of an SFML for the remaining decommissioning activities. This, coupled with conservatively estimated masses and planned decommissioning operations provides significant and adequate margin of safety to ensure that a criticality is not credible.

7. CONCLUSIONS

The identified SFML to bound all planned TMI-2 decommissioning operations (i.e., normal conditions) and credible operational upsets is 1200 kg uranium or 1361 kg UO_2. This limit credits several key factors:

- 10 wt.% of the impurities identified in 'Mix 3' from the Defueling Completion Report, which is considered representative of the debris that remains in the RV;
- Boron and iron are further reduced by 50% and 10%, respectively, in the 10 wt.% impurity fraction identified in 'Mix 3'; and
- Actual exposure histories applied to the average enrichment for all three batches of original TMI-2 fuel (burn-up credit).

And applies multiple conservatisms:

- A decayed fuel composition to the year 2022 which reduces key fission product poisons beyond the value used in the existing SFML calculation;
- Neglecting the removal of ~65% of the highest enrichment fuel assembly;
- Optimum moderation (fuel pellet to pitch ratio);
- Effectively infinite reflection;
- Optimum spherical core geometry; and
- Theoretical fuel density above the as-built specification for TMI-2.

The derived SFML bounds the entire expected fissile mass inventory throughout all physically separated areas within the reactor building. The bounding fissile mass used to produce the SFML is assembled in idealized conditions that cannot credibly exist during decommissioning operations. Even if the expected remaining fissile mass throughout the building (1097 kg UO_2), including hold up in all piping and cubicles were to be brought together, a criticality is not feasible. There are no credible operational upsets to realize the ideal configuration but even in the event that the upset occurs, it would require fissile mass in excess of that analyzed, which is

greater than what is anticipated, in addition to a greatly reduced impurity concentration to present a criticality hazard.

8. REFERENCES

[1] M. Pritchard, "TMI2-EN-RPT-0003 Rev. 0, TMI-2 Safe Fuel Mass Limit Computational Input Consensus," Nucler Safety & Technology Services, 2020.

[2] E. Schrult, "Letter C312-93-2004, TMI-2 Post-Defueling Survey Report for the Reactor Vessel," GPU Nuclear Corporation, Middleton, PA, February 1, 1993.

[3] GPU Nuclear Corporation, "TMI Nuclear Station Unit 2 Defueling Completion Report Rev. 4," 1989.

[4] E. Schrult, "TMI-2 Post-Defueling Survey Report for the Reactor Vessel," GPU Nuclear, Middleton, PA, 1993.

[5] EnergySolutions, "CG-EN-PR-204 Rev. 1, Control and Use of Acquired Analytical Software," 2016.

[6] Oak Ridge National Laboratory, "ORNL/TM-2005/39, SCALE: A Comprehensive Modeling and Simulation Suite for Nuclear Safety Analysis and Design, Version 6.2.4," Available from Radiation Safety Information Computational Center, Oak Ridge, TN, 2020.

[7] LA-UR-17-29981, *MCNP Users Manual - Code Version 6.2,* 2017.

[8] M. Chadwick, "ENDF/B-VII.1 Nuclear Data for Science and Technology: Cross Sections, Covariances, Fission Product Yields and Decay Data," *Nuclear Data Sheets,* vol. 112, 2011.

[9] "ANSI/ANS-8.24-2017, Validation of Neutron Transport Methods for Nuclear Criticality Safety Calculations," American Nuclear Society, La Grange Park, IL, 2017.

[10] W. M. Bowen and C. Bennett, "NUREG/CR-4604, Statistical Methods for Nuclear Material Management," Pacific Northwest Laboratory, Prepared for U.S. Nuclear Regulatory Commission, Richland, WA, 1988.

[11] J. Dean and J. R.W. Tayloe, "NUREG/CR-6698, Guide for Validation of Nuclear Criticality Safety Calculational Methodology," Science Application International Corporation, Prepared for U.S. Nuclear Regulatory Commission, Oak Ridge, TN, 2000.

[12] D. Faunce, "TMI2-EN-RPT-0002, MCNP Version 6.2 Bias Determination for Low Enrichment Uranium Using the ENDF/B-VIII.0 Cross Section Library," EnergySolutions, 2020.

[13] C. S. Olsen, D. W. Akers and R. K. McCardell, GEND-INF-084, Examination of the Debris from the Lower Head of the TMI-2 Reactor, Idaho Falls, Idaho: EG&G Idaho, Inc., 1988.

[14] G. O. Hayner, "GEND-INF-060 Vol. 2, TMI-2 H8A Core Debris Sample Examination Final Report," Prepared for EG&G Idaho, Inc and the U.S. DOE Three Mile Island Operations Office, Lynchburg, Virginia, 1985.

[15] D. W. Akers, E. R. Carlson, B. A. Cook, S. A. Ploger and J. O. Carlson, "GEND-INF-075, TMI-2 Core Debris Grab Samples - Examination and Analysis Part 1," EG&G Idaho, Inc., Idaho Falls, Idaho, 1986.

[16] GPU Nuclear Corporation, "4710-3220-89-1 Rev. 2, Criticality Safety Evaluation for Increasing the TMI-2 Safe Fuel Mass Limit," Submitted to Nuclear Regulatory Commission as Appendix B to the Defueling Completion Report Rev. 4, 1989.

[17] M. Pritchard, "NSTS-ES-01 Rev. 0, Safe Fuel Mass Limit Criticality Safety Analysis for TMI-2 Decommissioning," Nuclear Safety & Technology Services, 2020.

[18] "GPU Nuclear letter 4410-84-L-0199, Reactor Coolant System Criticality Report," November 8, 1984.

[19] *Letter, C.V. Parks, Oak Ridge National Laboratory, to D.S. Williams, GPU Nuclear Corporation,* November 6, 1987.

[20] GPU Nuclear Corporation, 15737-2-N09-005 Rev. 2, Criticality Safety Evaluation for Increasing the TMI-2 Safe Fuel Mass Limit, 1989.

[21] M. Marchetti, D. Laux and L. Fongaro, "Physical and Mechanical Characterization of Irradiated Uranium Dioxide with a Broad Burnup Range and Different Dopants Using Acoustic Microscopy," *Journal of Nuclear Materials,* vol. 494, pp. 322-329, 2017.

[22] C. S. Olsen, D. W. Akers and R. K. McCardell, "GEND-INF-084, Examination of the Debris from the Lower Head of the TMI-2 Reactor," EG&G Idaho, Prepared for the U.S. Department of Energy Idaho Operations Office, Idaho Falls, Idaho, January 1988.

[23] E. Clayton, "PNNL-19176 Rev. 6, Anomalies of Nuclear Criticality," Pacific Northwest Laboratory, Richland, Washington, 2010.

[24] GPU Nuclear Corporation, "4410-88-L-0162/0356P, TMI-2 Post-Defueling Survey Report for The Upper Plenum Assembly," Middletown, PA, September 30, 1988.

[25] GPU Nuclear Corporation, "4410-89-L-0097/0356P, TMI-2 Post-Defueling Survey Report for the Pressurizer, Reactor Building Basement, and Letdown Cooler Room," three reports packaged together, Middletown, PA, September 22, 1989.

[26] GPU Nuclear Corporation, "4410-90-L-0019/0356P, Post-Defueling Survey Report for the Reactor Vessel Head Assembly," Middletown, PA, March 14, 1990.

[27] C. Distenfeld, "C312-91-2064 Rev. 1, TMI-2 Post-Defueling Survey Report for the 'A' and 'B' Once-Through Steam Generators," GPU Nuclear Corporation, Middletown, PA, August 20, 1991.

[28] F. Deininger, "Letter C312-91-2045, TMI-2 Post-Defueling Survey Report for the Auxiliary & Fuel Handling Buildings," GPU Nuclear Corporation, Middletown, PA, June 7, 1991.

[29] F. Deininger, "C312-91-2052, TMI-2 Post-Defueling Survey Report for Reactor Building Miscellaneous Components," GPU Nuclear Corporation, Middletown, PA, June 18, 1991.

[30] P. Deininger, "Letter C312-91-2055, TMI-2 Post-Defueling Survey Report for the Reactor Coolant System," GPU Nuclear Corporation, Middletown, PA, July 3, 1991.

9. APPENDIX A – FUEL DEBRIS COMPOSITION

Table 9-1 – Fuel Composition as Calculated in 1988 (Ref. [3])

Nuclide	ZAID	Number Density (atoms/barn-cm)
^{235}U	92235	5.21E-4
^{238}U	92238	2.25E-2
^{16}O	8016	4.60E-2
^{239}Pu	94239	4.01E-5
^{240}Pu	94240	2.00E-6
^{241}Pu	94241	2.49E-7
^{149}Sm	62149	1.01E-7
^{151}Sm	62151	1.79E-7
^{151}Eu	63151	8.20E-9
^{153}Eu	63153	1.32E-7
^{154}Eu	63154	4.51E-9
^{155}Eu	63155	6.12E-9

Table 9-2 – Fuel Composition as Calculated for 2022

Nuclide	ZAID	Number Density (atoms/barn-cm)
^{4}He	2004	5.160E-08
^{207}Tl	81207	1.785E-21
^{209}Tl	81209	1.251E-29
^{206}Pb	82206	3.238E-22
^{207}Pb	82207	1.618E-15
^{208}Pb	82208	7.470E-25
^{209}Pb	82209	5.044E-26
^{210}Pb	82210	1.586E-21
^{211}Pb	82211	1.355E-20
^{212}Pb	82212	1.501E-28
^{214}Pb	82214	1.715E-26
^{209}Bi	83209	6.484E-22
^{210}Bi	83210	9.806E-25
^{211}Bi	83211	8.030E-22
^{212}Bi	83212	1.424E-29
^{213}Bi	83213	1.178E-26
^{214}Bi	83214	1.274E-26
^{210}Po	84210	2.512E-23
^{211}Po	84211	8.906E-27
^{215}Po	84215	1.114E-26
^{218}Po	84218	1.983E-27
^{219}Rn	86219	2.476E-23
^{222}Rn	86222	3.524E-24

^{221}Fr	87221	1.266E-27
^{223}Fr	87223	1.137E-22
^{223}Ra	88223	6.176E-18
^{224}Ra	88224	1.239E-27
^{225}Ra	88225	5.545E-24
^{226}Ra	88226	5.386E-19
^{228}Ra	88228	8.651E-25
^{225}Ac	89225	3.721E-24
^{227}Ac	89227	4.287E-15
^{228}Ac	89228	1.056E-28
^{227}Th	90227	9.954E-18
^{228}Th	90228	2.356E-25
^{229}Th	90229	9.976E-19
^{230}Th	90230	5.350E-15
^{231}Th	90231	2.155E-15
^{232}Th	90232	3.402E-15
^{234}Th	90234	3.323E-13
^{231}Pa	91231	1.693E-11
^{233}Pa	91233	2.232E-16
^{234}Pa	91234	6.159E-18
^{233}U	92233	2.580E-14
^{234}U	92234	1.149E-10
^{235}U	92235	5.210E-04
^{236}U	92236	6.961E-09
^{237}U	92237	1.594E-15
^{238}U	92238	2.250E-02
^{237}Np	93237	6.478E-09
^{239}Pu	94239	4.006E-05
^{240}Pu	94240	1.993E-06
^{241}Pu	94241	5.023E-08
^{241}Am	95241	1.923E-07
^{149}Sm	62149	1.010E-07
^{151}Sm	62151	1.388E-07
^{151}Eu	63151	4.838E-08
^{153}Eu	63153	1.320E-07
^{154}Sm	62154	7.550E-13
^{154}Eu	63154	3.156E-10
^{154}Gd	64154	4.194E-09
^{155}Eu	63155	4.972E-11
^{155}Gd	64155	6.070E-09
^{16}O	8016	4.600E-02

*Highlighted rows are nuclides excluded from the simulations.

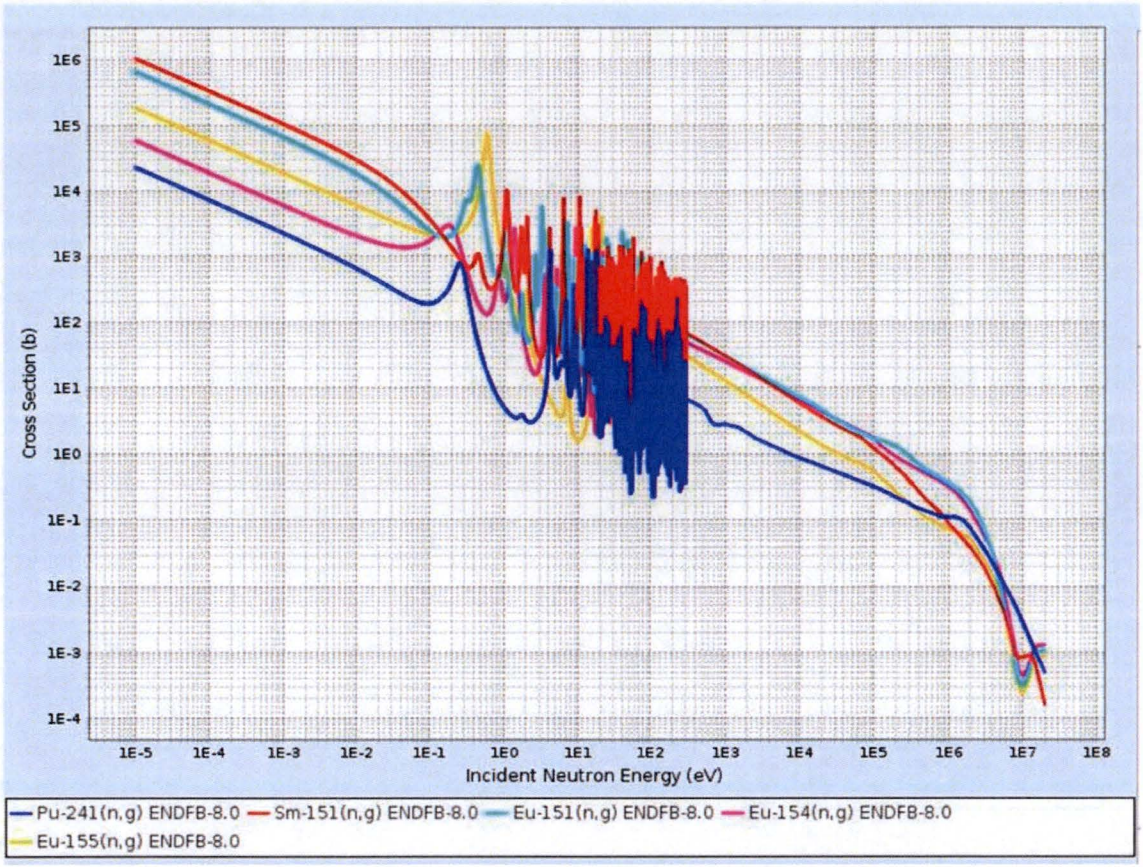

Figure 9-1. Energy Dependent Cross Section for Nuclides that Increased in the Decayed Composition

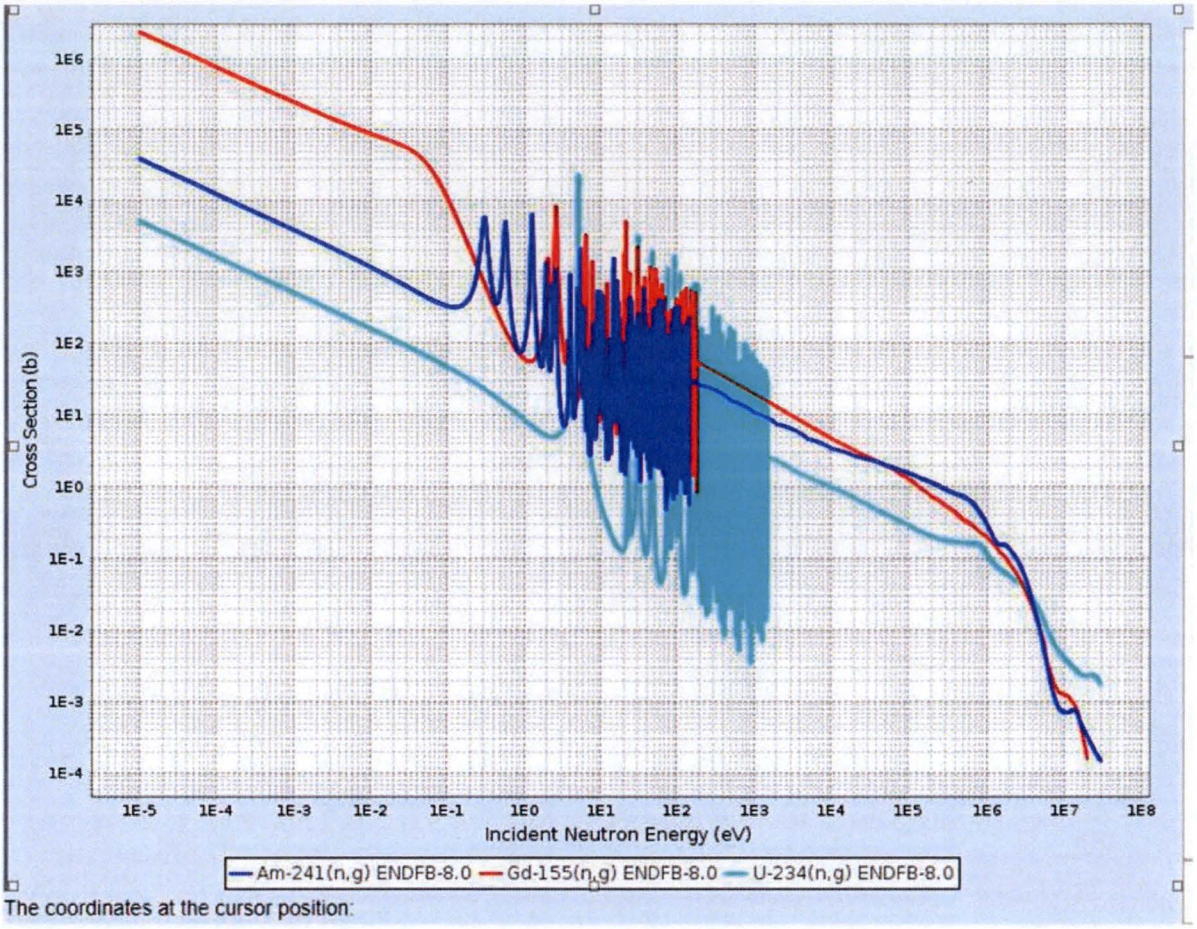

Figure 9-2. Energy Dependent Cross Section for Nuclides that Increased in the Decayed Composition

10. APPENDIX B – SAMPLE MCNP6 COMPUTER INPUT

TMI-sphereV8W_noBmod_0.4_1200_0.1_0.3.in

```
TMI-2 - sphere model water reflector with all impurities, no poison water
c Separation 0.4 cm
c No Soluble poison is in moderating water
c Refined fuel composition from V5 - from 'origen decay comp' file
c Simple sphere model with fuel plus impurities
c Iron content fixed at 10% reduced from reference
c  Parameters
c U mass (kg) = 1200
c Impurities wt frac: 0.1
c Fuel wt frac:0.9
c Impurities Boron multiplier = 0.3
c Iron multiplier = 0.9
c Fuel Density = 10.97
c Borated moderating water, no boron in reflector water
c Boron in water by weight = 0
c Water Boron multiplier = 0
c pitch = 1.6
c HexVolume = 3.5472
c Fuel Vol= 0.90478
c U Concentration = 2.2161
c  Hexagonal prism unit cell
c  UO2 fuel, enrichment=2.24%
c
c
c  -------------------CELL CARDS-----------------------------------------
c      FUEL UNIT CELL
10 100 -10.97          -4              u=2              imp:n=1     $ fuel inside pellet
20 400 -0.998207  4              u=2              imp:n=1     $ water around fuel pellet
c      LATTICE as UNIVERSE 1 FILLED WITH UNIVERSE 2
50 0             -3 lat=2 fill=2 u=1              imp:n=1     $ hexagonal lattice
c      SQUARE LATTICE AS UNIVERSE 3 FILLED WITH UNIVERSE 1
60 0             -5              u=3 lat=1 fill=1 imp:n=1
70 0             -1                               fill=3 imp:n=1   $ space filled by Universe 3
(lattice)
c      WATER REFLECTOR
80 400 -0.998207 -2 1                             imp:n=1    $ water outside core
c      NEVERLAND
500 0   2                                         imp:n=0

c  -------------------SURFACE CARDS---------------------------------------
c    rph    xyz of bottom of prism, height, 0 p 0, vector to 2nd facet, vector to 3rd facet
c
c       CORE AND REFLECTOR
1    sph    0 0 0   50.563                        $ whole core sphere for lattice
2    sph    0 0 0   80.563                  $ water reflector sphere
c       FUEL PELLET
3    rhp    0 0 -10  0 0 20  0 0.8           0       $ hexagonal prism cell, p=2
4    sph    0 0 0  0.60                       $ fuel sphere, r=0.50
5    rpp    -500 500 -500 500 -0.80 0.80   $ divider for unit cells

c --------------------DATA CARDS-----------------------------------------
c -------------------KCODE SOURCE----------------------------------------
kcode 10000 1.0 50 1050                           $ 10000 particles per cycle, 1050 cycles, skip
50 cycles
sdef pos= 0 0 0
c
c ------------------MATERIALS------------------------------------------
c
c ------------UO2 fuel; Density=10.97 g/cc 2.24% enr; ORNL Report------------
m100    2004.00c -2.986e-08                                                $ He-4
c       81207.00c -5.342e-20                                               $ Tl-207
c       81209.00c -3.779e-28                                               $ Tl-209
       82206.00c -9.643e-21                                               $ Pb-206
       82207.00c -4.843e-14                                               $ Pb-207
       82208.00c -2.246e-23                                               $ Pb-208
```

```
c       82209.00c -1.524e-24                                    $ Pb-209
c       82210.00c -4.814e-20                                    $ Pb-210
c       82211.00c -4.132e-19                                    $ Pb-211
c       82212.00c -4.601e-27                                    $ Pb-212
c       82214.00c -5.307e-25                                    $ Pb-214
        83209.00c -1.959e-20                                   $ Bi-209
c       83210.00c -2.977e-23                                    $ Bi-210
c       83211.00c -2.450e-20                                    $ Bi-211
c       83212.00c -4.363e-28                                    $ Bi-212
c       83213.00c -3.628e-25                                    $ Bi-213
c       83214.00c -3.942e-25                                    $ Bi-214
c       84210.00c -7.627e-22                                    $ Po-210
c       84211.00c -2.716e-25                                    $ Po-211
c       84215.00c -3.462e-25                                    $ Po-215
c       84218.00c -6.251e-26                                    $ Po-218
c       86219.00c -7.842e-22                                    $ Rn-219
c       86222.00c -1.131e-22                                    $ Rn-222
c       87221.00c -4.046e-26                                    $ Fr-221
c       87223.00c -3.666e-21                                    $ Fr-223
        88223.00c -1.991e-16                                   $ Ra-223
        88224.00c -4.014e-26                                   $ Ra-224
        88226.00c -1.760e-17                                   $ Ra-226
        88225.00c -1.803e-22                                   $ Ra-225
c       88228.00c -2.852e-23                                    $ Ra-228
        89225.00c -1.211e-22                                   $ Ac-225
        89227.00c -1.407e-13                                   $ Ac-227
c       89228.00c -3.480e-27                                    $ Ac-228
        90227.00c -3.267e-16                                   $ Th-227
        90228.00c -7.769e-24                                   $ Th-228
        90229.00c -3.304e-17                                   $ Th-229
        90230.00c -1.780e-13                                   $ Th-230
        90231.00c -7.200e-14                                   $ Th-231
        90232.00c -1.142e-13                                   $ Th-232
        90234.00c -1.125e-11                                   $ Th-234
        91231.00c -5.654e-10                                   $ Pa-231
        91233.00c -7.519e-15                                   $ Pa-233
c       91234.00c -2.084e-16                                    $ Pa-234
        92233.00c -8.695e-13                                   $ U-233
        92234.00c -3.887e-09                                   $ U-234
        92235.00c -1.771e-02                                  $ U-235
        92236.00c -2.376e-07                                    $ U-236
        92237.00c -5.462e-14                                    $ U-237
         92238.00c  -7.744e-01                                  $ U-238
         93237.00c -2.220e-07                                    $ Np-237
         8016.00c  -1.064e-01                                       $ O-16
         94239.00c  -1.385e-03                                  $ Pu-239
         94240.00c  -6.917e-05                                  $ Pu-240
         94241.00c  -1.751e-06                                  $ Pu-241
         95241.00c  -6.702e-06                                  $ Am-241
         62149.00c  -2.175e-06                                  $ Sm-149
         62151.00c  -3.029e-06                                  $ Sm-151
         62154.00c  -1.680e-11                                  $ Sm-154
         63151.00c  -1.056e-06                                  $ Eu-151
         63153.00c  -2.918e-06                                  $ Eu-153
         64154.00c  -7.023e-09                                  $ Eu-154
         63155.00c  -1.114e-09                                  $ Eu-155
         64154.00c  -9.333e-08                                 $ Gd-154
         64155.00c  -1.360e-07                                 $ Gd-155
         40090.00c  -3.973e-02                                  $ Zr-90
         40091.00c  -8.760e-03                                  $ Zr-91
         40092.00c  -1.353e-02                                  $ Zr-92
         40094.00c  -1.402e-02                                  $ Zr-94
         40096.00c  -2.307e-03                                  $ Zr-96
         26054.00c  -7.651e-04                                  $ Fe-54
         26056.00c  -1.245e-02                                  $ Fe-56
         26057.00c  -2.927e-04                                  $ Fe-57
         26058.00c  -3.963e-05                                  $ Fe-58
         5010.00c  -3.751e-05                                  $ B-10
         5011.00c  -1.661e-04                                  $ B-11
         24050.00c  -1.931e-04                                  $ Cr-50
```

```
        24052.00c  -3.872e-03                                                $ Cr-52
        24053.00c  -4.476e-04                                                $ Cr-53
        24054.00c  -1.135e-04                                                $ Cr-54
        42092.00c  -1.309e-04                                                $ Mo-92
        42094.00c  -8.359e-05                                                $ Mo-94
        42095.00c  -1.455e-04                                                $ Mo-95
        42096.00c  -1.543e-04                                                $ Mo-96
        42097.00c  -8.933e-05                                                $ Mo-97
        42098.00c  -2.284e-04                                                $ Mo-98
        42100.00c  -9.321e-05                                                $ Mo-100
        25055.00c  -3.701e-04                                                $ Mn-55
c
c ------------MODERATING WATER; Density = 0.998207; PNNL-15870 --------------
m200    5010.00c   -0.000e+00                              $ B-10
        5011.00c   -0.000e+00                               $ B-11
        1001.00c   -1.119e-01                                $ H-1
        8016.00c   -8.881e-01                              $ O-16
MT200   h-h2o.40t                                             $ S(a,b) for light water
c
c ------------CONCRETE; Density = 2.3; PNNL-15870 ------------------------
m300   1001.00c 1.68018E-01
       1002.00c 1.93243E-05
       8016.00c 5.62969E-01
       8017.00c 2.14009E-04
       11023.00c 2.13651E-02
       13027.00c 2.13429E-02
       14028.00c 1.87425E-01
       14029.00c 9.52136E-03
       14030.00c 6.28389E-03
       20040.00c 1.80258E-02
       20042.00c 1.20307E-04
       20043.00c 2.51028E-05
       20044.00c 3.87884E-04
       20046.00c 7.43786E-07
       20048.00c 3.47720E-05
       26054.00c 2.48181E-04
       26056.00c 3.89591E-03
       26057.00c 8.99736E-05
       26058.00c 1.19738E-05
MT300  h-h2o.40t fe-56.40t                          $ S(a,b) for light water, iron
c
c --------------REFLECTOR WATER; Density =0.998207; PNNL-15870 ------------
m400   1001.00c  0.66733
       8016.00c  0.33267
MT400  h-h2o.40t                                       $ S(a,b) for light water
print
```

11. APPENDIX C – SAMPLE ORIGEN COMPUTER INPUT

TMIFuelDecay.inp

```
'TMI Decayed Source Input
=origen

case{
    title="TMI Decayed Source"
    lib{
        file="end7dec"  % ORIGEN Decay library
    }
    mat{
        units = moles
        iso=[
                U235 =8.6515E-04
                U238 =3.7363E-02
                O16  =7.6386E-02
                Pu239=6.6589E-05
                Pu240=3.3211E-06
          Pu241=4.1348E-07
          Sm149=1.6772E-07
          Sm151=2.9724E-07
          Eu151=1.3617E-08
          Eu153=2.1919E-07
               Eu154=7.4892E-09
          Eu155=1.0163E-08
        ]
    }
    time{
        units = YEARS
        start = 1989
        t = [1990 1991 1993 1997 2005 2013 2019 2021 2022]
    }
    print{
        nuc{ total=yes units=[MOLES] }
        cutoff_step = 5
        rel_cutoff = no
        cutoffs[ ALL=1.0E-30 ]
    }
    save=yes
}
end
```

12. APPENDIX D – ELECTRONIC FILES

12.1. Computer Runs

The files listed below do not include the files associated with the scoping calculation to determine optimum moderation. A list of those files is included with the electronic archive.

Filename	File Date	Computer Code	Version	Computer
TMI-sphereV8W_1200_onlyimp_0.05.in	12/8/2020	MCNP	6.2.0	NSTS-LS01
TMI-sphereV8W_1200_onlyimp_0.05.ino	12/8/2020	MCNP	6.2.0	NSTS-LS01
TMI-sphereV8W_1200_onlyimp_0.15.in	12/8/2020	MCNP	6.2.0	NSTS-LS01
TMI-sphereV8W_1200_onlyimp_0.15.ino	12/8/2020	MCNP	6.2.0	NSTS-LS01
TMI-sphereV8W_1200_onlyimp_0.1621.in	12/8/2020	MCNP	6.2.0	NSTS-LS01
TMI-sphereV8W_1200_onlyimp_0.1621.ino	12/8/2020	MCNP	6.2.0	NSTS-LS01
TMI-sphereV8W_1200_onlyimp_0.1.in	12/8/2020	MCNP	6.2.0	NSTS-LS01
TMI-sphereV8W_1200_onlyimp_0.1.ino	12/8/2020	MCNP	6.2.0	NSTS-LS01
TMI-sphereV8W_noBmod_0.4_1125_0.05_0.2.in	12/8/2020	MCNP	6.2.0	NSTS-LS01
TMI-sphereV8W_noBmod_0.4_1125_0.05_0.2.ino	12/8/2020	MCNP	6.2.0	NSTS-LS01
TMI-sphereV8W_noBmod_0.4_1125_0.05_0.3.in	12/8/2020	MCNP	6.2.0	NSTS-LS01
TMI-sphereV8W_noBmod_0.4_1125_0.05_0.3.ino	12/8/2020	MCNP	6.2.0	NSTS-LS01
TMI-sphereV8W_noBmod_0.4_1125_0.05_0.5.in	12/8/2020	MCNP	6.2.0	NSTS-LS01
TMI-sphereV8W_noBmod_0.4_1125_0.05_0.5.ino	12/8/2020	MCNP	6.2.0	NSTS-LS01

TMI-sphereV8W_noBmod_0.4_1125_0.05_0.8.in	12/8/2020	MCNP	6.2.0	NSTS-LS01
TMI-sphereV8W_noBmod_0.4_1125_0.05_0.8.ino	12/8/2020	MCNP	6.2.0	NSTS-LS01
TMI-sphereV8W_noBmod_0.4_1125_0.05_1.in	12/8/2020	MCNP	6.2.0	NSTS-LS01
TMI-sphereV8W_noBmod_0.4_1125_0.05_1.ino	12/8/2020	MCNP	6.2.0	NSTS-LS01
TMI-sphereV8W_noBmod_0.4_1125_0.1_0.2.in	12/8/2020	MCNP	6.2.0	NSTS-LS01
TMI-sphereV8W_noBmod_0.4_1125_0.1_0.2.ino	12/8/2020	MCNP	6.2.0	NSTS-LS01
TMI-sphereV8W_noBmod_0.4_1125_0.1_0.3.in	12/8/2020	MCNP	6.2.0	NSTS-LS01
TMI-sphereV8W_noBmod_0.4_1125_0.1_0.3.ino	12/8/2020	MCNP	6.2.0	NSTS-LS01
TMI-sphereV8W_noBmod_0.4_1125_0.1_0.5.in	12/8/2020	MCNP	6.2.0	NSTS-LS01
TMI-sphereV8W_noBmod_0.4_1125_0.1_0.5.ino	12/8/2020	MCNP	6.2.0	NSTS-LS01
TMI-sphereV8W_noBmod_0.4_1125_0.1_0.8.in	12/8/2020	MCNP	6.2.0	NSTS-LS01
TMI-sphereV8W_noBmod_0.4_1125_0.1_0.8.ino	12/8/2020	MCNP	6.2.0	NSTS-LS01
TMI-sphereV8W_noBmod_0.4_1125_0.1_1.in	12/8/2020	MCNP	6.2.0	NSTS-LS01
TMI-sphereV8W_noBmod_0.4_1125_0.1_1.ino	12/8/2020	MCNP	6.2.0	NSTS-LS01
TMI-sphereV8W_noBmod_0.4_1125_0.15_0.2.in	12/8/2020	MCNP	6.2.0	NSTS-LS01
TMI-sphereV8W_noBmod_0.4_1125_0.15_0.2.ino	12/8/2020	MCNP	6.2.0	NSTS-LS01
TMI-sphereV8W_noBmod_0.4_1125_0.15_0.3.in	12/8/2020	MCNP	6.2.0	NSTS-LS01
TMI-sphereV8W_noBmod_0.4_1125_0.15_0.3.ino	12/8/2020	MCNP	6.2.0	NSTS-LS01
TMI-sphereV8W_noBmod_0.4_1125_0.15_0.5.in	12/8/2020	MCNP	6.2.0	NSTS-LS01
TMI-sphereV8W_noBmod_0.4_1125_0.15_0.5.ino	12/8/2020	MCNP	6.2.0	NSTS-LS01
TMI-sphereV8W_noBmod_0.4_1125_0.15_0.8.in	12/8/2020	MCNP	6.2.0	NSTS-LS01
TMI-sphereV8W_noBmod_0.4_1125_0.15_0.8.ino	12/8/2020	MCNP	6.2.0	NSTS-LS01
TMI-sphereV8W_noBmod_0.4_1125_0.15_1.in	12/8/2020	MCNP	6.2.0	NSTS-LS01
TMI-sphereV8W_noBmod_0.4_1125_0.15_1.ino	12/8/2020	MCNP	6.2.0	NSTS-LS01
TMI-sphereV8W_noBmod_0.4_1125_0.1621_0.2.in	12/8/2020	MCNP	6.2.0	NSTS-LS01
TMI-sphereV8W_noBmod_0.4_1125_0.1621_0.2.ino	12/8/2020	MCNP	6.2.0	NSTS-LS01
TMI-sphereV8W_noBmod_0.4_1125_0.1621_0.3.in	12/8/2020	MCNP	6.2.0	NSTS-LS01
TMI-sphereV8W_noBmod_0.4_1125_0.1621_0.3.ino	12/8/2020	MCNP	6.2.0	NSTS-LS01
TMI-sphereV8W_noBmod_0.4_1125_0.1621_0.5.in	12/8/2020	MCNP	6.2.0	NSTS-LS01
TMI-sphereV8W_noBmod_0.4_1125_0.1621_0.5.ino	12/8/2020	MCNP	6.2.0	NSTS-LS01
TMI-sphereV8W_noBmod_0.4_1125_0.1621_0.8.in	12/8/2020	MCNP	6.2.0	NSTS-LS01
TMI-sphereV8W_noBmod_0.4_1125_0.1621_0.8.ino	12/8/2020	MCNP	6.2.0	NSTS-LS01
TMI-sphereV8W_noBmod_0.4_1125_0.1621_1.in	12/8/2020	MCNP	6.2.0	NSTS-LS01
TMI-sphereV8W_noBmod_0.4_1125_0.1621_1.ino	12/8/2020	MCNP	6.2.0	NSTS-LS01
TMI-sphereV8W_noBmod_0.4_1200_0.05_0.2.in	12/8/2020	MCNP	6.2.0	NSTS-LS01
TMI-sphereV8W_noBmod_0.4_1200_0.05_0.2.ino	12/8/2020	MCNP	6.2.0	NSTS-LS01
TMI-sphereV8W_noBmod_0.4_1200_0.05_0.3.in	12/8/2020	MCNP	6.2.0	NSTS-LS01
TMI-sphereV8W_noBmod_0.4_1200_0.05_0.3.ino	12/8/2020	MCNP	6.2.0	NSTS-LS01
TMI-sphereV8W_noBmod_0.4_1200_0.05_0.5.in	12/8/2020	MCNP	6.2.0	NSTS-LS01
TMI-sphereV8W_noBmod_0.4_1200_0.05_0.5.ino	12/8/2020	MCNP	6.2.0	NSTS-LS01
TMI-sphereV8W_noBmod_0.4_1200_0.05_0.8.in	12/8/2020	MCNP	6.2.0	NSTS-LS01
TMI-sphereV8W_noBmod_0.4_1200_0.05_0.8.ino	12/8/2020	MCNP	6.2.0	NSTS-LS01
TMI-sphereV8W_noBmod_0.4_1200_0.05_1.in	12/8/2020	MCNP	6.2.0	NSTS-LS01
TMI-sphereV8W_noBmod_0.4_1200_0.05_1.ino	12/8/2020	MCNP	6.2.0	NSTS-LS01
TMI-sphereV8W_noBmod_0.4_1200_0.1_0.2.in	12/8/2020	MCNP	6.2.0	NSTS-LS01
TMI-sphereV8W_noBmod_0.4_1200_0.1_0.2.ino	12/8/2020	MCNP	6.2.0	NSTS-LS01
TMI-sphereV8W_noBmod_0.4_1200_0.1_0.3.in	12/8/2020	MCNP	6.2.0	NSTS-LS01
TMI-sphereV8W_noBmod_0.4_1200_0.1_0.3.ino	12/8/2020	MCNP	6.2.0	NSTS-LS01
TMI-sphereV8W_noBmod_0.4_1200_0.1_0.5.in	12/8/2020	MCNP	6.2.0	NSTS-LS01
TMI-sphereV8W_noBmod_0.4_1200_0.1_0.5.ino	12/8/2020	MCNP	6.2.0	NSTS-LS01
TMI-sphereV8W_noBmod_0.4_1200_0.1_0.8.in	12/8/2020	MCNP	6.2.0	NSTS-LS01
TMI-sphereV8W_noBmod_0.4_1200_0.1_0.8.ino	12/8/2020	MCNP	6.2.0	NSTS-LS01
TMI-sphereV8W_noBmod_0.4_1200_0.1_1.in	12/8/2020	MCNP	6.2.0	NSTS-LS01
TMI-sphereV8W_noBmod_0.4_1200_0.1_1.ino	12/8/2020	MCNP	6.2.0	NSTS-LS01
TMI-sphereV8W_noBmod_0.4_1200_0.15_0.2.in	12/8/2020	MCNP	6.2.0	NSTS-LS01
TMI-sphereV8W_noBmod_0.4_1200_0.15_0.2.ino	12/8/2020	MCNP	6.2.0	NSTS-LS01
TMI-sphereV8W_noBmod_0.4_1200_0.15_0.3.in	12/8/2020	MCNP	6.2.0	NSTS-LS01
TMI-sphereV8W_noBmod_0.4_1200_0.15_0.3.ino	12/8/2020	MCNP	6.2.0	NSTS-LS01
TMI-sphereV8W_noBmod_0.4_1200_0.15_0.5.in	12/8/2020	MCNP	6.2.0	NSTS-LS01
TMI-sphereV8W_noBmod_0.4_1200_0.15_0.5.ino	12/8/2020	MCNP	6.2.0	NSTS-LS01
TMI-sphereV8W_noBmod_0.4_1200_0.15_0.8.in	12/8/2020	MCNP	6.2.0	NSTS-LS01
TMI-sphereV8W_noBmod_0.4_1200_0.15_0.8.ino	12/8/2020	MCNP	6.2.0	NSTS-LS01

TMI-sphereV8W_noBmod_0.4_1200_0.15_1.in	12/8/2020	MCNP	6.2.0	NSTS-LS01
TMI-sphereV8W_noBmod_0.4_1200_0.15_1.ino	12/8/2020	MCNP	6.2.0	NSTS-LS01
TMI-sphereV8W_noBmod_0.4_1200_0.1621_0.2.in	12/8/2020	MCNP	6.2.0	NSTS-LS01
TMI-sphereV8W_noBmod_0.4_1200_0.1621_0.2.ino	12/8/2020	MCNP	6.2.0	NSTS-LS01
TMI-sphereV8W_noBmod_0.4_1200_0.1621_0.3.in	12/8/2020	MCNP	6.2.0	NSTS-LS01
TMI-sphereV8W_noBmod_0.4_1200_0.1621_0.3.ino	12/8/2020	MCNP	6.2.0	NSTS-LS01
TMI-sphereV8W_noBmod_0.4_1200_0.1621_0.5.in	12/8/2020	MCNP	6.2.0	NSTS-LS01
TMI-sphereV8W_noBmod_0.4_1200_0.1621_0.5.ino	12/8/2020	MCNP	6.2.0	NSTS-LS01
TMI-sphereV8W_noBmod_0.4_1200_0.1621_0.8.in	12/8/2020	MCNP	6.2.0	NSTS-LS01
TMI-sphereV8W_noBmod_0.4_1200_0.1621_0.8.ino	12/8/2020	MCNP	6.2.0	NSTS-LS01
TMI-sphereV8W_noBmod_0.4_1200_0.1621_1.in	12/8/2020	MCNP	6.2.0	NSTS-LS01
TMI-sphereV8W_noBmod_0.4_1200_0.1621_1.ino	12/8/2020	MCNP	6.2.0	NSTS-LS01
TMI-sphereV8W_noBmod_0.4_1500_0.05_0.2.in	12/8/2020	MCNP	6.2.0	NSTS-LS01
TMI-sphereV8W_noBmod_0.4_1500_0.05_0.2.ino	12/8/2020	MCNP	6.2.0	NSTS-LS01
TMI-sphereV8W_noBmod_0.4_1500_0.05_0.3.in	12/8/2020	MCNP	6.2.0	NSTS-LS01
TMI-sphereV8W_noBmod_0.4_1500_0.05_0.3.ino	12/8/2020	MCNP	6.2.0	NSTS-LS01
TMI-sphereV8W_noBmod_0.4_1500_0.05_0.5.in	12/8/2020	MCNP	6.2.0	NSTS-LS01
TMI-sphereV8W_noBmod_0.4_1500_0.05_0.5.ino	12/8/2020	MCNP	6.2.0	NSTS-LS01
TMI-sphereV8W_noBmod_0.4_1500_0.05_0.8.in	12/8/2020	MCNP	6.2.0	NSTS-LS01
TMI-sphereV8W_noBmod_0.4_1500_0.05_0.8.ino	12/8/2020	MCNP	6.2.0	NSTS-LS01
TMI-sphereV8W_noBmod_0.4_1500_0.05_1.in	12/8/2020	MCNP	6.2.0	NSTS-LS01
TMI-sphereV8W_noBmod_0.4_1500_0.05_1.ino	12/8/2020	MCNP	6.2.0	NSTS-LS01
TMI-sphereV8W_noBmod_0.4_1500_0.1_0.2.in	12/8/2020	MCNP	6.2.0	NSTS-LS01
TMI-sphereV8W_noBmod_0.4_1500_0.1_0.2.ino	12/8/2020	MCNP	6.2.0	NSTS-LS01
TMI-sphereV8W_noBmod_0.4_1500_0.1_0.3.in	12/8/2020	MCNP	6.2.0	NSTS-LS01
TMI-sphereV8W_noBmod_0.4_1500_0.1_0.3.ino	12/8/2020	MCNP	6.2.0	NSTS-LS01
TMI-sphereV8W_noBmod_0.4_1500_0.1_0.5.in	12/8/2020	MCNP	6.2.0	NSTS-LS01
TMI-sphereV8W_noBmod_0.4_1500_0.1_0.5.ino	12/8/2020	MCNP	6.2.0	NSTS-LS01
TMI-sphereV8W_noBmod_0.4_1500_0.1_0.8.in	12/8/2020	MCNP	6.2.0	NSTS-LS01
TMI-sphereV8W_noBmod_0.4_1500_0.1_0.8.ino	12/8/2020	MCNP	6.2.0	NSTS-LS01
TMI-sphereV8W_noBmod_0.4_1500_0.1_1.in	12/8/2020	MCNP	6.2.0	NSTS-LS01
TMI-sphereV8W_noBmod_0.4_1500_0.1_1.ino	12/8/2020	MCNP	6.2.0	NSTS-LS01
TMI-sphereV8W_noBmod_0.4_1500_0.15_0.2.in	12/8/2020	MCNP	6.2.0	NSTS-LS01
TMI-sphereV8W_noBmod_0.4_1500_0.15_0.2.ino	12/8/2020	MCNP	6.2.0	NSTS-LS01
TMI-sphereV8W_noBmod_0.4_1500_0.15_0.3.in	12/8/2020	MCNP	6.2.0	NSTS-LS01
TMI-sphereV8W_noBmod_0.4_1500_0.15_0.3.ino	12/8/2020	MCNP	6.2.0	NSTS-LS01
TMI-sphereV8W_noBmod_0.4_1500_0.15_0.5.in	12/8/2020	MCNP	6.2.0	NSTS-LS01
TMI-sphereV8W_noBmod_0.4_1500_0.15_0.5.ino	12/8/2020	MCNP	6.2.0	NSTS-LS01
TMI-sphereV8W_noBmod_0.4_1500_0.15_0.8.in	12/8/2020	MCNP	6.2.0	NSTS-LS01
TMI-sphereV8W_noBmod_0.4_1500_0.15_0.8.ino	12/8/2020	MCNP	6.2.0	NSTS-LS01
TMI-sphereV8W_noBmod_0.4_1500_0.15_1.in	12/8/2020	MCNP	6.2.0	NSTS-LS01
TMI-sphereV8W_noBmod_0.4_1500_0.15_1.ino	12/8/2020	MCNP	6.2.0	NSTS-LS01
TMI-sphereV8W_noBmod_0.4_1500_0.1621_0.2.in	12/8/2020	MCNP	6.2.0	NSTS-LS01
TMI-sphereV8W_noBmod_0.4_1500_0.1621_0.2.ino	12/8/2020	MCNP	6.2.0	NSTS-LS01
TMI-sphereV8W_noBmod_0.4_1500_0.1621_0.3.in	12/8/2020	MCNP	6.2.0	NSTS-LS01
TMI-sphereV8W_noBmod_0.4_1500_0.1621_0.3.ino	12/8/2020	MCNP	6.2.0	NSTS-LS01
TMI-sphereV8W_noBmod_0.4_1500_0.1621_0.5.in	12/8/2020	MCNP	6.2.0	NSTS-LS01
TMI-sphereV8W_noBmod_0.4_1500_0.1621_0.5.ino	12/8/2020	MCNP	6.2.0	NSTS-LS01
TMI-sphereV8W_noBmod_0.4_1500_0.1621_0.8.in	12/8/2020	MCNP	6.2.0	NSTS-LS01
TMI-sphereV8W_noBmod_0.4_1500_0.1621_0.8.ino	12/8/2020	MCNP	6.2.0	NSTS-LS01
TMI-sphereV8W_noBmod_0.4_1500_0.1621_1.in	12/8/2020	MCNP	6.2.0	NSTS-LS01
TMI-sphereV8W_noBmod_0.4_1500_0.1621_1.ino	12/8/2020	MCNP	6.2.0	NSTS-LS01
TMI-sphereV8W_noBmod_0.4_925_0.05_0.2.in	12/8/2020	MCNP	6.2.0	NSTS-LS01
TMI-sphereV8W_noBmod_0.4_925_0.05_0.2.ino	12/8/2020	MCNP	6.2.0	NSTS-LS01
TMI-sphereV8W_noBmod_0.4_925_0.05_0.3.in	12/8/2020	MCNP	6.2.0	NSTS-LS01
TMI-sphereV8W_noBmod_0.4_925_0.05_0.3.ino	12/8/2020	MCNP	6.2.0	NSTS-LS01
TMI-sphereV8W_noBmod_0.4_925_0.05_0.5.in	12/8/2020	MCNP	6.2.0	NSTS-LS01
TMI-sphereV8W_noBmod_0.4_925_0.05_0.5.ino	12/8/2020	MCNP	6.2.0	NSTS-LS01
TMI-sphereV8W_noBmod_0.4_925_0.05_0.8.in	12/8/2020	MCNP	6.2.0	NSTS-LS01
TMI-sphereV8W_noBmod_0.4_925_0.05_0.8.ino	12/8/2020	MCNP	6.2.0	NSTS-LS01
TMI-sphereV8W_noBmod_0.4_925_0.05_1.in	12/8/2020	MCNP	6.2.0	NSTS-LS01
TMI-sphereV8W_noBmod_0.4_925_0.05_1.ino	12/8/2020	MCNP	6.2.0	NSTS-LS01

TMI-sphereV8W_noBmod_0.4_925_0.1_0.2.in	12/8/2020	MCNP	6.2.0	NSTS-LS01
TMI-sphereV8W_noBmod_0.4_925_0.1_0.2.ino	12/8/2020	MCNP	6.2.0	NSTS-LS01
TMI-sphereV8W_noBmod_0.4_925_0.1_0.3.in	12/8/2020	MCNP	6.2.0	NSTS-LS01
TMI-sphereV8W_noBmod_0.4_925_0.1_0.3.ino	12/8/2020	MCNP	6.2.0	NSTS-LS01
TMI-sphereV8W_noBmod_0.4_925_0.1_0.5.in	12/8/2020	MCNP	6.2.0	NSTS-LS01
TMI-sphereV8W_noBmod_0.4_925_0.1_0.5.ino	12/8/2020	MCNP	6.2.0	NSTS-LS01
TMI-sphereV8W_noBmod_0.4_925_0.1_0.8.in	12/8/2020	MCNP	6.2.0	NSTS-LS01
TMI-sphereV8W_noBmod_0.4_925_0.1_0.8.ino	12/8/2020	MCNP	6.2.0	NSTS-LS01
TMI-sphereV8W_noBmod_0.4_925_0.1_1.in	12/8/2020	MCNP	6.2.0	NSTS-LS01
TMI-sphereV8W_noBmod_0.4_925_0.1_1.ino	12/8/2020	MCNP	6.2.0	NSTS-LS01
TMI-sphereV8W_noBmod_0.4_925_0.15_0.2.in	12/8/2020	MCNP	6.2.0	NSTS-LS01
TMI-sphereV8W_noBmod_0.4_925_0.15_0.2.ino	12/8/2020	MCNP	6.2.0	NSTS-LS01
TMI-sphereV8W_noBmod_0.4_925_0.15_0.3.in	12/8/2020	MCNP	6.2.0	NSTS-LS01
TMI-sphereV8W_noBmod_0.4_925_0.15_0.3.ino	12/8/2020	MCNP	6.2.0	NSTS-LS01
TMI-sphereV8W_noBmod_0.4_925_0.15_0.5.in	12/8/2020	MCNP	6.2.0	NSTS-LS01
TMI-sphereV8W_noBmod_0.4_925_0.15_0.5.ino	12/8/2020	MCNP	6.2.0	NSTS-LS01
TMI-sphereV8W_noBmod_0.4_925_0.15_0.8.in	12/8/2020	MCNP	6.2.0	NSTS-LS01
TMI-sphereV8W_noBmod_0.4_925_0.15_0.8.ino	12/8/2020	MCNP	6.2.0	NSTS-LS01
TMI-sphereV8W_noBmod_0.4_925_0.15_1.in	12/8/2020	MCNP	6.2.0	NSTS-LS01
TMI-sphereV8W_noBmod_0.4_925_0.15_1.ino	12/8/2020	MCNP	6.2.0	NSTS-LS01
TMI-sphereV8W_noBmod_0.4_925_0.1621_0.2.in	12/8/2020	MCNP	6.2.0	NSTS-LS01
TMI-sphereV8W_noBmod_0.4_925_0.1621_0.2.ino	12/8/2020	MCNP	6.2.0	NSTS-LS01
TMI-sphereV8W_noBmod_0.4_925_0.1621_0.3.in	12/8/2020	MCNP	6.2.0	NSTS-LS01
TMI-sphereV8W_noBmod_0.4_925_0.1621_0.3.ino	12/8/2020	MCNP	6.2.0	NSTS-LS01
TMI-sphereV8W_noBmod_0.4_925_0.1621_0.5.in	12/8/2020	MCNP	6.2.0	NSTS-LS01
TMI-sphereV8W_noBmod_0.4_925_0.1621_0.5.ino	12/8/2020	MCNP	6.2.0	NSTS-LS01
TMI-sphereV8W_noBmod_0.4_925_0.1621_0.8.in	12/8/2020	MCNP	6.2.0	NSTS-LS01
TMI-sphereV8W_noBmod_0.4_925_0.1621_0.8.ino	12/8/2020	MCNP	6.2.0	NSTS-LS01
TMI-sphereV8W_noBmod_0.4_925_0.1621_1.in	12/8/2020	MCNP	6.2.0	NSTS-LS01
TMI-sphereV8W_noBmod_0.4_925_0.1621_1.ino	12/8/2020	MCNP	6.2.0	NSTS-LS01
TMI-sphereV8W_onlyimp_1125_0.05.in	12/8/2020	MCNP	6.2.0	NSTS-LS01
TMI-sphereV8W_onlyimp_1125_0.05.ino	12/8/2020	MCNP	6.2.0	NSTS-LS01
TMI-sphereV8W_onlyimp_1125_0.15.in	12/8/2020	MCNP	6.2.0	NSTS-LS01
TMI-sphereV8W_onlyimp_1125_0.15.ino	12/8/2020	MCNP	6.2.0	NSTS-LS01
TMI-sphereV8W_onlyimp_1125_0.1621.in	12/8/2020	MCNP	6.2.0	NSTS-LS01
TMI-sphereV8W_onlyimp_1125_0.1621.ino	12/8/2020	MCNP	6.2.0	NSTS-LS01
TMI-sphereV8W_onlyimp_1125_0.1.in	12/8/2020	MCNP	6.2.0	NSTS-LS01
TMI-sphereV8W_onlyimp_1125_0.1.ino	12/8/2020	MCNP	6.2.0	NSTS-LS01
TMI-sphereV8W_onlyimp_1500_0.05.in	12/8/2020	MCNP	6.2.0	NSTS-LS01
TMI-sphereV8W_onlyimp_1500_0.05.ino	12/8/2020	MCNP	6.2.0	NSTS-LS01
TMI-sphereV8W_onlyimp_1500_0.15.in	12/8/2020	MCNP	6.2.0	NSTS-LS01
TMI-sphereV8W_onlyimp_1500_0.15.ino	12/8/2020	MCNP	6.2.0	NSTS-LS01
TMI-sphereV8W_onlyimp_1500_0.1621.in	12/8/2020	MCNP	6.2.0	NSTS-LS01
TMI-sphereV8W_onlyimp_1500_0.1621.ino	12/8/2020	MCNP	6.2.0	NSTS-LS01
TMI-sphereV8W_onlyimp_1500_0.1.in	12/8/2020	MCNP	6.2.0	NSTS-LS01
TMI-sphereV8W_onlyimp_1500_0.1.ino	12/8/2020	MCNP	6.2.0	NSTS-LS01
TMI-sphereV8W_onlyimp_1750_0.05.in	12/8/2020	MCNP	6.2.0	NSTS-LS01
TMI-sphereV8W_onlyimp_1750_0.05.ino	12/8/2020	MCNP	6.2.0	NSTS-LS01
TMI-sphereV8W_onlyimp_1750_0.15.in	12/8/2020	MCNP	6.2.0	NSTS-LS01
TMI-sphereV8W_onlyimp_1750_0.15.ino	12/8/2020	MCNP	6.2.0	NSTS-LS01
TMI-sphereV8W_onlyimp_1750_0.1621.in	12/8/2020	MCNP	6.2.0	NSTS-LS01
TMI-sphereV8W_onlyimp_1750_0.1621.ino	12/8/2020	MCNP	6.2.0	NSTS-LS01
TMI-sphereV8W_onlyimp_1750_0.1.in	12/8/2020	MCNP	6.2.0	NSTS-LS01
TMI-sphereV8W_onlyimp_1750_0.1.ino	12/8/2020	MCNP	6.2.0	NSTS-LS01
TMI-sphereV8W_onlyimp_925_0.05.in	12/8/2020	MCNP	6.2.0	NSTS-LS01
TMI-sphereV8W_onlyimp_925_0.05.ino	12/8/2020	MCNP	6.2.0	NSTS-LS01
TMI-sphereV8W_onlyimp_925_0.15.in	12/8/2020	MCNP	6.2.0	NSTS-LS01
TMI-sphereV8W_onlyimp_925_0.15.ino	12/8/2020	MCNP	6.2.0	NSTS-LS01
TMI-sphereV8W_onlyimp_925_0.1621.in	12/8/2020	MCNP	6.2.0	NSTS-LS01
TMI-sphereV8W_onlyimp_925_0.1621.ino	12/8/2020	MCNP	6.2.0	NSTS-LS01
TMI-sphereV8W_onlyimp_925_0.1.in	12/8/2020	MCNP	6.2.0	NSTS-LS01
TMI-sphereV8W_onlyimp_925_0.1.ino	12/8/2020	MCNP	6.2.0	NSTS-LS01

TMI-sphereV8C_noBmod_1125_0.05_0.2.in	12/10/2020	MCNP	6.2.0	NSTS-LS01
TMI-sphereV8C_noBmod_1125_0.05_0.2.ino	12/10/2020	MCNP	6.2.0	NSTS-LS01
TMI-sphereV8C_noBmod_1125_0.05_0.3.in	12/10/2020	MCNP	6.2.0	NSTS-LS01
TMI-sphereV8C_noBmod_1125_0.05_0.3.ino	12/10/2020	MCNP	6.2.0	NSTS-LS01
TMI-sphereV8C_noBmod_1125_0.05_0.5.in	12/10/2020	MCNP	6.2.0	NSTS-LS01
TMI-sphereV8C_noBmod_1125_0.05_0.5.ino	12/10/2020	MCNP	6.2.0	NSTS-LS01
TMI-sphereV8C_noBmod_1125_0.05_0.8.in	12/10/2020	MCNP	6.2.0	NSTS-LS01
TMI-sphereV8C_noBmod_1125_0.05_0.8.ino	12/10/2020	MCNP	6.2.0	NSTS-LS01
TMI-sphereV8C_noBmod_1125_0.05_1.in	12/10/2020	MCNP	6.2.0	NSTS-LS01
TMI-sphereV8C_noBmod_1125_0.05_1.ino	12/10/2020	MCNP	6.2.0	NSTS-LS01
TMI-sphereV8C_noBmod_1125_0.1_0.2.in	12/10/2020	MCNP	6.2.0	NSTS-LS01
TMI-sphereV8C_noBmod_1125_0.1_0.2.ino	12/10/2020	MCNP	6.2.0	NSTS-LS01
TMI-sphereV8C_noBmod_1125_0.1_0.3.in	12/10/2020	MCNP	6.2.0	NSTS-LS01
TMI-sphereV8C_noBmod_1125_0.1_0.3.ino	12/10/2020	MCNP	6.2.0	NSTS-LS01
TMI-sphereV8C_noBmod_1125_0.1_0.5.in	12/10/2020	MCNP	6.2.0	NSTS-LS01
TMI-sphereV8C_noBmod_1125_0.1_0.5.ino	12/10/2020	MCNP	6.2.0	NSTS-LS01
TMI-sphereV8C_noBmod_1125_0.1_0.8.in	12/10/2020	MCNP	6.2.0	NSTS-LS01
TMI-sphereV8C_noBmod_1125_0.1_0.8.ino	12/10/2020	MCNP	6.2.0	NSTS-LS01
TMI-sphereV8C_noBmod_1125_0.1_1.in	12/10/2020	MCNP	6.2.0	NSTS-LS01
TMI-sphereV8C_noBmod_1125_0.1_1.ino	12/10/2020	MCNP	6.2.0	NSTS-LS01
TMI-sphereV8C_noBmod_1125_0.1_1.inr	12/10/2020	MCNP	6.2.0	NSTS-LS01
TMI-sphereV8C_noBmod_1125_0.1_1.ins	12/10/2020	MCNP	6.2.0	NSTS-LS01
TMI-sphereV8C_noBmod_1125_0.15_0.2.in	12/10/2020	MCNP	6.2.0	NSTS-LS01
TMI-sphereV8C_noBmod_1125_0.15_0.2.ino	12/10/2020	MCNP	6.2.0	NSTS-LS01
TMI-sphereV8C_noBmod_1125_0.15_0.2.inr	12/10/2020	MCNP	6.2.0	NSTS-LS01
TMI-sphereV8C_noBmod_1125_0.15_0.2.ins	12/10/2020	MCNP	6.2.0	NSTS-LS01
TMI-sphereV8C_noBmod_1125_0.15_0.3.in	12/10/2020	MCNP	6.2.0	NSTS-LS01
TMI-sphereV8C_noBmod_1125_0.15_0.3.ino	12/10/2020	MCNP	6.2.0	NSTS-LS01
TMI-sphereV8C_noBmod_1125_0.15_0.3.inr	12/10/2020	MCNP	6.2.0	NSTS-LS01
TMI-sphereV8C_noBmod_1125_0.15_0.3.ins	12/10/2020	MCNP	6.2.0	NSTS-LS01
TMI-sphereV8C_noBmod_1125_0.15_0.5.in	12/10/2020	MCNP	6.2.0	NSTS-LS01
TMI-sphereV8C_noBmod_1125_0.15_0.5.ino	12/10/2020	MCNP	6.2.0	NSTS-LS01
TMI-sphereV8C_noBmod_1125_0.15_0.5.inr	12/10/2020	MCNP	6.2.0	NSTS-LS01
TMI-sphereV8C_noBmod_1125_0.15_0.5.ins	12/10/2020	MCNP	6.2.0	NSTS-LS01
TMI-sphereV8C_noBmod_1125_0.15_0.8.in	12/10/2020	MCNP	6.2.0	NSTS-LS01
TMI-sphereV8C_noBmod_1125_0.15_0.8.ino	12/10/2020	MCNP	6.2.0	NSTS-LS01
TMI-sphereV8C_noBmod_1125_0.1621_0.2.in	12/10/2020	MCNP	6.2.0	NSTS-LS01
TMI-sphereV8C_noBmod_1125_0.1621_0.2.ino	12/10/2020	MCNP	6.2.0	NSTS-LS01
TMI-sphereV8C_noBmod_1125_0.1621_0.5.in	12/10/2020	MCNP	6.2.0	NSTS-LS01
TMI-sphereV8C_noBmod_1125_0.1621_0.5.ino	12/10/2020	MCNP	6.2.0	NSTS-LS01
TMI-sphereV8C_noBmod_1125_0.1621_1.in	12/10/2020	MCNP	6.2.0	NSTS-LS01
TMI-sphereV8C_noBmod_1125_0.1621_1.ino	12/10/2020	MCNP	6.2.0	NSTS-LS01
TMI-sphereV8C_noBmod_1200_0.05_0.3.in	12/10/2020	MCNP	6.2.0	NSTS-LS01
TMI-sphereV8C_noBmod_1200_0.05_0.3.ino	12/10/2020	MCNP	6.2.0	NSTS-LS01
TMI-sphereV8C_noBmod_1200_0.05_0.8.in	12/10/2020	MCNP	6.2.0	NSTS-LS01
TMI-sphereV8C_noBmod_1200_0.05_0.8.ino	12/10/2020	MCNP	6.2.0	NSTS-LS01
TMI-sphereV8C_noBmod_1200_0.1_0.2.in	12/10/2020	MCNP	6.2.0	NSTS-LS01
TMI-sphereV8C_noBmod_1200_0.1_0.2.ino	12/10/2020	MCNP	6.2.0	NSTS-LS01
TMI-sphereV8C_noBmod_1200_0.1_0.5.in	12/10/2020	MCNP	6.2.0	NSTS-LS01
TMI-sphereV8C_noBmod_1200_0.1_0.5.ino	12/10/2020	MCNP	6.2.0	NSTS-LS01
TMI-sphereV8C_noBmod_1200_0.1_1.in	12/10/2020	MCNP	6.2.0	NSTS-LS01
TMI-sphereV8C_noBmod_1200_0.1_1.ino	12/10/2020	MCNP	6.2.0	NSTS-LS01
TMI-sphereV8C_noBmod_1200_0.15_0.3.in	12/10/2020	MCNP	6.2.0	NSTS-LS01
TMI-sphereV8C_noBmod_1200_0.15_0.3.ino	12/10/2020	MCNP	6.2.0	NSTS-LS01
TMI-sphereV8C_noBmod_1200_0.15_0.8.in	12/10/2020	MCNP	6.2.0	NSTS-LS01
TMI-sphereV8C_noBmod_1200_0.15_0.8.ino	12/10/2020	MCNP	6.2.0	NSTS-LS01
TMI-sphereV8C_noBmod_1200_0.15_1.in	12/10/2020	MCNP	6.2.0	NSTS-LS01
TMI-sphereV8C_noBmod_1200_0.15_1.ino	12/10/2020	MCNP	6.2.0	NSTS-LS01
TMI-sphereV8C_noBmod_1200_0.1621_0.2.in	12/10/2020	MCNP	6.2.0	NSTS-LS01
TMI-sphereV8C_noBmod_1200_0.1621_0.2.ino	12/10/2020	MCNP	6.2.0	NSTS-LS01
TMI-sphereV8C_noBmod_1200_0.1621_0.3.in	12/10/2020	MCNP	6.2.0	NSTS-LS01
TMI-sphereV8C_noBmod_1200_0.1621_0.3.ino	12/10/2020	MCNP	6.2.0	NSTS-LS01

TMI-sphereV8C_noBmod_1200_0.1621_0.5.in	12/10/2020	MCNP	6.2.0	NSTS-LS01
TMI-sphereV8C_noBmod_1200_0.1621_0.5.ino	12/10/2020	MCNP	6.2.0	NSTS-LS01
TMI-sphereV8C_noBmod_1200_0.1621_0.8.in	12/10/2020	MCNP	6.2.0	NSTS-LS01
TMI-sphereV8C_noBmod_1200_0.1621_0.8.ino	12/10/2020	MCNP	6.2.0	NSTS-LS01
TMI-sphereV8C_noBmod_1200_0.1621_1.in	12/10/2020	MCNP	6.2.0	NSTS-LS01
TMI-sphereV8C_noBmod_1200_0.1621_1.ino	12/10/2020	MCNP	6.2.0	NSTS-LS01
TMI-sphereV8C_noBmod_1500_0.05_0.2.in	12/10/2020	MCNP	6.2.0	NSTS-LS01
TMI-sphereV8C_noBmod_1500_0.05_0.2.ino	12/10/2020	MCNP	6.2.0	NSTS-LS01
TMI-sphereV8C_noBmod_1500_0.05_0.3.in	12/10/2020	MCNP	6.2.0	NSTS-LS01
TMI-sphereV8C_noBmod_1500_0.05_0.3.ino	12/10/2020	MCNP	6.2.0	NSTS-LS01
TMI-sphereV8C_noBmod_1500_0.05_0.5.in	12/10/2020	MCNP	6.2.0	NSTS-LS01
TMI-sphereV8C_noBmod_1500_0.05_0.5.ino	12/10/2020	MCNP	6.2.0	NSTS-LS01
TMI-sphereV8C_noBmod_1500_0.05_0.8.in	12/10/2020	MCNP	6.2.0	NSTS-LS01
TMI-sphereV8C_noBmod_1500_0.05_0.8.ino	12/10/2020	MCNP	6.2.0	NSTS-LS01
TMI-sphereV8C_noBmod_1500_0.05_1.in	12/10/2020	MCNP	6.2.0	NSTS-LS01
TMI-sphereV8C_noBmod_1500_0.05_1.ino	12/10/2020	MCNP	6.2.0	NSTS-LS01
TMI-sphereV8C_noBmod_1500_0.1_0.2.in	12/10/2020	MCNP	6.2.0	NSTS-LS01
TMI-sphereV8C_noBmod_1500_0.1_0.2.ino	12/10/2020	MCNP	6.2.0	NSTS-LS01
TMI-sphereV8C_noBmod_1500_0.1_0.3.in	12/10/2020	MCNP	6.2.0	NSTS-LS01
TMI-sphereV8C_noBmod_1500_0.1_0.3.ino	12/10/2020	MCNP	6.2.0	NSTS-LS01
TMI-sphereV8C_noBmod_1500_0.1_0.5.in	12/10/2020	MCNP	6.2.0	NSTS-LS01
TMI-sphereV8C_noBmod_1500_0.1_0.5.ino	12/10/2020	MCNP	6.2.0	NSTS-LS01
TMI-sphereV8C_noBmod_1500_0.1_0.8.in	12/10/2020	MCNP	6.2.0	NSTS-LS01
TMI-sphereV8C_noBmod_1500_0.1_0.8.ino	12/10/2020	MCNP	6.2.0	NSTS-LS01
TMI-sphereV8C_noBmod_1500_0.1_0.8.inr	12/10/2020	MCNP	6.2.0	NSTS-LS01
TMI-sphereV8C_noBmod_1500_0.1_0.8.ins	12/10/2020	MCNP	6.2.0	NSTS-LS01
TMI-sphereV8C_noBmod_1500_0.1_1.in	12/10/2020	MCNP	6.2.0	NSTS-LS01
TMI-sphereV8C_noBmod_1500_0.1_1.ino	12/10/2020	MCNP	6.2.0	NSTS-LS01
TMI-sphereV8C_noBmod_1500_0.1_1.inr	12/10/2020	MCNP	6.2.0	NSTS-LS01
TMI-sphereV8C_noBmod_1500_0.1_1.ins	12/10/2020	MCNP	6.2.0	NSTS-LS01
TMI-sphereV8C_noBmod_1500_0.15_0.2.in	12/10/2020	MCNP	6.2.0	NSTS-LS01
TMI-sphereV8C_noBmod_1500_0.15_0.2.ino	12/10/2020	MCNP	6.2.0	NSTS-LS01
TMI-sphereV8C_noBmod_1500_0.15_0.2.inr	12/10/2020	MCNP	6.2.0	NSTS-LS01
TMI-sphereV8C_noBmod_1500_0.15_0.2.ins	12/10/2020	MCNP	6.2.0	NSTS-LS01
TMI-sphereV8C_noBmod_1500_0.15_0.3.in	12/10/2020	MCNP	6.2.0	NSTS-LS01
TMI-sphereV8C_noBmod_1500_0.15_0.3.ino	12/10/2020	MCNP	6.2.0	NSTS-LS01
TMI-sphereV8C_noBmod_1500_0.15_0.5.in	12/10/2020	MCNP	6.2.0	NSTS-LS01
TMI-sphereV8C_noBmod_1500_0.15_0.5.ino	12/10/2020	MCNP	6.2.0	NSTS-LS01
TMI-sphereV8C_noBmod_1500_0.15_0.8.in	12/10/2020	MCNP	6.2.0	NSTS-LS01
TMI-sphereV8C_noBmod_1500_0.15_0.8.ino	12/10/2020	MCNP	6.2.0	NSTS-LS01
TMI-sphereV8C_noBmod_1500_0.15_1.in	12/10/2020	MCNP	6.2.0	NSTS-LS01
TMI-sphereV8C_noBmod_1500_0.15_1.ino	12/10/2020	MCNP	6.2.0	NSTS-LS01
TMI-sphereV8C_noBmod_1500_0.1621_0.2.in	12/10/2020	MCNP	6.2.0	NSTS-LS01
TMI-sphereV8C_noBmod_1500_0.1621_0.2.ino	12/10/2020	MCNP	6.2.0	NSTS-LS01
TMI-sphereV8C_noBmod_1500_0.1621_0.3.in	12/10/2020	MCNP	6.2.0	NSTS-LS01
TMI-sphereV8C_noBmod_1500_0.1621_0.3.ino	12/10/2020	MCNP	6.2.0	NSTS-LS01
TMI-sphereV8C_noBmod_1500_0.1621_0.5.in	12/10/2020	MCNP	6.2.0	NSTS-LS01
TMI-sphereV8C_noBmod_1500_0.1621_0.5.ino	12/10/2020	MCNP	6.2.0	NSTS-LS01
TMI-sphereV8C_noBmod_1500_0.1621_0.8.in	12/10/2020	MCNP	6.2.0	NSTS-LS01
TMI-sphereV8C_noBmod_1500_0.1621_0.8.ino	12/10/2020	MCNP	6.2.0	NSTS-LS01
TMI-sphereV8C_noBmod_1500_0.1621_1.in	12/10/2020	MCNP	6.2.0	NSTS-LS01
TMI-sphereV8C_noBmod_1500_0.1621_1.ino	12/10/2020	MCNP	6.2.0	NSTS-LS01
TMI-sphereV8C_noBmod_925_0.05_0.2.in	12/10/2020	MCNP	6.2.0	NSTS-LS01
TMI-sphereV8C_noBmod_925_0.05_0.2.ino	12/10/2020	MCNP	6.2.0	NSTS-LS01
TMI-sphereV8C_noBmod_925_0.05_0.3.in	12/10/2020	MCNP	6.2.0	NSTS-LS01
TMI-sphereV8C_noBmod_925_0.05_0.3.ino	12/10/2020	MCNP	6.2.0	NSTS-LS01
TMI-sphereV8C_noBmod_925_0.05_0.5.in	12/10/2020	MCNP	6.2.0	NSTS-LS01
TMI-sphereV8C_noBmod_925_0.05_0.5.ino	12/10/2020	MCNP	6.2.0	NSTS-LS01
TMI-sphereV8C_noBmod_925_0.05_0.8.in	12/10/2020	MCNP	6.2.0	NSTS-LS01
TMI-sphereV8C_noBmod_925_0.05_0.8.ino	12/10/2020	MCNP	6.2.0	NSTS-LS01
TMI-sphereV8C_noBmod_925_0.05_1.in	12/10/2020	MCNP	6.2.0	NSTS-LS01
TMI-sphereV8C_noBmod_925_0.05_1.ino	12/10/2020	MCNP	6.2.0	NSTS-LS01

TMI-sphereV8C_noBmod_925_0.1_0.2.in	12/10/2020	MCNP	6.2.0	NSTS-LS01
TMI-sphereV8C_noBmod_925_0.1_0.2.ino	12/10/2020	MCNP	6.2.0	NSTS-LS01
TMI-sphereV8C_noBmod_925_0.1_0.3.in	12/10/2020	MCNP	6.2.0	NSTS-LS01
TMI-sphereV8C_noBmod_925_0.1_0.3.ino	12/10/2020	MCNP	6.2.0	NSTS-LS01
TMI-sphereV8C_noBmod_925_0.1_0.5.in	12/10/2020	MCNP	6.2.0	NSTS-LS01
TMI-sphereV8C_noBmod_925_0.1_0.5.ino	12/10/2020	MCNP	6.2.0	NSTS-LS01
TMI-sphereV8C_noBmod_925_0.1_0.8.in	12/10/2020	MCNP	6.2.0	NSTS-LS01
TMI-sphereV8C_noBmod_925_0.1_0.8.ino	12/10/2020	MCNP	6.2.0	NSTS-LS01
TMI-sphereV8C_noBmod_925_0.1_1.in	12/10/2020	MCNP	6.2.0	NSTS-LS01
TMI-sphereV8C_noBmod_925_0.1_1.ino	12/10/2020	MCNP	6.2.0	NSTS-LS01
TMI-sphereV8C_noBmod_925_0.15_0.2.in	12/10/2020	MCNP	6.2.0	NSTS-LS01
TMI-sphereV8C_noBmod_925_0.15_0.2.ino	12/10/2020	MCNP	6.2.0	NSTS-LS01
TMI-sphereV8C_noBmod_925_0.15_0.3.in	12/10/2020	MCNP	6.2.0	NSTS-LS01
TMI-sphereV8C_noBmod_925_0.15_0.3.ino	12/10/2020	MCNP	6.2.0	NSTS-LS01
TMI-sphereV8C_noBmod_925_0.15_0.5.in	12/10/2020	MCNP	6.2.0	NSTS-LS01
TMI-sphereV8C_noBmod_925_0.15_0.5.ino	12/10/2020	MCNP	6.2.0	NSTS-LS01
TMI-sphereV8C_noBmod_925_0.15_0.8.in	12/10/2020	MCNP	6.2.0	NSTS-LS01
TMI-sphereV8C_noBmod_925_0.15_0.8.ino	12/10/2020	MCNP	6.2.0	NSTS-LS01
TMI-sphereV8C_noBmod_925_0.15_1.in	12/10/2020	MCNP	6.2.0	NSTS-LS01
TMI-sphereV8C_noBmod_925_0.15_1.ino	12/10/2020	MCNP	6.2.0	NSTS-LS01
TMI-sphereV8C_noBmod_925_0.1621_0.2.in	12/10/2020	MCNP	6.2.0	NSTS-LS01
TMI-sphereV8C_noBmod_925_0.1621_0.2.ino	12/10/2020	MCNP	6.2.0	NSTS-LS01
TMI-sphereV8C_noBmod_925_0.1621_0.3.in	12/10/2020	MCNP	6.2.0	NSTS-LS01
TMI-sphereV8C_noBmod_925_0.1621_0.3.ino	12/10/2020	MCNP	6.2.0	NSTS-LS01
TMI-sphereV8C_noBmod_925_0.1621_0.5.in	12/10/2020	MCNP	6.2.0	NSTS-LS01
TMI-sphereV8C_noBmod_925_0.1621_0.5.ino	12/10/2020	MCNP	6.2.0	NSTS-LS01
TMI-sphereV8C_noBmod_925_0.1621_0.8.in	12/10/2020	MCNP	6.2.0	NSTS-LS01
TMI-sphereV8C_noBmod_925_0.1621_0.8.ino	12/10/2020	MCNP	6.2.0	NSTS-LS01
TMI-sphereV8C_noBmod_925_0.1621_1.in	12/10/2020	MCNP	6.2.0	NSTS-LS01
TMI-sphereV8C_noBmod_925_0.1621_1.ino	12/10/2020	MCNP	6.2.0	NSTS-LS01
TMI-sphereV8W_noBimp_1125_0.05_100.in	12/8/2020	MCNP	6.2.0	NSTS-LS01
TMI-sphereV8W_noBimp_1125_0.05_100.ino	12/8/2020	MCNP	6.2.0	NSTS-LS01
TMI-sphereV8W_noBimp_1125_0.05_25.in	12/8/2020	MCNP	6.2.0	NSTS-LS01
TMI-sphereV8W_noBimp_1125_0.05_25.ino	12/8/2020	MCNP	6.2.0	NSTS-LS01
TMI-sphereV8W_noBimp_1125_0.05_50.in	12/8/2020	MCNP	6.2.0	NSTS-LS01
TMI-sphereV8W_noBimp_1125_0.05_50.ino	12/8/2020	MCNP	6.2.0	NSTS-LS01
TMI-sphereV8W_noBimp_1125_0.05_75.in	12/8/2020	MCNP	6.2.0	NSTS-LS01
TMI-sphereV8W_noBimp_1125_0.05_75.ino	12/8/2020	MCNP	6.2.0	NSTS-LS01
TMI-sphereV8W_noBimp_1125_0.1_100.in	12/8/2020	MCNP	6.2.0	NSTS-LS01
TMI-sphereV8W_noBimp_1125_0.1_100.ino	12/8/2020	MCNP	6.2.0	NSTS-LS01
TMI-sphereV8W_noBimp_1125_0.1_25.in	12/8/2020	MCNP	6.2.0	NSTS-LS01
TMI-sphereV8W_noBimp_1125_0.1_25.ino	12/8/2020	MCNP	6.2.0	NSTS-LS01
TMI-sphereV8W_noBimp_1125_0.1_50.in	12/8/2020	MCNP	6.2.0	NSTS-LS01
TMI-sphereV8W_noBimp_1125_0.1_50.ino	12/8/2020	MCNP	6.2.0	NSTS-LS01
TMI-sphereV8W_noBimp_1125_0.15_100.in	12/8/2020	MCNP	6.2.0	NSTS-LS01
TMI-sphereV8W_noBimp_1125_0.15_100.ino	12/8/2020	MCNP	6.2.0	NSTS-LS01
TMI-sphereV8W_noBimp_1125_0.15_25.in	12/8/2020	MCNP	6.2.0	NSTS-LS01
TMI-sphereV8W_noBimp_1125_0.15_25.ino	12/8/2020	MCNP	6.2.0	NSTS-LS01
TMI-sphereV8W_noBimp_1125_0.15_50.in	12/8/2020	MCNP	6.2.0	NSTS-LS01
TMI-sphereV8W_noBimp_1125_0.15_50.ino	12/8/2020	MCNP	6.2.0	NSTS-LS01
TMI-sphereV8W_noBimp_1125_0.15_75.in	12/8/2020	MCNP	6.2.0	NSTS-LS01
TMI-sphereV8W_noBimp_1125_0.15_75.ino	12/8/2020	MCNP	6.2.0	NSTS-LS01
TMI-sphereV8W_noBimp_1125_0.1621_100.in	12/8/2020	MCNP	6.2.0	NSTS-LS01
TMI-sphereV8W_noBimp_1125_0.1621_100.ino	12/8/2020	MCNP	6.2.0	NSTS-LS01
TMI-sphereV8W_noBimp_1125_0.1621_25.in	12/8/2020	MCNP	6.2.0	NSTS-LS01
TMI-sphereV8W_noBimp_1125_0.1621_25.ino	12/8/2020	MCNP	6.2.0	NSTS-LS01
TMI-sphereV8W_noBimp_1125_0.1621_50.in	12/8/2020	MCNP	6.2.0	NSTS-LS01
TMI-sphereV8W_noBimp_1125_0.1621_50.ino	12/8/2020	MCNP	6.2.0	NSTS-LS01
TMI-sphereV8W_noBimp_1125_0.1621_75.in	12/8/2020	MCNP	6.2.0	NSTS-LS01
TMI-sphereV8W_noBimp_1125_0.1621_75.ino	12/8/2020	MCNP	6.2.0	NSTS-LS01
TMI-sphereV8W_noBimp_1125_0.1_75.in	12/8/2020	MCNP	6.2.0	NSTS-LS01
TMI-sphereV8W_noBimp_1125_0.1_75.ino	12/8/2020	MCNP	6.2.0	NSTS-LS01

TMI-sphereV8W_noBimp_1200_0.05_100.in	12/8/2020	MCNP	6.2.0	NSTS-LS01
TMI-sphereV8W_noBimp_1200_0.05_100.ino	12/8/2020	MCNP	6.2.0	NSTS-LS01
TMI-sphereV8W_noBimp_1200_0.05_25.in	12/8/2020	MCNP	6.2.0	NSTS-LS01
TMI-sphereV8W_noBimp_1200_0.05_25.ino	12/8/2020	MCNP	6.2.0	NSTS-LS01
TMI-sphereV8W_noBimp_1200_0.05_50.in	12/8/2020	MCNP	6.2.0	NSTS-LS01
TMI-sphereV8W_noBimp_1200_0.05_50.ino	12/8/2020	MCNP	6.2.0	NSTS-LS01
TMI-sphereV8W_noBimp_1200_0.05_75.in	12/8/2020	MCNP	6.2.0	NSTS-LS01
TMI-sphereV8W_noBimp_1200_0.05_75.ino	12/8/2020	MCNP	6.2.0	NSTS-LS01
TMI-sphereV8W_noBimp_1200_0.1_100.in	12/8/2020	MCNP	6.2.0	NSTS-LS01
TMI-sphereV8W_noBimp_1200_0.1_100.ino	12/8/2020	MCNP	6.2.0	NSTS-LS01
TMI-sphereV8W_noBimp_1200_0.1_25.in	12/8/2020	MCNP	6.2.0	NSTS-LS01
TMI-sphereV8W_noBimp_1200_0.1_25.ino	12/8/2020	MCNP	6.2.0	NSTS-LS01
TMI-sphereV8W_noBimp_1200_0.1_50.in	12/8/2020	MCNP	6.2.0	NSTS-LS01
TMI-sphereV8W_noBimp_1200_0.1_50.ino	12/8/2020	MCNP	6.2.0	NSTS-LS01
TMI-sphereV8W_noBimp_1200_0.15_100.in	12/8/2020	MCNP	6.2.0	NSTS-LS01
TMI-sphereV8W_noBimp_1200_0.15_100.ino	12/8/2020	MCNP	6.2.0	NSTS-LS01
TMI-sphereV8W_noBimp_1200_0.15_25.in	12/8/2020	MCNP	6.2.0	NSTS-LS01
TMI-sphereV8W_noBimp_1200_0.15_25.ino	12/8/2020	MCNP	6.2.0	NSTS-LS01
TMI-sphereV8W_noBimp_1200_0.15_50.in	12/8/2020	MCNP	6.2.0	NSTS-LS01
TMI-sphereV8W_noBimp_1200_0.15_50.ino	12/8/2020	MCNP	6.2.0	NSTS-LS01
TMI-sphereV8W_noBimp_1200_0.15_75.in	12/8/2020	MCNP	6.2.0	NSTS-LS01
TMI-sphereV8W_noBimp_1200_0.15_75.ino	12/8/2020	MCNP	6.2.0	NSTS-LS01
TMI-sphereV8W_noBimp_1200_0.1621_100.in	12/8/2020	MCNP	6.2.0	NSTS-LS01
TMI-sphereV8W_noBimp_1200_0.1621_100.ino	12/8/2020	MCNP	6.2.0	NSTS-LS01
TMI-sphereV8W_noBimp_1200_0.1621_25.in	12/8/2020	MCNP	6.2.0	NSTS-LS01
TMI-sphereV8W_noBimp_1200_0.1621_25.ino	12/8/2020	MCNP	6.2.0	NSTS-LS01
TMI-sphereV8W_noBimp_1200_0.1621_50.in	12/8/2020	MCNP	6.2.0	NSTS-LS01
TMI-sphereV8W_noBimp_1200_0.1621_50.ino	12/8/2020	MCNP	6.2.0	NSTS-LS01
TMI-sphereV8W_noBimp_1200_0.1621_75.in	12/8/2020	MCNP	6.2.0	NSTS-LS01
TMI-sphereV8W_noBimp_1200_0.1621_75.ino	12/8/2020	MCNP	6.2.0	NSTS-LS01
TMI-sphereV8W_noBimp_1200_0.1_75.in	12/8/2020	MCNP	6.2.0	NSTS-LS01
TMI-sphereV8W_noBimp_1200_0.1_75.ino	12/8/2020	MCNP	6.2.0	NSTS-LS01
TMI-sphereV8W_noBimp_1500_0.05_100.in	12/8/2020	MCNP	6.2.0	NSTS-LS01
TMI-sphereV8W_noBimp_1500_0.05_100.ino	12/8/2020	MCNP	6.2.0	NSTS-LS01
TMI-sphereV8W_noBimp_1500_0.05_25.in	12/8/2020	MCNP	6.2.0	NSTS-LS01
TMI-sphereV8W_noBimp_1500_0.05_25.ino	12/8/2020	MCNP	6.2.0	NSTS-LS01
TMI-sphereV8W_noBimp_1500_0.05_50.in	12/8/2020	MCNP	6.2.0	NSTS-LS01
TMI-sphereV8W_noBimp_1500_0.05_50.ino	12/8/2020	MCNP	6.2.0	NSTS-LS01
TMI-sphereV8W_noBimp_1500_0.05_75.in	12/8/2020	MCNP	6.2.0	NSTS-LS01
TMI-sphereV8W_noBimp_1500_0.05_75.ino	12/8/2020	MCNP	6.2.0	NSTS-LS01
TMI-sphereV8W_noBimp_1500_0.1_100.in	12/8/2020	MCNP	6.2.0	NSTS-LS01
TMI-sphereV8W_noBimp_1500_0.1_100.ino	12/8/2020	MCNP	6.2.0	NSTS-LS01
TMI-sphereV8W_noBimp_1500_0.1_25.in	12/8/2020	MCNP	6.2.0	NSTS-LS01
TMI-sphereV8W_noBimp_1500_0.1_25.ino	12/8/2020	MCNP	6.2.0	NSTS-LS01
TMI-sphereV8W_noBimp_1500_0.1_50.in	12/8/2020	MCNP	6.2.0	NSTS-LS01
TMI-sphereV8W_noBimp_1500_0.1_50.ino	12/8/2020	MCNP	6.2.0	NSTS-LS01
TMI-sphereV8W_noBimp_1500_0.15_100.in	12/8/2020	MCNP	6.2.0	NSTS-LS01
TMI-sphereV8W_noBimp_1500_0.15_100.ino	12/8/2020	MCNP	6.2.0	NSTS-LS01
TMI-sphereV8W_noBimp_1500_0.15_25.in	12/8/2020	MCNP	6.2.0	NSTS-LS01
TMI-sphereV8W_noBimp_1500_0.15_25.ino	12/8/2020	MCNP	6.2.0	NSTS-LS01
TMI-sphereV8W_noBimp_1500_0.15_50.in	12/8/2020	MCNP	6.2.0	NSTS-LS01
TMI-sphereV8W_noBimp_1500_0.15_50.ino	12/8/2020	MCNP	6.2.0	NSTS-LS01
TMI-sphereV8W_noBimp_1500_0.15_75.in	12/8/2020	MCNP	6.2.0	NSTS-LS01
TMI-sphereV8W_noBimp_1500_0.15_75.ino	12/8/2020	MCNP	6.2.0	NSTS-LS01
TMI-sphereV8W_noBimp_1500_0.1621_100.in	12/8/2020	MCNP	6.2.0	NSTS-LS01
TMI-sphereV8W_noBimp_1500_0.1621_100.ino	12/8/2020	MCNP	6.2.0	NSTS-LS01
TMI-sphereV8W_noBimp_1500_0.1621_25.in	12/8/2020	MCNP	6.2.0	NSTS-LS01
TMI-sphereV8W_noBimp_1500_0.1621_25.ino	12/8/2020	MCNP	6.2.0	NSTS-LS01
TMI-sphereV8W_noBimp_1500_0.1621_50.in	12/8/2020	MCNP	6.2.0	NSTS-LS01
TMI-sphereV8W_noBimp_1500_0.1621_50.ino	12/8/2020	MCNP	6.2.0	NSTS-LS01
TMI-sphereV8W_noBimp_1500_0.1621_75.in	12/8/2020	MCNP	6.2.0	NSTS-LS01
TMI-sphereV8W_noBimp_1500_0.1621_75.ino	12/8/2020	MCNP	6.2.0	NSTS-LS01

TMI-sphereV8W_noBimp_1500_0.1_75.in	12/8/2020	MCNP	6.2.0	NSTS-LS01
TMI-sphereV8W_noBimp_1500_0.1_75.ino	12/8/2020	MCNP	6.2.0	NSTS-LS01
TMI-sphereV8W_noBimp_1750_0.05_100.in	12/8/2020	MCNP	6.2.0	NSTS-LS01
TMI-sphereV8W_noBimp_1750_0.05_100.ino	12/8/2020	MCNP	6.2.0	NSTS-LS01
TMI-sphereV8W_noBimp_1750_0.05_25.in	12/8/2020	MCNP	6.2.0	NSTS-LS01
TMI-sphereV8W_noBimp_1750_0.05_25.ino	12/8/2020	MCNP	6.2.0	NSTS-LS01
TMI-sphereV8W_noBimp_1750_0.05_50.in	12/8/2020	MCNP	6.2.0	NSTS-LS01
TMI-sphereV8W_noBimp_1750_0.05_50.ino	12/8/2020	MCNP	6.2.0	NSTS-LS01
TMI-sphereV8W_noBimp_1750_0.05_75.in	12/8/2020	MCNP	6.2.0	NSTS-LS01
TMI-sphereV8W_noBimp_1750_0.05_75.ino	12/8/2020	MCNP	6.2.0	NSTS-LS01
TMI-sphereV8W_noBimp_1750_0.1_100.in	12/8/2020	MCNP	6.2.0	NSTS-LS01
TMI-sphereV8W_noBimp_1750_0.1_100.ino	12/8/2020	MCNP	6.2.0	NSTS-LS01
TMI-sphereV8W_noBimp_1750_0.1_25.in	12/8/2020	MCNP	6.2.0	NSTS-LS01
TMI-sphereV8W_noBimp_1750_0.1_25.ino	12/8/2020	MCNP	6.2.0	NSTS-LS01
TMI-sphereV8W_noBimp_1750_0.1_50.in	12/8/2020	MCNP	6.2.0	NSTS-LS01
TMI-sphereV8W_noBimp_1750_0.1_50.ino	12/8/2020	MCNP	6.2.0	NSTS-LS01
TMI-sphereV8W_noBimp_1750_0.15_100.in	12/8/2020	MCNP	6.2.0	NSTS-LS01
TMI-sphereV8W_noBimp_1750_0.15_100.ino	12/8/2020	MCNP	6.2.0	NSTS-LS01
TMI-sphereV8W_noBimp_1750_0.15_25.in	12/8/2020	MCNP	6.2.0	NSTS-LS01
TMI-sphereV8W_noBimp_1750_0.15_25.ino	12/8/2020	MCNP	6.2.0	NSTS-LS01
TMI-sphereV8W_noBimp_1750_0.15_50.in	12/8/2020	MCNP	6.2.0	NSTS-LS01
TMI-sphereV8W_noBimp_1750_0.15_50.ino	12/8/2020	MCNP	6.2.0	NSTS-LS01
TMI-sphereV8W_noBimp_1750_0.15_75.in	12/8/2020	MCNP	6.2.0	NSTS-LS01
TMI-sphereV8W_noBimp_1750_0.15_75.ino	12/8/2020	MCNP	6.2.0	NSTS-LS01
TMI-sphereV8W_noBimp_1750_0.1621_100.in	12/8/2020	MCNP	6.2.0	NSTS-LS01
TMI-sphereV8W_noBimp_1750_0.1621_100.ino	12/8/2020	MCNP	6.2.0	NSTS-LS01
TMI-sphereV8W_noBimp_1750_0.1621_25.in	12/8/2020	MCNP	6.2.0	NSTS-LS01
TMI-sphereV8W_noBimp_1750_0.1621_25.ino	12/8/2020	MCNP	6.2.0	NSTS-LS01
TMI-sphereV8W_noBimp_1750_0.1621_50.in	12/8/2020	MCNP	6.2.0	NSTS-LS01
TMI-sphereV8W_noBimp_1750_0.1621_50.ino	12/8/2020	MCNP	6.2.0	NSTS-LS01
TMI-sphereV8W_noBimp_1750_0.1621_75.in	12/8/2020	MCNP	6.2.0	NSTS-LS01
TMI-sphereV8W_noBimp_1750_0.1621_75.ino	12/8/2020	MCNP	6.2.0	NSTS-LS01
TMI-sphereV8W_noBimp_1750_0.1_75.in	12/8/2020	MCNP	6.2.0	NSTS-LS01
TMI-sphereV8W_noBimp_1750_0.1_75.ino	12/8/2020	MCNP	6.2.0	NSTS-LS01
TMI-sphereV8W_noBimp_925_0.05_100.in	12/8/2020	MCNP	6.2.0	NSTS-LS01
TMI-sphereV8W_noBimp_925_0.05_100.ino	12/8/2020	MCNP	6.2.0	NSTS-LS01
TMI-sphereV8W_noBimp_925_0.05_25.in	12/8/2020	MCNP	6.2.0	NSTS-LS01
TMI-sphereV8W_noBimp_925_0.05_25.ino	12/8/2020	MCNP	6.2.0	NSTS-LS01
TMI-sphereV8W_noBimp_925_0.05_50.in	12/8/2020	MCNP	6.2.0	NSTS-LS01
TMI-sphereV8W_noBimp_925_0.05_50.ino	12/8/2020	MCNP	6.2.0	NSTS-LS01
TMI-sphereV8W_noBimp_925_0.05_75.in	12/8/2020	MCNP	6.2.0	NSTS-LS01
TMI-sphereV8W_noBimp_925_0.05_75.ino	12/8/2020	MCNP	6.2.0	NSTS-LS01
TMI-sphereV8W_noBimp_925_0.1_100.in	12/8/2020	MCNP	6.2.0	NSTS-LS01
TMI-sphereV8W_noBimp_925_0.1_100.ino	12/8/2020	MCNP	6.2.0	NSTS-LS01
TMI-sphereV8W_noBimp_925_0.1_25.in	12/8/2020	MCNP	6.2.0	NSTS-LS01
TMI-sphereV8W_noBimp_925_0.1_25.ino	12/8/2020	MCNP	6.2.0	NSTS-LS01
TMI-sphereV8W_noBimp_925_0.1_50.in	12/8/2020	MCNP	6.2.0	NSTS-LS01
TMI-sphereV8W_noBimp_925_0.1_50.ino	12/8/2020	MCNP	6.2.0	NSTS-LS01
TMI-sphereV8W_noBimp_925_0.15_100.in	12/8/2020	MCNP	6.2.0	NSTS-LS01
TMI-sphereV8W_noBimp_925_0.15_100.ino	12/8/2020	MCNP	6.2.0	NSTS-LS01
TMI-sphereV8W_noBimp_925_0.15_25.in	12/8/2020	MCNP	6.2.0	NSTS-LS01
TMI-sphereV8W_noBimp_925_0.15_25.ino	12/8/2020	MCNP	6.2.0	NSTS-LS01
TMI-sphereV8W_noBimp_925_0.15_50.in	12/8/2020	MCNP	6.2.0	NSTS-LS01
TMI-sphereV8W_noBimp_925_0.15_50.ino	12/8/2020	MCNP	6.2.0	NSTS-LS01
TMI-sphereV8W_noBimp_925_0.15_75.in	12/8/2020	MCNP	6.2.0	NSTS-LS01
TMI-sphereV8W_noBimp_925_0.15_75.ino	12/8/2020	MCNP	6.2.0	NSTS-LS01
TMI-sphereV8W_noBimp_925_0.1621_100.in	12/8/2020	MCNP	6.2.0	NSTS-LS01
TMI-sphereV8W_noBimp_925_0.1621_100.ino	12/8/2020	MCNP	6.2.0	NSTS-LS01
TMI-sphereV8W_noBimp_925_0.1621_25.in	12/8/2020	MCNP	6.2.0	NSTS-LS01
TMI-sphereV8W_noBimp_925_0.1621_25.ino	12/8/2020	MCNP	6.2.0	NSTS-LS01
TMI-sphereV8W_noBimp_925_0.1621_50.in	12/8/2020	MCNP	6.2.0	NSTS-LS01
TMI-sphereV8W_noBimp_925_0.1621_50.ino	12/8/2020	MCNP	6.2.0	NSTS-LS01

TMI-sphereV8W_noBimp_925_0.1621_75.in	12/8/2020	MCNP	6.2.0	NSTS-LS01
TMI-sphereV8W_noBimp_925_0.1621_75.ino	12/8/2020	MCNP	6.2.0	NSTS-LS01
TMI-sphereV8W_noBimp_925_0.1_75.in	12/8/2020	MCNP	6.2.0	NSTS-LS01
TMI-sphereV8W_noBimp_925_0.1_75.ino	12/8/2020	MCNP	6.2.0	NSTS-LS01
TMI-sphereV8W_noBnoB_1125_0.05.in	12/8/2020	MCNP	6.2.0	NSTS-LS01
TMI-sphereV8W_noBnoB_1125_0.05.ino	12/8/2020	MCNP	6.2.0	NSTS-LS01
TMI-sphereV8W_noBnoB_1125_0.15.in	12/8/2020	MCNP	6.2.0	NSTS-LS01
TMI-sphereV8W_noBnoB_1125_0.15.ino	12/8/2020	MCNP	6.2.0	NSTS-LS01
TMI-sphereV8W_noBnoB_1125_0.1621.in	12/8/2020	MCNP	6.2.0	NSTS-LS01
TMI-sphereV8W_noBnoB_1125_0.1621.ino	12/8/2020	MCNP	6.2.0	NSTS-LS01
TMI-sphereV8W_noBnoB_1125_0.1.in	12/8/2020	MCNP	6.2.0	NSTS-LS01
TMI-sphereV8W_noBnoB_1125_0.1.ino	12/8/2020	MCNP	6.2.0	NSTS-LS01
TMI-sphereV8W_noBnoB_1200_0.05.in	12/8/2020	MCNP	6.2.0	NSTS-LS01
TMI-sphereV8W_noBnoB_1200_0.05.ino	12/8/2020	MCNP	6.2.0	NSTS-LS01
TMI-sphereV8W_noBnoB_1200_0.15.in	12/8/2020	MCNP	6.2.0	NSTS-LS01
TMI-sphereV8W_noBnoB_1200_0.15.ino	12/8/2020	MCNP	6.2.0	NSTS-LS01
TMI-sphereV8W_noBnoB_1200_0.1621.in	12/8/2020	MCNP	6.2.0	NSTS-LS01
TMI-sphereV8W_noBnoB_1200_0.1621.ino	12/8/2020	MCNP	6.2.0	NSTS-LS01
TMI-sphereV8W_noBnoB_1200_0.1.in	12/8/2020	MCNP	6.2.0	NSTS-LS01
TMI-sphereV8W_noBnoB_1200_0.1.ino	12/8/2020	MCNP	6.2.0	NSTS-LS01
TMI-sphereV8W_noBnoB_1500_0.05.in	12/8/2020	MCNP	6.2.0	NSTS-LS01
TMI-sphereV8W_noBnoB_1500_0.05.ino	12/8/2020	MCNP	6.2.0	NSTS-LS01
TMI-sphereV8W_noBnoB_1500_0.15.in	12/8/2020	MCNP	6.2.0	NSTS-LS01
TMI-sphereV8W_noBnoB_1500_0.15.ino	12/8/2020	MCNP	6.2.0	NSTS-LS01
TMI-sphereV8W_noBnoB_1500_0.1621.in	12/8/2020	MCNP	6.2.0	NSTS-LS01
TMI-sphereV8W_noBnoB_1500_0.1621.ino	12/8/2020	MCNP	6.2.0	NSTS-LS01
TMI-sphereV8W_noBnoB_1500_0.1.in	12/8/2020	MCNP	6.2.0	NSTS-LS01
TMI-sphereV8W_noBnoB_1500_0.1.ino	12/8/2020	MCNP	6.2.0	NSTS-LS01
TMI-sphereV8W_noBnoB_1750_0.05.in	12/8/2020	MCNP	6.2.0	NSTS-LS01
TMI-sphereV8W_noBnoB_1750_0.05.ino	12/8/2020	MCNP	6.2.0	NSTS-LS01
TMI-sphereV8W_noBnoB_1750_0.15.in	12/8/2020	MCNP	6.2.0	NSTS-LS01
TMI-sphereV8W_noBnoB_1750_0.15.ino	12/8/2020	MCNP	6.2.0	NSTS-LS01
TMI-sphereV8W_noBnoB_1750_0.1621.in	12/8/2020	MCNP	6.2.0	NSTS-LS01
TMI-sphereV8W_noBnoB_1750_0.1621.ino	12/8/2020	MCNP	6.2.0	NSTS-LS01
TMI-sphereV8W_noBnoB_1750_0.1.in	12/8/2020	MCNP	6.2.0	NSTS-LS01
TMI-sphereV8W_noBnoB_1750_0.1.ino	12/8/2020	MCNP	6.2.0	NSTS-LS01
TMI-sphereV8W_noBnoB_925_0.05.in	12/8/2020	MCNP	6.2.0	NSTS-LS01
TMI-sphereV8W_noBnoB_925_0.05.ino	12/8/2020	MCNP	6.2.0	NSTS-LS01
TMI-sphereV8W_noBnoB_925_0.15.in	12/8/2020	MCNP	6.2.0	NSTS-LS01
TMI-sphereV8W_noBnoB_925_0.15.ino	12/8/2020	MCNP	6.2.0	NSTS-LS01
TMI-sphereV8W_noBnoB_925_0.1621.in	12/8/2020	MCNP	6.2.0	NSTS-LS01
TMI-sphereV8W_noBnoB_925_0.1621.ino	12/8/2020	MCNP	6.2.0	NSTS-LS01
TMI-sphereV8W_noBnoB_925_0.1.in	12/8/2020	MCNP	6.2.0	NSTS-LS01
TMI-sphereV8W_noBnoB_925_0.1.ino	12/8/2020	MCNP	6.2.0	NSTS-LS01
TMI-sphereV8W_noBimp_1125_0.05_100.in	12/8/2020	MCNP	6.2.0	NSTS-LS01
TMI-sphereV8W_noBimp_1125_0.05_100.ino	12/8/2020	MCNP	6.2.0	NSTS-LS01
TMI-sphereV8W_noBimp_1125_0.05_25.in	12/8/2020	MCNP	6.2.0	NSTS-LS01
TMI-sphereV8W_noBimp_1125_0.05_25.ino	12/8/2020	MCNP	6.2.0	NSTS-LS01
TMI-sphereV8W_noBimp_1125_0.05_50.in	12/8/2020	MCNP	6.2.0	NSTS-LS01
TMI-sphereV8W_noBimp_1125_0.05_50.ino	12/8/2020	MCNP	6.2.0	NSTS-LS01
TMI-sphereV8W_noBimp_1125_0.05_75.in	12/8/2020	MCNP	6.2.0	NSTS-LS01
TMI-sphereV8W_noBimp_1125_0.05_75.ino	12/8/2020	MCNP	6.2.0	NSTS-LS01
TMI-sphereV8W_noBimp_1125_0.1_100.in	12/8/2020	MCNP	6.2.0	NSTS-LS01
TMI-sphereV8W_noBimp_1125_0.1_100.ino	12/8/2020	MCNP	6.2.0	NSTS-LS01
TMI-sphereV8W_noBimp_1125_0.1_25.in	12/8/2020	MCNP	6.2.0	NSTS-LS01
TMI-sphereV8W_noBimp_1125_0.1_25.ino	12/8/2020	MCNP	6.2.0	NSTS-LS01
TMI-sphereV8W_noBimp_1125_0.1_50.in	12/8/2020	MCNP	6.2.0	NSTS-LS01
TMI-sphereV8W_noBimp_1125_0.1_50.ino	12/8/2020	MCNP	6.2.0	NSTS-LS01
TMI-sphereV8W_noBimp_1125_0.15_100.in	12/8/2020	MCNP	6.2.0	NSTS-LS01
TMI-sphereV8W_noBimp_1125_0.15_100.ino	12/8/2020	MCNP	6.2.0	NSTS-LS01
TMI-sphereV8W_noBimp_1125_0.15_25.in	12/8/2020	MCNP	6.2.0	NSTS-LS01
TMI-sphereV8W_noBimp_1125_0.15_25.ino	12/8/2020	MCNP	6.2.0	NSTS-LS01

TMI-sphereV8W_noBimp_1125_0.15_50.in	12/8/2020	MCNP	6.2.0	NSTS-LS01
TMI-sphereV8W_noBimp_1125_0.15_50.ino	12/8/2020	MCNP	6.2.0	NSTS-LS01
TMI-sphereV8W_noBimp_1125_0.15_75.in	12/8/2020	MCNP	6.2.0	NSTS-LS01
TMI-sphereV8W_noBimp_1125_0.15_75.ino	12/8/2020	MCNP	6.2.0	NSTS-LS01
TMI-sphereV8W_noBimp_1125_0.1621_100.in	12/8/2020	MCNP	6.2.0	NSTS-LS01
TMI-sphereV8W_noBimp_1125_0.1621_100.ino	12/8/2020	MCNP	6.2.0	NSTS-LS01
TMI-sphereV8W_noBimp_1125_0.1621_25.in	12/8/2020	MCNP	6.2.0	NSTS-LS01
TMI-sphereV8W_noBimp_1125_0.1621_25.ino	12/8/2020	MCNP	6.2.0	NSTS-LS01
TMI-sphereV8W_noBimp_1125_0.1621_50.in	12/8/2020	MCNP	6.2.0	NSTS-LS01
TMI-sphereV8W_noBimp_1125_0.1621_50.ino	12/8/2020	MCNP	6.2.0	NSTS-LS01
TMI-sphereV8W_noBimp_1125_0.1621_75.in	12/8/2020	MCNP	6.2.0	NSTS-LS01
TMI-sphereV8W_noBimp_1125_0.1621_75.ino	12/8/2020	MCNP	6.2.0	NSTS-LS01
TMI-sphereV8W_noBimp_1125_0.1_75.in	12/8/2020	MCNP	6.2.0	NSTS-LS01
TMI-sphereV8W_noBimp_1125_0.1_75.ino	12/8/2020	MCNP	6.2.0	NSTS-LS01
TMI-sphereV8W_noBimp_1200_0.05_100.in	12/8/2020	MCNP	6.2.0	NSTS-LS01
TMI-sphereV8W_noBimp_1200_0.05_100.ino	12/8/2020	MCNP	6.2.0	NSTS-LS01
TMI-sphereV8W_noBimp_1200_0.05_25.in	12/8/2020	MCNP	6.2.0	NSTS-LS01
TMI-sphereV8W_noBimp_1200_0.05_25.ino	12/8/2020	MCNP	6.2.0	NSTS-LS01
TMI-sphereV8W_noBimp_1200_0.05_50.in	12/8/2020	MCNP	6.2.0	NSTS-LS01
TMI-sphereV8W_noBimp_1200_0.05_50.ino	12/8/2020	MCNP	6.2.0	NSTS-LS01
TMI-sphereV8W_noBimp_1200_0.05_75.in	12/8/2020	MCNP	6.2.0	NSTS-LS01
TMI-sphereV8W_noBimp_1200_0.05_75.ino	12/8/2020	MCNP	6.2.0	NSTS-LS01
TMI-sphereV8W_noBimp_1200_0.1_100.in	12/8/2020	MCNP	6.2.0	NSTS-LS01
TMI-sphereV8W_noBimp_1200_0.1_100.ino	12/8/2020	MCNP	6.2.0	NSTS-LS01
TMI-sphereV8W_noBimp_1200_0.1_25.in	12/8/2020	MCNP	6.2.0	NSTS-LS01
TMI-sphereV8W_noBimp_1200_0.1_25.ino	12/8/2020	MCNP	6.2.0	NSTS-LS01
TMI-sphereV8W_noBimp_1200_0.1_50.in	12/8/2020	MCNP	6.2.0	NSTS-LS01
TMI-sphereV8W_noBimp_1200_0.1_50.ino	12/8/2020	MCNP	6.2.0	NSTS-LS01
TMI-sphereV8W_noBimp_1200_0.15_100.in	12/8/2020	MCNP	6.2.0	NSTS-LS01
TMI-sphereV8W_noBimp_1200_0.15_100.ino	12/8/2020	MCNP	6.2.0	NSTS-LS01
TMI-sphereV8W_noBimp_1200_0.15_25.in	12/8/2020	MCNP	6.2.0	NSTS-LS01
TMI-sphereV8W_noBimp_1200_0.15_25.ino	12/8/2020	MCNP	6.2.0	NSTS-LS01
TMI-sphereV8W_noBimp_1200_0.15_50.in	12/8/2020	MCNP	6.2.0	NSTS-LS01
TMI-sphereV8W_noBimp_1200_0.15_50.ino	12/8/2020	MCNP	6.2.0	NSTS-LS01
TMI-sphereV8W_noBimp_1200_0.15_75.in	12/8/2020	MCNP	6.2.0	NSTS-LS01
TMI-sphereV8W_noBimp_1200_0.15_75.ino	12/8/2020	MCNP	6.2.0	NSTS-LS01
TMI-sphereV8W_noBimp_1200_0.1621_100.in	12/8/2020	MCNP	6.2.0	NSTS-LS01
TMI-sphereV8W_noBimp_1200_0.1621_100.ino	12/8/2020	MCNP	6.2.0	NSTS-LS01
TMI-sphereV8W_noBimp_1200_0.1621_25.in	12/8/2020	MCNP	6.2.0	NSTS-LS01
TMI-sphereV8W_noBimp_1200_0.1621_25.ino	12/8/2020	MCNP	6.2.0	NSTS-LS01
TMI-sphereV8W_noBimp_1200_0.1621_50.in	12/8/2020	MCNP	6.2.0	NSTS-LS01
TMI-sphereV8W_noBimp_1200_0.1621_50.ino	12/8/2020	MCNP	6.2.0	NSTS-LS01
TMI-sphereV8W_noBimp_1200_0.1621_75.in	12/8/2020	MCNP	6.2.0	NSTS-LS01
TMI-sphereV8W_noBimp_1200_0.1621_75.ino	12/8/2020	MCNP	6.2.0	NSTS-LS01
TMI-sphereV8W_noBimp_1200_0.1_75.in	12/8/2020	MCNP	6.2.0	NSTS-LS01
TMI-sphereV8W_noBimp_1200_0.1_75.ino	12/8/2020	MCNP	6.2.0	NSTS-LS01
TMI-sphereV8W_noBimp_1500_0.05_100.in	12/8/2020	MCNP	6.2.0	NSTS-LS01
TMI-sphereV8W_noBimp_1500_0.05_100.ino	12/8/2020	MCNP	6.2.0	NSTS-LS01
TMI-sphereV8W_noBimp_1500_0.05_25.in	12/8/2020	MCNP	6.2.0	NSTS-LS01
TMI-sphereV8W_noBimp_1500_0.05_25.ino	12/8/2020	MCNP	6.2.0	NSTS-LS01
TMI-sphereV8W_noBimp_1500_0.05_50.in	12/8/2020	MCNP	6.2.0	NSTS-LS01
TMI-sphereV8W_noBimp_1500_0.05_50.ino	12/8/2020	MCNP	6.2.0	NSTS-LS01
TMI-sphereV8W_noBimp_1500_0.05_75.in	12/8/2020	MCNP	6.2.0	NSTS-LS01
TMI-sphereV8W_noBimp_1500_0.05_75.ino	12/8/2020	MCNP	6.2.0	NSTS-LS01
TMI-sphereV8W_noBimp_1500_0.1_100.in	12/8/2020	MCNP	6.2.0	NSTS-LS01
TMI-sphereV8W_noBimp_1500_0.1_100.ino	12/8/2020	MCNP	6.2.0	NSTS-LS01
TMI-sphereV8W_noBimp_1500_0.1_25.in	12/8/2020	MCNP	6.2.0	NSTS-LS01
TMI-sphereV8W_noBimp_1500_0.1_25.ino	12/8/2020	MCNP	6.2.0	NSTS-LS01
TMI-sphereV8W_noBimp_1500_0.1_50.in	12/8/2020	MCNP	6.2.0	NSTS-LS01
TMI-sphereV8W_noBimp_1500_0.1_50.ino	12/8/2020	MCNP	6.2.0	NSTS-LS01
TMI-sphereV8W_noBimp_1500_0.15_100.in	12/8/2020	MCNP	6.2.0	NSTS-LS01
TMI-sphereV8W_noBimp_1500_0.15_100.ino	12/8/2020	MCNP	6.2.0	NSTS-LS01

TMI-sphereV8W_noBimp_1500_0.15_25.in	12/8/2020	MCNP	6.2.0	NSTS-LS01
TMI-sphereV8W_noBimp_1500_0.15_25.ino	12/8/2020	MCNP	6.2.0	NSTS-LS01
TMI-sphereV8W_noBimp_1500_0.15_50.in	12/8/2020	MCNP	6.2.0	NSTS-LS01
TMI-sphereV8W_noBimp_1500_0.15_50.ino	12/8/2020	MCNP	6.2.0	NSTS-LS01
TMI-sphereV8W_noBimp_1500_0.15_75.in	12/8/2020	MCNP	6.2.0	NSTS-LS01
TMI-sphereV8W_noBimp_1500_0.15_75.ino	12/8/2020	MCNP	6.2.0	NSTS-LS01
TMI-sphereV8W_noBimp_1500_0.1621_100.in	12/8/2020	MCNP	6.2.0	NSTS-LS01
TMI-sphereV8W_noBimp_1500_0.1621_100.ino	12/8/2020	MCNP	6.2.0	NSTS-LS01
TMI-sphereV8W_noBimp_1500_0.1621_25.in	12/8/2020	MCNP	6.2.0	NSTS-LS01
TMI-sphereV8W_noBimp_1500_0.1621_25.ino	12/8/2020	MCNP	6.2.0	NSTS-LS01
TMI-sphereV8W_noBimp_1500_0.1621_50.in	12/8/2020	MCNP	6.2.0	NSTS-LS01
TMI-sphereV8W_noBimp_1500_0.1621_50.ino	12/8/2020	MCNP	6.2.0	NSTS-LS01
TMI-sphereV8W_noBimp_1500_0.1621_75.in	12/8/2020	MCNP	6.2.0	NSTS-LS01
TMI-sphereV8W_noBimp_1500_0.1621_75.ino	12/8/2020	MCNP	6.2.0	NSTS-LS01
TMI-sphereV8W_noBimp_1500_0.1_75.in	12/8/2020	MCNP	6.2.0	NSTS-LS01
TMI-sphereV8W_noBimp_1500_0.1_75.ino	12/8/2020	MCNP	6.2.0	NSTS-LS01
TMI-sphereV8W_noBimp_1750_0.05_100.in	12/8/2020	MCNP	6.2.0	NSTS-LS01
TMI-sphereV8W_noBimp_1750_0.05_100.ino	12/8/2020	MCNP	6.2.0	NSTS-LS01
TMI-sphereV8W_noBimp_1750_0.05_25.in	12/8/2020	MCNP	6.2.0	NSTS-LS01
TMI-sphereV8W_noBimp_1750_0.05_25.ino	12/8/2020	MCNP	6.2.0	NSTS-LS01
TMI-sphereV8W_noBimp_1750_0.05_50.in	12/8/2020	MCNP	6.2.0	NSTS-LS01
TMI-sphereV8W_noBimp_1750_0.05_50.ino	12/8/2020	MCNP	6.2.0	NSTS-LS01
TMI-sphereV8W_noBimp_1750_0.05_75.in	12/8/2020	MCNP	6.2.0	NSTS-LS01
TMI-sphereV8W_noBimp_1750_0.05_75.ino	12/8/2020	MCNP	6.2.0	NSTS-LS01
TMI-sphereV8W_noBimp_1750_0.1_100.in	12/8/2020	MCNP	6.2.0	NSTS-LS01
TMI-sphereV8W_noBimp_1750_0.1_100.ino	12/8/2020	MCNP	6.2.0	NSTS-LS01
TMI-sphereV8W_noBimp_1750_0.1_25.in	12/8/2020	MCNP	6.2.0	NSTS-LS01
TMI-sphereV8W_noBimp_1750_0.1_25.ino	12/8/2020	MCNP	6.2.0	NSTS-LS01
TMI-sphereV8W_noBimp_1750_0.1_50.in	12/8/2020	MCNP	6.2.0	NSTS-LS01
TMI-sphereV8W_noBimp_1750_0.1_50.ino	12/8/2020	MCNP	6.2.0	NSTS-LS01
TMI-sphereV8W_noBimp_1750_0.15_100.in	12/8/2020	MCNP	6.2.0	NSTS-LS01
TMI-sphereV8W_noBimp_1750_0.15_100.ino	12/8/2020	MCNP	6.2.0	NSTS-LS01
TMI-sphereV8W_noBimp_1750_0.15_25.in	12/8/2020	MCNP	6.2.0	NSTS-LS01
TMI-sphereV8W_noBimp_1750_0.15_25.ino	12/8/2020	MCNP	6.2.0	NSTS-LS01
TMI-sphereV8W_noBimp_1750_0.15_50.in	12/8/2020	MCNP	6.2.0	NSTS-LS01
TMI-sphereV8W_noBimp_1750_0.15_50.ino	12/8/2020	MCNP	6.2.0	NSTS-LS01
TMI-sphereV8W_noBimp_1750_0.15_75.in	12/8/2020	MCNP	6.2.0	NSTS-LS01
TMI-sphereV8W_noBimp_1750_0.15_75.ino	12/8/2020	MCNP	6.2.0	NSTS-LS01
TMI-sphereV8W_noBimp_1750_0.1621_100.in	12/8/2020	MCNP	6.2.0	NSTS-LS01
TMI-sphereV8W_noBimp_1750_0.1621_100.ino	12/8/2020	MCNP	6.2.0	NSTS-LS01
TMI-sphereV8W_noBimp_1750_0.1621_25.in	12/8/2020	MCNP	6.2.0	NSTS-LS01
TMI-sphereV8W_noBimp_1750_0.1621_25.ino	12/8/2020	MCNP	6.2.0	NSTS-LS01
TMI-sphereV8W_noBimp_1750_0.1621_50.in	12/8/2020	MCNP	6.2.0	NSTS-LS01
TMI-sphereV8W_noBimp_1750_0.1621_50.ino	12/8/2020	MCNP	6.2.0	NSTS-LS01
TMI-sphereV8W_noBimp_1750_0.1621_75.in	12/8/2020	MCNP	6.2.0	NSTS-LS01
TMI-sphereV8W_noBimp_1750_0.1621_75.ino	12/8/2020	MCNP	6.2.0	NSTS-LS01
TMI-sphereV8W_noBimp_1750_0.1_75.in	12/8/2020	MCNP	6.2.0	NSTS-LS01
TMI-sphereV8W_noBimp_1750_0.1_75.ino	12/8/2020	MCNP	6.2.0	NSTS-LS01
TMI-sphereV8W_noBimp_925_0.05_100.in	12/8/2020	MCNP	6.2.0	NSTS-LS01
TMI-sphereV8W_noBimp_925_0.05_100.ino	12/8/2020	MCNP	6.2.0	NSTS-LS01
TMI-sphereV8W_noBimp_925_0.05_25.in	12/8/2020	MCNP	6.2.0	NSTS-LS01
TMI-sphereV8W_noBimp_925_0.05_25.ino	12/8/2020	MCNP	6.2.0	NSTS-LS01
TMI-sphereV8W_noBimp_925_0.05_50.in	12/8/2020	MCNP	6.2.0	NSTS-LS01
TMI-sphereV8W_noBimp_925_0.05_50.ino	12/8/2020	MCNP	6.2.0	NSTS-LS01
TMI-sphereV8W_noBimp_925_0.05_75.in	12/8/2020	MCNP	6.2.0	NSTS-LS01
TMI-sphereV8W_noBimp_925_0.05_75.ino	12/8/2020	MCNP	6.2.0	NSTS-LS01
TMI-sphereV8W_noBimp_925_0.1_100.in	12/8/2020	MCNP	6.2.0	NSTS-LS01
TMI-sphereV8W_noBimp_925_0.1_100.ino	12/8/2020	MCNP	6.2.0	NSTS-LS01
TMI-sphereV8W_noBimp_925_0.1_25.in	12/8/2020	MCNP	6.2.0	NSTS-LS01
TMI-sphereV8W_noBimp_925_0.1_25.ino	12/8/2020	MCNP	6.2.0	NSTS-LS01
TMI-sphereV8W_noBimp_925_0.1_50.in	12/8/2020	MCNP	6.2.0	NSTS-LS01
TMI-sphereV8W_noBimp_925_0.1_50.ino	12/8/2020	MCNP	6.2.0	NSTS-LS01

TMI-sphereV8W_noBimp_925_0.15_100.in	12/8/2020	MCNP	6.2.0	NSTS-LS01
TMI-sphereV8W_noBimp_925_0.15_100.ino	12/8/2020	MCNP	6.2.0	NSTS-LS01
TMI-sphereV8W_noBimp_925_0.15_25.in	12/8/2020	MCNP	6.2.0	NSTS-LS01
TMI-sphereV8W_noBimp_925_0.15_25.ino	12/8/2020	MCNP	6.2.0	NSTS-LS01
TMI-sphereV8W_noBimp_925_0.15_50.in	12/8/2020	MCNP	6.2.0	NSTS-LS01
TMI-sphereV8W_noBimp_925_0.15_50.ino	12/8/2020	MCNP	6.2.0	NSTS-LS01
TMI-sphereV8W_noBimp_925_0.15_75.in	12/8/2020	MCNP	6.2.0	NSTS-LS01
TMI-sphereV8W_noBimp_925_0.15_75.ino	12/8/2020	MCNP	6.2.0	NSTS-LS01
TMI-sphereV8W_noBimp_925_0.1621_100.in	12/8/2020	MCNP	6.2.0	NSTS-LS01
TMI-sphereV8W_noBimp_925_0.1621_100.ino	12/8/2020	MCNP	6.2.0	NSTS-LS01
TMI-sphereV8W_noBimp_925_0.1621_25.in	12/8/2020	MCNP	6.2.0	NSTS-LS01
TMI-sphereV8W_noBimp_925_0.1621_25.ino	12/8/2020	MCNP	6.2.0	NSTS-LS01
TMI-sphereV8W_noBimp_925_0.1621_50.in	12/8/2020	MCNP	6.2.0	NSTS-LS01
TMI-sphereV8W_noBimp_925_0.1621_50.ino	12/8/2020	MCNP	6.2.0	NSTS-LS01
TMI-sphereV8W_noBimp_925_0.1621_75.in	12/8/2020	MCNP	6.2.0	NSTS-LS01
TMI-sphereV8W_noBimp_925_0.1621_75.ino	12/8/2020	MCNP	6.2.0	NSTS-LS01
TMI-sphereV8W_noBimp_925_0.1_75.in	12/8/2020	MCNP	6.2.0	NSTS-LS01
TMI-sphereV8W_noBimp_925_0.1_75.ino	12/8/2020	MCNP	6.2.0	NSTS-LS01
TMI-sphereV8W_noBnoB_1125_0.05.in	12/8/2020	MCNP	6.2.0	NSTS-LS01
TMI-sphereV8W_noBnoB_1125_0.05.ino	12/8/2020	MCNP	6.2.0	NSTS-LS01
TMI-sphereV8W_noBnoB_1125_0.15.in	12/8/2020	MCNP	6.2.0	NSTS-LS01
TMI-sphereV8W_noBnoB_1125_0.15.ino	12/8/2020	MCNP	6.2.0	NSTS-LS01
TMI-sphereV8W_noBnoB_1125_0.1621.in	12/8/2020	MCNP	6.2.0	NSTS-LS01
TMI-sphereV8W_noBnoB_1125_0.1621.ino	12/8/2020	MCNP	6.2.0	NSTS-LS01
TMI-sphereV8W_noBnoB_1125_0.1.in	12/8/2020	MCNP	6.2.0	NSTS-LS01
TMI-sphereV8W_noBnoB_1125_0.1.ino	12/8/2020	MCNP	6.2.0	NSTS-LS01
TMI-sphereV8W_noBnoB_1200_0.05.in	12/8/2020	MCNP	6.2.0	NSTS-LS01
TMI-sphereV8W_noBnoB_1200_0.05.ino	12/8/2020	MCNP	6.2.0	NSTS-LS01
TMI-sphereV8W_noBnoB_1200_0.15.in	12/8/2020	MCNP	6.2.0	NSTS-LS01
TMI-sphereV8W_noBnoB_1200_0.15.ino	12/8/2020	MCNP	6.2.0	NSTS-LS01
TMI-sphereV8W_noBnoB_1200_0.1621.in	12/8/2020	MCNP	6.2.0	NSTS-LS01
TMI-sphereV8W_noBnoB_1200_0.1621.ino	12/8/2020	MCNP	6.2.0	NSTS-LS01
TMI-sphereV8W_noBnoB_1200_0.1.in	12/8/2020	MCNP	6.2.0	NSTS-LS01
TMI-sphereV8W_noBnoB_1200_0.1.ino	12/8/2020	MCNP	6.2.0	NSTS-LS01
TMI-sphereV8W_noBnoB_1500_0.05.in	12/8/2020	MCNP	6.2.0	NSTS-LS01
TMI-sphereV8W_noBnoB_1500_0.05.ino	12/8/2020	MCNP	6.2.0	NSTS-LS01
TMI-sphereV8W_noBnoB_1500_0.15.in	12/8/2020	MCNP	6.2.0	NSTS-LS01
TMI-sphereV8W_noBnoB_1500_0.15.ino	12/8/2020	MCNP	6.2.0	NSTS-LS01
TMI-sphereV8W_noBnoB_1500_0.1621.in	12/8/2020	MCNP	6.2.0	NSTS-LS01
TMI-sphereV8W_noBnoB_1500_0.1621.ino	12/8/2020	MCNP	6.2.0	NSTS-LS01
TMI-sphereV8W_noBnoB_1500_0.1.in	12/8/2020	MCNP	6.2.0	NSTS-LS01
TMI-sphereV8W_noBnoB_1500_0.1.ino	12/8/2020	MCNP	6.2.0	NSTS-LS01
TMI-sphereV8W_noBnoB_1750_0.05.in	12/8/2020	MCNP	6.2.0	NSTS-LS01
TMI-sphereV8W_noBnoB_1750_0.05.ino	12/8/2020	MCNP	6.2.0	NSTS-LS01
TMI-sphereV8W_noBnoB_1750_0.15.in	12/8/2020	MCNP	6.2.0	NSTS-LS01
TMI-sphereV8W_noBnoB_1750_0.15.ino	12/8/2020	MCNP	6.2.0	NSTS-LS01
TMI-sphereV8W_noBnoB_1750_0.1621.in	12/8/2020	MCNP	6.2.0	NSTS-LS01
TMI-sphereV8W_noBnoB_1750_0.1621.ino	12/8/2020	MCNP	6.2.0	NSTS-LS01
TMI-sphereV8W_noBnoB_1750_0.1.in	12/8/2020	MCNP	6.2.0	NSTS-LS01
TMI-sphereV8W_noBnoB_1750_0.1.ino	12/8/2020	MCNP	6.2.0	NSTS-LS01
TMI-sphereV8W_noBnoB_925_0.05.in	12/8/2020	MCNP	6.2.0	NSTS-LS01
TMI-sphereV8W_noBnoB_925_0.05.ino	12/8/2020	MCNP	6.2.0	NSTS-LS01
TMI-sphereV8W_noBnoB_925_0.15.in	12/8/2020	MCNP	6.2.0	NSTS-LS01
TMI-sphereV8W_noBnoB_925_0.15.ino	12/8/2020	MCNP	6.2.0	NSTS-LS01
TMI-sphereV8W_noBnoB_925_0.1621.in	12/8/2020	MCNP	6.2.0	NSTS-LS01
TMI-sphereV8W_noBnoB_925_0.1621.ino	12/8/2020	MCNP	6.2.0	NSTS-LS01
TMI-sphereV8W_noBnoB_925_0.1.in	12/8/2020	MCNP	6.2.0	NSTS-LS01
TMI-sphereV8W_noBnoB_925_0.1.ino	12/8/2020	MCNP	6.2.0	NSTS-LS01
TMI-sphereV8C_noBimp_1125_0.05_100.in	12/10/2020	MCNP	6.2.0	NSTS-LS01
TMI-sphereV8C_noBimp_1125_0.05_100.ino	12/10/2020	MCNP	6.2.0	NSTS-LS01
TMI-sphereV8C_noBimp_1125_0.05_25.in	12/10/2020	MCNP	6.2.0	NSTS-LS01
TMI-sphereV8C_noBimp_1125_0.05_25.ino	12/10/2020	MCNP	6.2.0	NSTS-LS01

TMI-sphereV8C_noBimp_1125_0.05_50.in	12/10/2020	MCNP	6.2.0	NSTS-LS01
TMI-sphereV8C_noBimp_1125_0.05_50.ino	12/10/2020	MCNP	6.2.0	NSTS-LS01
TMI-sphereV8C_noBimp_1125_0.05_75.in	12/10/2020	MCNP	6.2.0	NSTS-LS01
TMI-sphereV8C_noBimp_1125_0.05_75.ino	12/10/2020	MCNP	6.2.0	NSTS-LS01
TMI-sphereV8C_noBimp_1125_0.1_100.in	12/10/2020	MCNP	6.2.0	NSTS-LS01
TMI-sphereV8C_noBimp_1125_0.1_100.ino	12/10/2020	MCNP	6.2.0	NSTS-LS01
TMI-sphereV8C_noBimp_1125_0.1_25.in	12/10/2020	MCNP	6.2.0	NSTS-LS01
TMI-sphereV8C_noBimp_1125_0.1_25.ino	12/10/2020	MCNP	6.2.0	NSTS-LS01
TMI-sphereV8C_noBimp_1125_0.1_50.in	12/10/2020	MCNP	6.2.0	NSTS-LS01
TMI-sphereV8C_noBimp_1125_0.1_50.ino	12/10/2020	MCNP	6.2.0	NSTS-LS01
TMI-sphereV8C_noBimp_1125_0.15_100.in	12/10/2020	MCNP	6.2.0	NSTS-LS01
TMI-sphereV8C_noBimp_1125_0.15_100.ino	12/10/2020	MCNP	6.2.0	NSTS-LS01
TMI-sphereV8C_noBimp_1125_0.15_25.in	12/10/2020	MCNP	6.2.0	NSTS-LS01
TMI-sphereV8C_noBimp_1125_0.15_25.ino	12/10/2020	MCNP	6.2.0	NSTS-LS01
TMI-sphereV8C_noBimp_1125_0.15_50.in	12/10/2020	MCNP	6.2.0	NSTS-LS01
TMI-sphereV8C_noBimp_1125_0.15_50.ino	12/10/2020	MCNP	6.2.0	NSTS-LS01
TMI-sphereV8C_noBimp_1125_0.15_75.in	12/10/2020	MCNP	6.2.0	NSTS-LS01
TMI-sphereV8C_noBimp_1125_0.15_75.ino	12/10/2020	MCNP	6.2.0	NSTS-LS01
TMI-sphereV8C_noBimp_1125_0.1621_100.in	12/10/2020	MCNP	6.2.0	NSTS-LS01
TMI-sphereV8C_noBimp_1125_0.1621_100.ino	12/10/2020	MCNP	6.2.0	NSTS-LS01
TMI-sphereV8C_noBimp_1125_0.1621_25.in	12/10/2020	MCNP	6.2.0	NSTS-LS01
TMI-sphereV8C_noBimp_1125_0.1621_25.ino	12/10/2020	MCNP	6.2.0	NSTS-LS01
TMI-sphereV8C_noBimp_1125_0.1621_50.in	12/10/2020	MCNP	6.2.0	NSTS-LS01
TMI-sphereV8C_noBimp_1125_0.1621_50.ino	12/10/2020	MCNP	6.2.0	NSTS-LS01
TMI-sphereV8C_noBimp_1125_0.1621_75.in	12/10/2020	MCNP	6.2.0	NSTS-LS01
TMI-sphereV8C_noBimp_1125_0.1621_75.ino	12/10/2020	MCNP	6.2.0	NSTS-LS01
TMI-sphereV8C_noBimp_1125_0.1_75.in	12/10/2020	MCNP	6.2.0	NSTS-LS01
TMI-sphereV8C_noBimp_1125_0.1_75.ino	12/10/2020	MCNP	6.2.0	NSTS-LS01
TMI-sphereV8C_noBimp_1200_0.05_100.in	12/10/2020	MCNP	6.2.0	NSTS-LS01
TMI-sphereV8C_noBimp_1200_0.05_100.ino	12/10/2020	MCNP	6.2.0	NSTS-LS01
TMI-sphereV8C_noBimp_1200_0.05_25.in	12/10/2020	MCNP	6.2.0	NSTS-LS01
TMI-sphereV8C_noBimp_1200_0.05_25.ino	12/10/2020	MCNP	6.2.0	NSTS-LS01
TMI-sphereV8C_noBimp_1200_0.05_50.in	12/10/2020	MCNP	6.2.0	NSTS-LS01
TMI-sphereV8C_noBimp_1200_0.05_50.ino	12/10/2020	MCNP	6.2.0	NSTS-LS01
TMI-sphereV8C_noBimp_1200_0.05_75.in	12/10/2020	MCNP	6.2.0	NSTS-LS01
TMI-sphereV8C_noBimp_1200_0.05_75.ino	12/10/2020	MCNP	6.2.0	NSTS-LS01
TMI-sphereV8C_noBimp_1200_0.1_100.in	12/10/2020	MCNP	6.2.0	NSTS-LS01
TMI-sphereV8C_noBimp_1200_0.1_100.ino	12/10/2020	MCNP	6.2.0	NSTS-LS01
TMI-sphereV8C_noBimp_1200_0.1_25.in	12/10/2020	MCNP	6.2.0	NSTS-LS01
TMI-sphereV8C_noBimp_1200_0.1_25.ino	12/10/2020	MCNP	6.2.0	NSTS-LS01
TMI-sphereV8C_noBimp_1200_0.1_50.in	12/10/2020	MCNP	6.2.0	NSTS-LS01
TMI-sphereV8C_noBimp_1200_0.1_50.ino	12/10/2020	MCNP	6.2.0	NSTS-LS01
TMI-sphereV8C_noBimp_1200_0.15_100.in	12/10/2020	MCNP	6.2.0	NSTS-LS01
TMI-sphereV8C_noBimp_1200_0.15_100.ino	12/10/2020	MCNP	6.2.0	NSTS-LS01
TMI-sphereV8C_noBimp_1200_0.15_25.in	12/10/2020	MCNP	6.2.0	NSTS-LS01
TMI-sphereV8C_noBimp_1200_0.15_25.ino	12/10/2020	MCNP	6.2.0	NSTS-LS01
TMI-sphereV8C_noBimp_1200_0.15_50.in	12/10/2020	MCNP	6.2.0	NSTS-LS01
TMI-sphereV8C_noBimp_1200_0.15_50.ino	12/10/2020	MCNP	6.2.0	NSTS-LS01
TMI-sphereV8C_noBimp_1200_0.15_75.in	12/10/2020	MCNP	6.2.0	NSTS-LS01
TMI-sphereV8C_noBimp_1200_0.15_75.ino	12/10/2020	MCNP	6.2.0	NSTS-LS01
TMI-sphereV8C_noBimp_1200_0.1621_100.in	12/10/2020	MCNP	6.2.0	NSTS-LS01
TMI-sphereV8C_noBimp_1200_0.1621_100.ino	12/10/2020	MCNP	6.2.0	NSTS-LS01
TMI-sphereV8C_noBimp_1200_0.1621_25.in	12/10/2020	MCNP	6.2.0	NSTS-LS01
TMI-sphereV8C_noBimp_1200_0.1621_25.ino	12/10/2020	MCNP	6.2.0	NSTS-LS01
TMI-sphereV8C_noBimp_1200_0.1621_50.in	12/10/2020	MCNP	6.2.0	NSTS-LS01
TMI-sphereV8C_noBimp_1200_0.1621_50.ino	12/10/2020	MCNP	6.2.0	NSTS-LS01
TMI-sphereV8C_noBimp_1200_0.1621_75.in	12/10/2020	MCNP	6.2.0	NSTS-LS01
TMI-sphereV8C_noBimp_1200_0.1621_75.ino	12/10/2020	MCNP	6.2.0	NSTS-LS01
TMI-sphereV8C_noBimp_1200_0.1_75.in	12/10/2020	MCNP	6.2.0	NSTS-LS01
TMI-sphereV8C_noBimp_1200_0.1_75.ino	12/10/2020	MCNP	6.2.0	NSTS-LS01
TMI-sphereV8C_noBimp_1500_0.05_100.in	12/10/2020	MCNP	6.2.0	NSTS-LS01
TMI-sphereV8C_noBimp_1500_0.05_100.ino	12/10/2020	MCNP	6.2.0	NSTS-LS01

TMI-sphereV8C_noBimp_1500_0.05_25.in	12/10/2020	MCNP	6.2.0	NSTS-LS01
TMI-sphereV8C_noBimp_1500_0.05_25.ino	12/10/2020	MCNP	6.2.0	NSTS-LS01
TMI-sphereV8C_noBimp_1500_0.05_50.in	12/10/2020	MCNP	6.2.0	NSTS-LS01
TMI-sphereV8C_noBimp_1500_0.05_50.ino	12/10/2020	MCNP	6.2.0	NSTS-LS01
TMI-sphereV8C_noBimp_1500_0.05_75.in	12/10/2020	MCNP	6.2.0	NSTS-LS01
TMI-sphereV8C_noBimp_1500_0.05_75.ino	12/10/2020	MCNP	6.2.0	NSTS-LS01
TMI-sphereV8C_noBimp_1500_0.1_100.in	12/10/2020	MCNP	6.2.0	NSTS-LS01
TMI-sphereV8C_noBimp_1500_0.1_100.ino	12/10/2020	MCNP	6.2.0	NSTS-LS01
TMI-sphereV8C_noBimp_1500_0.1_25.in	12/10/2020	MCNP	6.2.0	NSTS-LS01
TMI-sphereV8C_noBimp_1500_0.1_25.ino	12/10/2020	MCNP	6.2.0	NSTS-LS01
TMI-sphereV8C_noBimp_1500_0.1_50.in	12/10/2020	MCNP	6.2.0	NSTS-LS01
TMI-sphereV8C_noBimp_1500_0.1_50.ino	12/10/2020	MCNP	6.2.0	NSTS-LS01
TMI-sphereV8C_noBimp_1500_0.15_100.in	12/10/2020	MCNP	6.2.0	NSTS-LS01
TMI-sphereV8C_noBimp_1500_0.15_100.ino	12/10/2020	MCNP	6.2.0	NSTS-LS01
TMI-sphereV8C_noBimp_1500_0.15_25.in	12/10/2020	MCNP	6.2.0	NSTS-LS01
TMI-sphereV8C_noBimp_1500_0.15_25.ino	12/10/2020	MCNP	6.2.0	NSTS-LS01
TMI-sphereV8C_noBimp_1500_0.15_50.in	12/10/2020	MCNP	6.2.0	NSTS-LS01
TMI-sphereV8C_noBimp_1500_0.15_50.ino	12/10/2020	MCNP	6.2.0	NSTS-LS01
TMI-sphereV8C_noBimp_1500_0.15_75.in	12/10/2020	MCNP	6.2.0	NSTS-LS01
TMI-sphereV8C_noBimp_1500_0.15_75.ino	12/10/2020	MCNP	6.2.0	NSTS-LS01
TMI-sphereV8C_noBimp_1500_0.1621_100.in	12/10/2020	MCNP	6.2.0	NSTS-LS01
TMI-sphereV8C_noBimp_1500_0.1621_100.ino	12/10/2020	MCNP	6.2.0	NSTS-LS01
TMI-sphereV8C_noBimp_1500_0.1621_25.in	12/10/2020	MCNP	6.2.0	NSTS-LS01
TMI-sphereV8C_noBimp_1500_0.1621_25.ino	12/10/2020	MCNP	6.2.0	NSTS-LS01
TMI-sphereV8C_noBimp_1500_0.1621_50.in	12/10/2020	MCNP	6.2.0	NSTS-LS01
TMI-sphereV8C_noBimp_1500_0.1621_50.ino	12/10/2020	MCNP	6.2.0	NSTS-LS01
TMI-sphereV8C_noBimp_1500_0.1621_75.in	12/10/2020	MCNP	6.2.0	NSTS-LS01
TMI-sphereV8C_noBimp_1500_0.1621_75.ino	12/10/2020	MCNP	6.2.0	NSTS-LS01
TMI-sphereV8C_noBimp_1500_0.1_75.in	12/10/2020	MCNP	6.2.0	NSTS-LS01
TMI-sphereV8C_noBimp_1500_0.1_75.ino	12/10/2020	MCNP	6.2.0	NSTS-LS01
TMI-sphereV8C_noBimp_1750_0.05_100.in	12/10/2020	MCNP	6.2.0	NSTS-LS01
TMI-sphereV8C_noBimp_1750_0.05_100.ino	12/10/2020	MCNP	6.2.0	NSTS-LS01
TMI-sphereV8C_noBimp_1750_0.05_25.in	12/10/2020	MCNP	6.2.0	NSTS-LS01
TMI-sphereV8C_noBimp_1750_0.05_25.ino	12/10/2020	MCNP	6.2.0	NSTS-LS01
TMI-sphereV8C_noBimp_1750_0.05_50.in	12/10/2020	MCNP	6.2.0	NSTS-LS01
TMI-sphereV8C_noBimp_1750_0.05_50.ino	12/10/2020	MCNP	6.2.0	NSTS-LS01
TMI-sphereV8C_noBimp_1750_0.05_75.in	12/10/2020	MCNP	6.2.0	NSTS-LS01
TMI-sphereV8C_noBimp_1750_0.05_75.ino	12/10/2020	MCNP	6.2.0	NSTS-LS01
TMI-sphereV8C_noBimp_1750_0.1_100.in	12/10/2020	MCNP	6.2.0	NSTS-LS01
TMI-sphereV8C_noBimp_1750_0.1_100.ino	12/10/2020	MCNP	6.2.0	NSTS-LS01
TMI-sphereV8C_noBimp_1750_0.1_25.in	12/10/2020	MCNP	6.2.0	NSTS-LS01
TMI-sphereV8C_noBimp_1750_0.1_25.ino	12/10/2020	MCNP	6.2.0	NSTS-LS01
TMI-sphereV8C_noBimp_1750_0.1_50.in	12/10/2020	MCNP	6.2.0	NSTS-LS01
TMI-sphereV8C_noBimp_1750_0.1_50.ino	12/10/2020	MCNP	6.2.0	NSTS-LS01
TMI-sphereV8C_noBimp_1750_0.15_100.in	12/10/2020	MCNP	6.2.0	NSTS-LS01
TMI-sphereV8C_noBimp_1750_0.15_100.ino	12/10/2020	MCNP	6.2.0	NSTS-LS01
TMI-sphereV8C_noBimp_1750_0.15_25.in	12/10/2020	MCNP	6.2.0	NSTS-LS01
TMI-sphereV8C_noBimp_1750_0.15_25.ino	12/10/2020	MCNP	6.2.0	NSTS-LS01
TMI-sphereV8C_noBimp_1750_0.15_50.in	12/10/2020	MCNP	6.2.0	NSTS-LS01
TMI-sphereV8C_noBimp_1750_0.15_50.ino	12/10/2020	MCNP	6.2.0	NSTS-LS01
TMI-sphereV8C_noBimp_1750_0.15_75.in	12/10/2020	MCNP	6.2.0	NSTS-LS01
TMI-sphereV8C_noBimp_1750_0.15_75.ino	12/10/2020	MCNP	6.2.0	NSTS-LS01
TMI-sphereV8C_noBimp_1750_0.1621_100.in	12/10/2020	MCNP	6.2.0	NSTS-LS01
TMI-sphereV8C_noBimp_1750_0.1621_100.ino	12/10/2020	MCNP	6.2.0	NSTS-LS01
TMI-sphereV8C_noBimp_1750_0.1621_25.in	12/10/2020	MCNP	6.2.0	NSTS-LS01
TMI-sphereV8C_noBimp_1750_0.1621_25.ino	12/10/2020	MCNP	6.2.0	NSTS-LS01
TMI-sphereV8C_noBimp_1750_0.1621_50.in	12/10/2020	MCNP	6.2.0	NSTS-LS01
TMI-sphereV8C_noBimp_1750_0.1621_50.ino	12/10/2020	MCNP	6.2.0	NSTS-LS01
TMI-sphereV8C_noBimp_1750_0.1621_75.in	12/10/2020	MCNP	6.2.0	NSTS-LS01
TMI-sphereV8C_noBimp_1750_0.1621_75.ino	12/10/2020	MCNP	6.2.0	NSTS-LS01
TMI-sphereV8C_noBimp_1750_0.1_75.in	12/10/2020	MCNP	6.2.0	NSTS-LS01
TMI-sphereV8C_noBimp_1750_0.1_75.ino	12/10/2020	MCNP	6.2.0	NSTS-LS01

TMI-sphereV8C_noBimp_925_0.05_100.in	12/10/2020	MCNP	6.2.0	NSTS-LS01
TMI-sphereV8C_noBimp_925_0.05_100.ino	12/10/2020	MCNP	6.2.0	NSTS-LS01
TMI-sphereV8C_noBimp_925_0.05_25.in	12/10/2020	MCNP	6.2.0	NSTS-LS01
TMI-sphereV8C_noBimp_925_0.05_25.ino	12/10/2020	MCNP	6.2.0	NSTS-LS01
TMI-sphereV8C_noBimp_925_0.05_50.in	12/10/2020	MCNP	6.2.0	NSTS-LS01
TMI-sphereV8C_noBimp_925_0.05_50.ino	12/10/2020	MCNP	6.2.0	NSTS-LS01
TMI-sphereV8C_noBimp_925_0.05_75.in	12/10/2020	MCNP	6.2.0	NSTS-LS01
TMI-sphereV8C_noBimp_925_0.05_75.ino	12/10/2020	MCNP	6.2.0	NSTS-LS01
TMI-sphereV8C_noBimp_925_0.1_100.in	12/10/2020	MCNP	6.2.0	NSTS-LS01
TMI-sphereV8C_noBimp_925_0.1_100.ino	12/10/2020	MCNP	6.2.0	NSTS-LS01
TMI-sphereV8C_noBimp_925_0.1_25.in	12/10/2020	MCNP	6.2.0	NSTS-LS01
TMI-sphereV8C_noBimp_925_0.1_25.ino	12/10/2020	MCNP	6.2.0	NSTS-LS01
TMI-sphereV8C_noBimp_925_0.1_50.in	12/10/2020	MCNP	6.2.0	NSTS-LS01
TMI-sphereV8C_noBimp_925_0.1_50.ino	12/10/2020	MCNP	6.2.0	NSTS-LS01
TMI-sphereV8C_noBimp_925_0.15_100.in	12/10/2020	MCNP	6.2.0	NSTS-LS01
TMI-sphereV8C_noBimp_925_0.15_100.ino	12/10/2020	MCNP	6.2.0	NSTS-LS01
TMI-sphereV8C_noBimp_925_0.15_25.in	12/10/2020	MCNP	6.2.0	NSTS-LS01
TMI-sphereV8C_noBimp_925_0.15_25.ino	12/10/2020	MCNP	6.2.0	NSTS-LS01
TMI-sphereV8C_noBimp_925_0.15_50.in	12/10/2020	MCNP	6.2.0	NSTS-LS01
TMI-sphereV8C_noBimp_925_0.15_50.ino	12/10/2020	MCNP	6.2.0	NSTS-LS01
TMI-sphereV8C_noBimp_925_0.15_75.in	12/10/2020	MCNP	6.2.0	NSTS-LS01
TMI-sphereV8C_noBimp_925_0.15_75.ino	12/10/2020	MCNP	6.2.0	NSTS-LS01
TMI-sphereV8C_noBimp_925_0.1621_100.in	12/10/2020	MCNP	6.2.0	NSTS-LS01
TMI-sphereV8C_noBimp_925_0.1621_100.ino	12/10/2020	MCNP	6.2.0	NSTS-LS01
TMI-sphereV8C_noBimp_925_0.1621_25.in	12/10/2020	MCNP	6.2.0	NSTS-LS01
TMI-sphereV8C_noBimp_925_0.1621_25.ino	12/10/2020	MCNP	6.2.0	NSTS-LS01
TMI-sphereV8C_noBimp_925_0.1621_50.in	12/10/2020	MCNP	6.2.0	NSTS-LS01
TMI-sphereV8C_noBimp_925_0.1621_50.ino	12/10/2020	MCNP	6.2.0	NSTS-LS01
TMI-sphereV8C_noBimp_925_0.1621_75.in	12/10/2020	MCNP	6.2.0	NSTS-LS01
TMI-sphereV8C_noBimp_925_0.1621_75.ino	12/10/2020	MCNP	6.2.0	NSTS-LS01
TMI-sphereV8C_noBimp_925_0.1_75.in	12/10/2020	MCNP	6.2.0	NSTS-LS01
TMI-sphereV8C_noBimp_925_0.1_75.ino	12/10/2020	MCNP	6.2.0	NSTS-LS01
TMIFuelDecay.inp	12/10/2020	ORIGEN/SCALE	6.2.4	LAPTOP-MEGANP
TMIFuelDecay.out	12/10/2020	ORIGEN/SCALE	6.2.4	21888-L

12.2. Other Electronic Files

Filename	File Date	Description
Final SFML Results.xlsb	12/16/2020	Repository of all final MCNP k_{eff} results, tables, and plots.
Material comp and scoping.xls	12/16/2020	ORIGEN output for material composition; MCNP k_{eff} results for optimum moderation determination.